Aus der Klinik und Poliklinik für Nuklearmedizin
Klinik der Ludwig-Maximilians-Universität München
Direktor: Prof. Dr. med. Peter Bartenstein

In Vivo Monitoring der Neuroinflammation während einer Immunmodulatorischen Therapie in Mausmodellen der Amyloid Pathologie

Dissertation

zum Erwerb des Doktorgrades der Medizin
an der Medizinischen Fakultät der
Ludwig-Maximilians-Universität zu München

vorgelegt von

Gloria Biechele
aus
Mindelheim

2022

Mit Genehmigung der Medizinischen
Fakultät der Universität München

Berichterstatter:	Priv.-Doz. Dr. med. Matthias Brendel, MHBA
Mitberichterstatter:	Prof. Dr. Markus Kipp Prof. Dr. Arthur Liesz Prof. Dr. Johannes Levin
Mitbetreuung durch den promovierten Mitarbeiter:	Priv.-Doz. Dr. med. Leonie Beyer
Dekan:	Prof. Dr. med. Thomas Gudermann
Tag der mündlichen Prüfung:	15.12.2022

I. Eidesstattliche Versicherung

Biechele, Gloria

Name, Vorname

Ich erkläre hiermit an Eides statt, dass ich die vorliegende Dissertation mit dem Titel

In Vivo Monitoring der Neuroinflammation während einer Immunmodulatorischen Therapie in Mausmodellen der Amyloid Pathologie

selbständig verfasst, mich außer der angegebenen keiner weiteren Hilfsmittel bedient und alle Erkenntnisse, die aus dem Schrifttum ganz oder annähernd übernommen sind, als solche kenntlich gemacht und nach ihrer Herkunft unter Bezeichnung der Fundstelle einzeln nachgewiesen habe.

Ich erkläre des Weiteren, dass die hier vorgelegte Dissertation nicht in gleicher oder in ähnlicher Form bei einer anderen Stelle zur Erlangung eines akademischen Grades eingereicht wurde.

München, 17.01.2023 — Gloria Biechele

Ort, Datum — Unterschrift Doktorandin

Kumulative Dissertation gemäß § 4a der Promotionsordnung

II. Inhaltsverzeichnis

III. Abkürzungsverzeichnis

APP	Amyloid Vorläuferprotein
Aβ	Amyloid Beta Peptid, β-Amyloid
AUC	Area under the curve (dt. Fläche unter der Kurve)
CA1	Cornu ammonis 1, Teil des Hippocampus
CB2R	Cannabinoid 2 Rezeptor
COX-1/-2	Cyclooxygenase Isoenzyme 1 und 2
CSF1R	koloniestimulierende Faktor 1 Rezeptor
^{11}C	Kohlenstoff-Isotop mit der Massenzahl 11
FAD	Familiäre Alzheimer Krankheit
^{18}F	Fluor-Isotop mit der Massenzahl 18
kDa	Kilo Dalton
MBq	Megabecquerel
mo	Monate
MRT	Magnetresonanztomographie
MWM	Morris-Wasserlabyrinth
NLRP3	NOD-, LRR-, and pyrin domain-containing 3, Inflammasom
PET	Positronen-Emissions-Tomographie
PPARγ	Peroxisomen-Proliferator-aktivierten-Rezeptor
P2X7R	P2X-ligandengesteuerter Ionenkanal 7 Rezeptor
P2Y12R	purinerger metabotroper Rezeptor 12
SUV	Standard-Aufnahmewert
SUVR	relativer Standard-Aufnahmewert zur Referenzregion
SUVH	relativer Standard-Aufnahmewert zum Herz
TG	transgen

TREM	triggernder Rezeptor auf myeloischen Zellen
TSPO	18-kDa-Translokator-Protein
Vehikel	mit Kontrollfutter behandelte Tiere
WT	Wildtyp
µPET	Kleintier PET
MCI	Mild cognitive Impairment (dt. Leichte kognitive Störung)

IV. Publikationen der kumulativen Dissertation

Die vorliegende kumulative Dissertation umfasst zwei bereits publizierte Manuskripte:

Biechele, G.; Blume, T.; Deussing, M.; Zott, B.; Shi, Y.; Xiang, X.; Franzmeier, N.; Kleinberger, G.; Peters, F.; Ochs, K.; Focke, C.; Sacher, C.; Wind, K.; Schmidt, C.; Lindner, S.; Gildehaus, F.; Eckenweber, F.; Beyer, L.; von Ungern-Sternberg, B.; Bartenstein, P.; Baumann, K.; Dorostkar, M.; Rominger, A.; Cumming, P.; Willem, M.; Adelsberger, H.; Herms, J.; Brendel, M. Pre-therapeutic Microglia Activation and Sex Determine Therapy Effects of chronic Immunomodulation. Theranostics. 2021 Aug 19; 11(18): 8964-8976. (IF 11.556)

Blume, T.; Deussing, M.; **Biechele, G.**; Peters, F.; Zott, B.; Schmidt, C.; Franzmeier, N.; Wind, K.; Eckenweber, F.; Sacher, C.; Shi, Y.; Ochs, K.; Kleinberger, G.; Xiang, X.; Focke, C.; Lindner, S.; Gildehaus, F.; Beyer, L.; Ungern-Sternberg, B.; Bartenstein, P.; Baumann, K.; Haass, C.; Adelsberger, H.; Rominger, A.; Cumming, P.; Willem, M.; Dorostkar, M., Herms, J., Brendel, M. Chronic PPARγ Stimulation Shifts Amyloidosis to Higher Fibrillarity but Improves Cognition. Front Aging Neurosci. 2022 Mar 30; 14: 854031. (IF 5.750)

Beschreibung des Eigenanteiles:

„**Pre-therapeutic microglia activation and sex determine therapy effects of chronic immunomodulation.”**

Erstellen des Studienkonzepts in Zusammenarbeit mit dem Betreuer. Selbstständige praktische Umsetzung des Studienkonzepts durch Ausführung der Kleintier-PET-Scans sowie der kognitiven Verhaltenstestung. Mitarbeit bei Versorgung und Fütterung der Versuchsmäuse, sowie regelmäßige Kontrolle des körperlichen Wohlergehens der Tiere. Nach Abschluss des praktischen Teils der Studie autonome Auswertung und Interpretation der erhobenen Daten der PET Scans sowie statistische Analyse, stets in enger Rücksprache mit dem Betreuer. Durchführung der kognitiven Verhaltenstestung und zuletzt Perfusion der Tiere. Eigenständiges Verfassen des primären Manuskriptentwurfs des Papers. Anschließende Überarbeitung des Entwurfs bis zur finalen Version in Abstimmung mit dem Betreuer.

„Chronic PPARγ stimulation shifts amyloidosis to higher fibrillarity but improves cognition “

Analog zur Erstautorschaft Planung und Ausführung der Kleintier-PET-Scans sowie der kognitiven Verhaltenstestung im Morris-Water-Maze. Perfusion der Tiere sowie anschließende Interaktion mit den Studienpartnern der Abteilung für Neuropathologie, welche obenstehende Publikation als Erstautorschaft veröffentlichten. Aufbereitung, Auswertung und Interpretation der PET- und Verhaltensergebnisse sowie Korrelation mit den neuropathologischen Quantifizierungen. Bereitstellung der PET-basierten Abbildungen und Absätze der Publikation.

1. Einführung

Infolge des demographischen Wandels, welchem unsere Gesellschaft unterliegt, haben Gesundheitssysteme in Industrienationen mit einer Reihe vermehrt auftretender Erkrankungen des hohen Alters zu kämpfen. Neben kardiovaskulären und endokrinologischen Problemstellungen zählen auch kognitive Verluste zu den häufigsten Beeinträchtigungen im alltäglichen Leben der Älteren (Jaul and Barron 2017). Etwa 8 Millionen Menschen sind derzeit in Deutschland älter als 80 Jahre, deren Demenzrisiko beträgt gerundet 20%, bei den über 90-Jährigen beträgt es bereits 40% (Thyrian, Boekholt et al. 2020). Infolge demographischer Veränderungen kommt es zu weit mehr Neuerkrankungen als zu Sterbefällen unter den bereits Erkrankten (Deutsche Alzheimer Gesellschaft e.V. 2020), was in einer wachsenden sozioökonomischen Belastung für das Gesundheitssystem in Gesellschaften längeren Lebens resultiert. 2016 betrugen die geschätzten Kosten aller Demenzerkrankungen in Deutschland 73 Milliarden €, was sich bis 2060 gemäß Hochrechnungen voraussichtlich auf 194 Milliarden € steigern wird (Michalowsky, Kaczynski et al. 2019).

Neben vaskulärer Demenz, Lewy-Body-Demenz und dem Komplex der frontotemporalen dementiellen Erkrankungen stellt die Alzheimer Krankheit laut der WHO mit 60-70% die mit Abstand häufigste Ursache einer Demenzerkrankung dar (WHO 2021). Laut der Alzheimer Gesellschaft wird Alzheimer als „Form der Demenz, die Gedächtnis, Denkprozess und Verhalten beeinträchtigt“ definiert, mit letztendlicher Erschwernis, alltägliche Aufgaben zu bewältigen (Alzheimer´s Association 2022). Gemäß der deutschen ICD-Kodierung muss für die Diagnosestellung eine Alltagsbeeinträchtigung über einen Zeitraum von mindestens 6 Monaten erfüllt sein. Angesichts der immensen Beeinträchtigung stellen die bislang zugelassenen Wirkstoffklassen Acetylcholinesterase-Inhibitoren und NMDA-

Antagonisten einen lediglich symptomatischem Therapieansatz dar (Birks 2006, Weller and Budson 2018). Trotz engagierter pathogenetischer Forschung und steigender ökonomischer Motivation existiert bisher keine zugelassene kausal wirksame oder krankheitsmodifizierende Behandlungsoption. (Lane, Hardy et al. 2018). Mit dem gegen β-Amyloid gerichteten Antikörper Aducanumab konnte allerdings als erste spezifische Therapie eine (Teil-) Zulassung erwirkt werden (FDA 2021).

1.1. Neuroinflammation bei Alzheimer Krankheit

Charakteristisch für die Alzheimer Krankheit ist die Akkumulation dreierlei neuropathologischer Komplexitäten: extrazelluläre β-Amyloid Peptid Plaques, intrazelluläre fibrilläre Tau Aggregate und die Aktivierung neuroinflammatorischer Pfade, reguliert durch Mikroglia und Astrozyten (Braak and Braak 1991, Querfurth and LaFerla 2010, Serrano-Pozo, Frosch et al. 2011, Heneka, Carson et al. 2015). Dieser Komplex wird als die „ATN-Sequenz“ konzeptualisiert, der zu Folge Amyloidose [A] der Tau-Pathologie [T] vorausgeht und sie beschleunigt, welche wiederum zu Neurodegeneration [N] führt (Tan, Ji et al. 2020). Dies wird nun zu einem „ATX(N)-System“ erweitert, wobei „X“ neuartige Biomarker für zusätzliche pathophysiologische Mechanismen, wie neuroimmune Dysregulation, synaptische Dysfunktion und Veränderungen der Blut-Hirn-Schranke im Rahmen regionaler Inflammation darstellt (Hampel, Cummings et al. 2021). Infolge des Auftretens von Aβ wurden je nach Krankheitsstadium zwei verschiedene Arten von Mikroglia beobachtet: Eine gering aktive, potentiell nützliche Entzündung und eine zur Hemmung der synaptischen Funktion bis zum Zelltod führende, schädliche Variante (Bamberger, Harris et al. 2003, Wang, Tan et al. 2015). Im Rahmen der Alzheimer-Pathophysiologie stellt die Neuroinflammation einen wichtigen Mediator für

Proteinaggregation und -ausbreitung, sowie für das Fortschreiten der Erkrankung dar und sorgt außerdem für eine positive Rückkopplungsschleife innerhalb der Krankheitskaskade (Ishizawa and Dickson 2001, Serrano-Pozo, Mielke et al. 2011, Villemagne, Burnham et al. 2013, Pascoal, Benedet et al. 2021). Studien zu oben genannten, multiplen Biomarkern bei an neurodegenerativen Erkrankungen leidenden Patienten kamen zu diskrepanten Ergebnissen. Während einige Autoren Aβ und Tau den gleichen Einfluss zur mikroglialen Aktivierung zuschreiben (Dani, Wood et al. 2018) und einige die Interaktion von Aβ und Mikrogliaaktivierung als Taktgeber der Tau-Ausbreitung unterstützen (Pascoal, Benedet et al. 2021), zeigte sich auch, dass die Auswirkungen der neuropathologischen Akkumulation auf die Kognition stark durch kortikale Atrophie moduliert werden (Frigerio, Boon et al. 2021, Su, Surendranathan et al. 2021). Ein detailliertes Verständnis des pathophysiologischen Zusammenspiels und seines Beitrags zur Inflammation könnte einen tieferen Einblick in die mechanistischen Prozesse gewähren und so zum Schlüssel für neue therapeutische Ansätze werden.

1.2. Immunmodulatorische Therapien bei Alzheimer Krankheit

Ob und wie sich Neuroinflammation letztendlich positiv oder negativ auf die erkrankungsbezogene Pathophysiologie und die patientenbezogene Lebensqualität auswirkt, ist noch unklar. Dennoch besteht berechtigtes Interesse, über eine Modulation der inflammatorischen Mechanismen neue Behandlungsstrategien gegen die Alzheimer Krankheit zu entwickeln (Ahmad, Fatima et al. 2019).

Aus präklinischen Arbeiten geht hervor, dass eine Immunmodulation über den Peroxisomen-Proliferator-aktivierten-Rezeptor (PPAR)-γ in der Lage ist, die neuronale Synapsendichte (Zou, Shi et al. 2016), sowie die räumliche Lernleistung (Mandrekar-Colucci, Karlo et al. 2012) in Alzheimer Mausmodellen zu bewahren. Als

ligandenabhängiger, nuklearer Rezeptor führt PPARγ im Zusammenspiel mit dem Leber X Rezeptor zu einem Anstieg der Apolipoprotein-E-Spiegel (apoE) im Gehirn, welche wiederum die proteolytische Entfernung von Aβ begünstigen. Als weitere Effekte sind die Stimulation von Astrozyten sowie die Polarisation von Mikroglia zu nennen, wodurch Letztere von einem proinflammatorischen M1-Zustand in einen entzündungshemmenden M2-Zustand mit verbesserter Phagozytoseaktivität konvertiert (Mandrekar-Colucci, Karlo et al. 2012). PPARγ-Agonisten begünstigen den Amyloidabbau und sind so in der Lage, bei behandelten Mäusen Gedächtnisverluste wiederherzustellen (Mandrekar-Colucci, Karlo et al. 2012, d'Angelo, Castelli et al. 2019). Dennoch wurde eine groß angelegte humane Studie zum Einsatz des PPARγ-Agonisten Pioglitazone bei Patienten mit leichter kognitiver Beeinträchtigung (engl. MCI = mild cognitive Impairment) eingestellt, nachdem eine Zwischenanalyse keinen Nutzen nachweisen konnte (Burns, Chiang et al. 2019).

Als weitere Möglichkeit der Immunmodulation sind NLRP3-Inflammasom-inhibitorische (NOD-, LRR-, and pyrin domain-containing 3) Strategien zu nennen. Das NLRP3-Inflammasom sorgt im Rahmen der Alzheimer Krankheit für die Sekretion der Interleukine IL-1β und IL-18 (Hanslik and Ulland 2020), welche für Neuroinflammation bis hin zu induziertem Zelltod verantwortlich sind (Wright, Zinn et al. 2013, Malik and Kanneganti 2017). NLRP3-Aktivierung begünstigt die pathologische Aggregation von Aβ und Tau und verhindert deren mikrogliale Clearance (Heneka, Kummer et al. 2013, Ising, Venegas et al. 2019). Eine therapeutische Inhibition dieses Inflammasoms stellt somit ein potentielles Mittel dar, Neuropathologien abzumildern, allerdings mit Einräumen schwerwiegender Folgen durch unbeabsichtigte immunsuppressive Wirkungen (Salliot, Dougados et al. 2009, Kullenberg, Lofqvist et al. 2016).

1.3. PET zur Bewertung von Neuroinflammation bei Menschen und Kleintieren

Die Positronen-Emissions-Tomographie als bildgebende Untersuchungsmethode ermöglicht dem Betrachter, mittels radioaktiv markierter Substanzen Stoffwechselaktivität und molekulare Strukturen im Körper sichtbar zu machen. Mithilfe geeigneter Tracer kann eine Vielzahl fehlgefalteter Proteine und stoffwechselpathologischer Vorgänge longitudinal in vivo dargestellt, sowie quantitativ und qualitativ bewertet werden. Zu diesen Vorgängen zählt auch die Neuroinflammation, welche bei der Alzheimer Krankheit vor allem auf reaktive Mikroglia und Astrozytose zurückzuführen ist (Leng and Edison 2021). Zunächst wurde die molekulare Bildgebung der Neuroinflammation mittels PET von Studien dominiert, die Isochinolincarboxamid [^{11}C]PK11195 als Liganden an das 18kDa Translokatorprotein (TSPO), auch bekannt als peripherer Benzodiazepinrezeptor, nutzten (Vivash and O'Brien 2016). TSPO benennt ein Protein an den Kontaktstellen der inneren und äußeren Mitochondrienmembran, welches an der Regulierung zahlreicher zellulärer Vorgänge beteiligt ist, unter anderem Entzündungsreaktion, oxidativer Stress und mitochondriale Homöostase (Scarf and Kassiou 2011, Bonsack and Sukumari-Ramesh 2018). Dennoch sind die detaillierten Funktionen von TSPO noch nicht vollständig geklärt und Gegenstand aktueller Forschung (Rupprecht, Wetzel et al. 2022, Shi, Cui et al. 2022). Aufgrund optimierbarer radiopharmazeutischer Eigenschaften (Chandra, Valkimadi et al. 2019) wurden TSPO-Tracer der zweiten und dritten Generation entwickelt, zu denen [^{18}F]GE-180 zählt (Fan, Calsolaro et al. 2016). Die TSPO-PET gewinnt an Relevanz zur Überwachung therapiebedingter Modifikation der mikroglialen Aktivierung in Mausmodellen (Scott, Zetterberg et al. 2018) sowie in humanen Studien (Wolf, Brackhan et al. 2020). In diesem Zusammenhang hat sich der TSPO-Ligand [^{18}F]GE-180 zur Darstellung aktivierter Mikroglia in Amyloid-Mausmodellen unter anti-

inflammatorischer Behandlung als leistungsfähig erwiesen (James, Belichenko et al. 2017). In vergangenen Studien konnten auch innerhalb unserer Arbeitsgruppe hohe Übereinstimmungen zwischen der [^{18}F]GE-180-PET Quantifizierung und immunhistochemischen Analysen mittels mikroglialer Marker nachgewiesen werden (Brendel, Probst et al. 2016, Parhizkar, Arzberger et al. 2019).

Neue Ansätze verfolgen auch nicht-TSPO PET-Marker zur Visualisierung neuroinflammation-bezogener Zielstrukturen. Zu diesen spezifischen und funktionellen Biomarkern zählen der P2X-ligandengesteuerte Ionenkanal 7 Rezeptor (P2X7R), die Cyclooxygenase Isoenzyme (COX-1 und COX-2), der Cannabinoid 2 Rezeptor (CB2R), der koloniestimulierende Faktor 1 Rezeptor (CSF1R), der purinerge metabotrope Rezeptor 12 (P2Y12R) und der triggernde Rezeptor auf myeloischen Zellen (TREM). Mithilfe dieser hochselektiven Biomarker kann es in Zukunft gelingen, Erkrankungen hinsichtlich ihrer beteiligten Immunzellen spezifisch zu charakterisieren (Gotzl, Brendel et al. 2019, Jain, Chaney et al. 2020). Zusammenfassend kann molekulare Bildgebung von Neuroinflammation wesentlich zur Therapieauswahl und -überwachung sich immunmodulatorisch auswirkender Therapien beitragen.

1.4. Mausmodelle der Alzheimer Krankheit

Die Entwicklung transgener Alzheimer-Mausmodelle trug grundlegend zum Verständnis molekularpathologischer Mechanismen, sowie zur Entwicklung und Prüfung therapeutischer Interventionen bei (Elder, Gama Sosa et al. 2010). Ein Großteil der Mausmodelle basiert auf der Verwendung von Genen, welche für die autosomal dominant vererbte, familiäre Alzheimer-Demenz (FAD) verantwortlich sind. Unter diesen Genen stellen das β-Amyloid precursor Protein (APP) Gen auf Chromosom 21 (St George-Hyslop 2000), das Presenilin 1 (PS1) Gen auf

Chromosom 14 und das Presenilin 2 (PS2) Gen auf Chromosom 1 (Puzzo, Gulisano et al. 2015) wichtige Genloci dar, welche in direktem Zusammenhang mit der Bildung und Akkumulation von β-Amyloid Plaques stehen (Platt, Reeves et al. 2013). APP als transmembranes Glykoprotein wird in diesem Rahmen komplex durch verschiedene proteolytische Sekretasen gespalten, was in der Bildung von löslichem Aβ resultiert. Beide oben genannten Presenilin-Gene codieren für solche Sekretasen (Puzzo, Gulisano et al. 2015).

Die transgene Mauslinie B6.PS2APP überexprimiert die Kombination aus homozygoter Presenilin-2-Mutation und humaner APP-Mutation (Richards, Higgins et al. 2003) mit nachfolgendem Vorkommen erster Plaques in zerebralem Cortex und Hippocampus ab einem Alter von 5 - 6 Monaten (Richards, Higgins et al. 2003, Ozmen, Albientz et al. 2009). Mit kognitiven Einschränkungen infolge der Amyloidakkumulation ist ab einem Alter von 8 Monaten zu rechnen (https://www.alzforum.org/research-models/ps2app).

Das *App*$^{NL\text{-}G\text{-}F}$-Mausmodell zählt zu den Knock-in Modellen der zweiten Generation (Saito, Matsuba et al. 2014), welche folgende drei zusätzlich integrierte Gene im APP-Genlocus enthalten: Eine sogenannte schwedische, beyreuther/iberische und eine arktische Mutation, welche zum Anstieg der totalen β-Amyloid-Produktion (Citron, Oltersdorf et al. 1992), zu einer erhöhten Aβ42/Aβ40-Ratio (Lichtenthaler, Ida et al. 1997) und zu begünstigter Plaque-Akkumulation (Nilsberth, Westlind-Danielsson et al. 2001) führen. Homozygote *App*$^{NL\text{-}G\text{-}F}$ -Mäuse weisen so ab einem Alter von 2 Monaten, ohne Überexpression von APP, sich progredient ausdehnende, zerebrale β-Amyloid Plaques mit umliegender reaktiver mikroglialer Aktivierung auf. Mit kognitiven Defiziten ist ab einem Alter von 8 Monaten zu rechnen (Saito, Matsuba et al. 2014, Masuda, Kobayashi et al. 2016).

Beide genannten Mausmodelle wurden mit C57Bl/6 Hintergrund generiert, welche als Wildtypen zur Überwachung der nicht-erkrankungsassoziierten Effekte dienten.

1.5. Abgeleitete Fragestellung

Immunmodulatorische Therapien mit dem PPARγ-Agonisten Pioglitazone zeigen heterogene Ergebnisse (Geldmacher, Fritsch et al. 2011, Mandrekar-Colucci, Karlo et al. 2012, Zou, Shi et al. 2016, Burns, Chiang et al. 2019). Aus vorangehenden Studien geht hervor, dass eine chronische Behandlung mit Pioglitazone mit reduzierter Neuroinflammation, Plaquemodifikation und verbesserter kognitiver Leistung einhergeht. Im Rahmen dieser Arbeit wurden die Effekte einer Behandlung von Pioglitazone zwischen Mäusen mit und ohne APP-Überexpression verglichen. Zudem wurden die longitudinalen Bildgebungsdaten hinsichtlich einer Stratifikationsmöglichkeit für optimiertes Therapieansprechen ausgewertet.

2. Inhalte der Promotionsarbeit

2.1. Die Therapieeffekte chronischer Immunmodulation werden durch prätherapeutische Mikrogliaaktivierung und das Geschlecht bestimmt

Diese Studie untersuchte zum einen die Hypothese, ob sich die TSPO-PET mit dem Tracer [^{18}F]GE-180 zum Monitoring anti-inflammatorischer Effekte bei chronischer Immunmodulation in Alzheimer-Mausmodellen eignet. Zum anderen wurde die Hypothese getestet, ob mikrogliale Aktivierung in der TSPO-PET in der Lage ist, therapieassoziierte Veränderungen und Ergebnisparameter zu prognostizieren. Darüber hinaus evaluierten wir Auswirkungen des Geschlechts auf die Immunmodulation. Schließlich wurden die in vivo PET-Ergebnisse und der zelluläre Ursprung der TSPO-PET Signalveränderungen (immun)histochemisch validiert und bestätigt.

Zwei verschiedene Aβ-Mausmodelle (PS2APP und *App^{NL-G-F}*) und eine Wildtyp-Kohorte wurden einem longitudinalen PET-Bildgebungsdesign (TSPO- und Aβ-PET) unterzogen. 23 weibliche PS2APP- und 15 Wildtyp-Mäuse durchliefen im Alter von 8 Monaten die Ausganguntersuchung und wurden dann im Alter von 9,5, 11,5 und 13 Monaten erneut mittels PET kontrolliert. Bei den 33 gemischtgeschlechtlichen *App^{NL-G-F}* -Mäusen erfolgte die Erstuntersuchung im Alter von 5 Monaten und die PET Bildgebung wurde dann mit 7,5 und 10 Monaten wiederholt. Nach Absolvieren der Erstuntersuchung wurde den Tieren für die gesamte Versuchszeit käfigweise zufällig entweder Pioglitazone- oder Kontrollfutter (Vehikel) zugeteilt. Zur Messung der zerebralen TSPO-Expression wurden [^{18}F]GE-180 TSPO-PET-Aufnahmen mit einer durchschnittlichen Dosis von 11,5 ± 2,2 MBq und einem Emissionsfenster von 60 – 90 Minuten nach Injektion durchgeführt. Zur Messung der fibrillären zerebralen Amyloidose wurden [^{18}F]florbetaben Aβ-PET-Aufnahmen mit einer durchschnittlichen

Dosis von 12,2 ± 2,0 MBq und einem Emissionsfenster von 30-60 Minuten nach Injektion durchgeführt, gemäß eines etablierten Protokolls (Overhoff, Brendel et al. 2016). Mithilfe von PMOD (Version 3.5; PMOD technologies, Basel, Schweiz) wurden die akquirierten Bilddaten zunächst räumlich koregistriert und dann auf ein für den Genotyp spezifisches „Template“ ausgerichtet. Durch Skalierung auf Gewicht und injizierte Radioaktivität konnten die Daten als Standardaufnahmewerte (engl. Standardized-Uptake-Value, SUV) normalisiert werden. Es wurden relative Standardaufnahmewerte (engl.: Standardized-Uptake-Value-Ratio, SUV_R) für das Aβ-PET mittels Pseudoreferenzregion und für das TSPO-PET mittels Myokardkorrektion (SUV_H) (Deussing, Blume et al. 2018) berechnet. Für die PS2APP-Kohorte diente die weiße Substanz (Overhoff, Brendel et al. 2016), für die *App*$^{NL-G-F}$-Kohorte das periaquäduktale Grau (Sacher, Blume et al. 2019) als pathologiearme Pseudoreferenzregion. Die TSPO-Daten wurden zur besseren Vergleichbarkeit zudem als Z-Scores = ([$Einzelwert_{TG}$ - $Mittelwert_{WT-Veh}$]/$Standardabweichung_{WT-Veh}$) für jedes individuelle Tier mit Amyloid Pathologie zu jedem Studienzeitpunkt standardisiert. Zudem erfolgte eine kognitive Verhaltenstestung (räumliches Lernen) mittels Morris-Wasserlabyrinth (MWM) (Bromley-Brits, Deng et al. 2011). Analysiert wurden die Latenz zum erstmaligen Erreichen der Plattform (engl.: escape latency), die Häufigkeit der Plattform-Durchquerungen (engl.: platform frequency) und die Aufenthaltszeit im Plattformquadranten, jeweils am Testtag. Die Einzelparameter wurden mittels einer Hauptkomponentenanalyse zu einem Score pro Tier kondensiert. Außerdem erfolgte die Entnahme randomisierter Gehirnhemisphären für (immun)histochemische sowie biochemische Analysen mit Iba1 als allgemeinen mikroglialen Marker und CD68 als speziellen Marker für mikrogliale Aktivierung.

Zunächst konnten wir zeigen, dass die TSPO-PET in der Lage war, veränderte Mikroglia-Aktivierung unter chronischer PPARγ-Stimulation nachzuweisen. Im Gegensatz zu den Vehikel-behandelten Wildtyp-Mäusen zeigten die Vehikel-behandelten PS2APP-Mäuse einen starken Anstieg des TSPO-PET-Signals mit einem Spitzenwert bei 11,5 Monaten (52-67 % Zunahme, alle Zeitpunkte: $p < 0,0001$) (**Abb. 1**). Prätherapeutisch konnte dabei kein Unterschied zwischen Pioglitazone- und Vehikel-behandelten PS2APP-Mäusen festgestellt werden (SUV_H: 0,24 ± 0,05 vs. 0,26 ± 0,01, $p = 0,647$). Das TSPO-PET-Signal der PS2APP-Tiere unter Pioglitazon-Behandlung wies im Verlauf von 9,5 (13 % Abnahme, $p = 0,0027$), 11,5 (17 % Abnahme, $p = 0,0046$) und 13 (13 % Abnahme, $p = 0,0071$) Monaten ein abgeschwächtes TSPO-PET-Signal auf, wohingegen das TSPO-PET-Signal der altersgleichen Vehikel-Gruppe kontinuierlich stieg (**Abb. 1**).

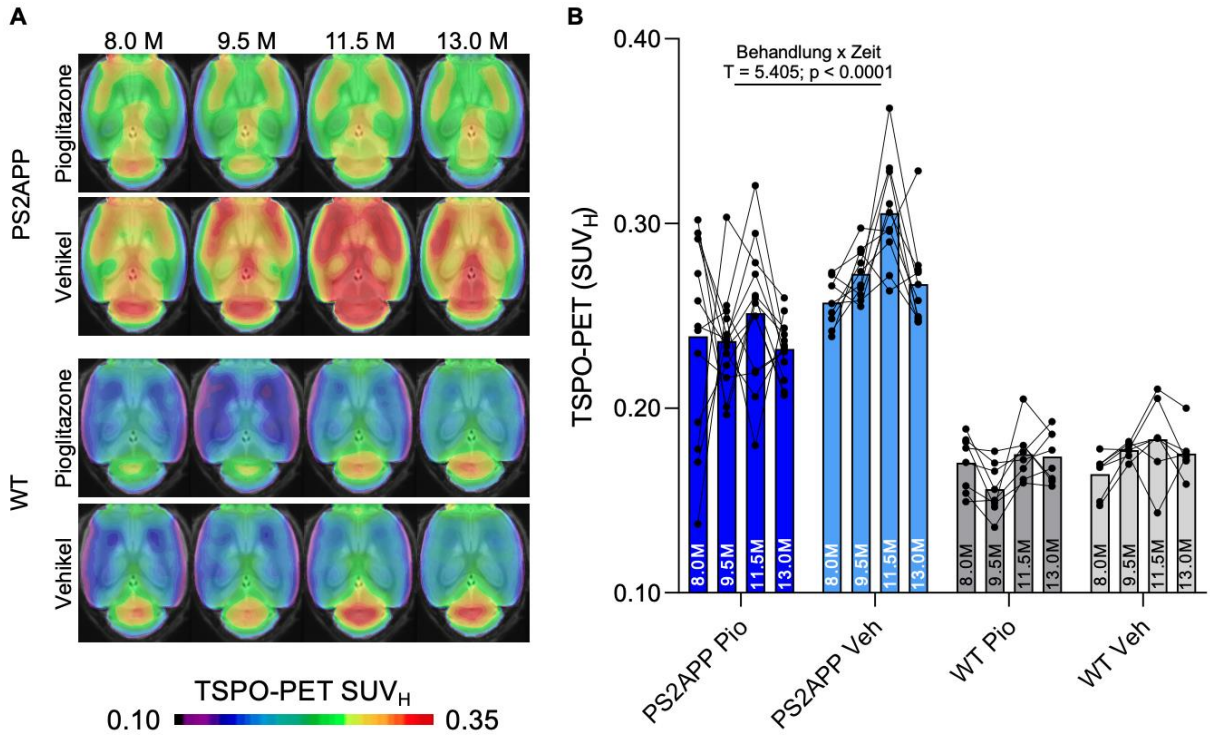

Abbildung 1: TSPO-PET-Monitoring von PS2APP- und Wildtyp-Mäusen (WT) während einer chronischen Therapie mit Pioglitazone. **A** In Projektion auf eine anatomische Standard-MRT-Aufnahme zeigen axiale Aufnahmen die Gruppenmittelwerte des [^{18}F]GE-180 TSPO-PET-Signals

(myocardium scaled standardized uptake value, SUV_H) zu verschiedenen Zeitpunkten in der Behandlungs- und Vehikelgruppe. Zum Zeitpunkt der Baseline-Scans waren alle Tiere therapienaiv. **B** Darstellung des kortikalen TSPO-PET-Signals als individueller Verlauf während der Beobachtungsperiode. Pio = Pioglitazone-Behandlung, Veh = Vehikel-Behandlung. Die Statistik basiert auf einem linear mixed model. PS2APP Pioglitazone n = 13, PS2APP Vehikel n = 10, WT Pioglitazone n = 8, WT Vehikel n = 7.

In einer unserer vorherigen Arbeiten zeigte sich, dass das Geschlecht der Mäuse einen Einfluss auf die zerebrale TSPO-Expression hat (Biechele, Franzmeier et al. 2020). Deshalb untersuchten wir den Einfluss des Geschlechts auf die PPARγ-induzierten Veränderungen. Zu diesem Zweck wurden altersgleiche weibliche und männliche *App*$^{NL\text{-}G\text{-}F}$-Mäuse longitudinalen TSPO- und Aβ-Scans während einer chronischen Pioglitazone-Behandlung unterzogen. Vehikel-behandelte, weibliche *App*$^{NL\text{-}G\text{-}F}$-Mäuse zeigten, verglichen mit den männlichen Tieren, im Alter von 7,5 (18 % Zunahme, p = 0,017) und 10 Monaten (25 % Zunahme, p = 0,0007) einen geschlechtsspezifischen Anstieg des TSPO-PET-Signals. Weibliche *App*$^{NL\text{-}G\text{-}F}$-Tiere unter Pioglitazone-Behandlung wiesen im Alter von 7,5 (15 % verringert, p = 0,030) und 10 Monaten (21 % verringert, p = 0,0053) einen geringeren Anstieg des TSPO-PET-Signals auf, als weibliche *App*$^{NL\text{-}G\text{-}F}$-Tiere unter Vehikel-Behandlung (**Abb. 2**). Männliche *App*$^{NL\text{-}G\text{-}F}$-Mäuse unter Pioglitazone-Behandlung zeigten eine Tendenz zu einem erhöhten Anstieg des TSPO-PET-Signal im Alter von 5 bis 10 Monaten im Vergleich zur transgenen Vehikel-Gruppe, welcher allerdings keine Signifikanz erreichte. Eine chronische PPARγ-Stimulation moduliert die Mikrogliaaktivierung folglich geschlechtsabhängig, aber unabhängig von dem Vorhandensein einer APP-Überexpression.

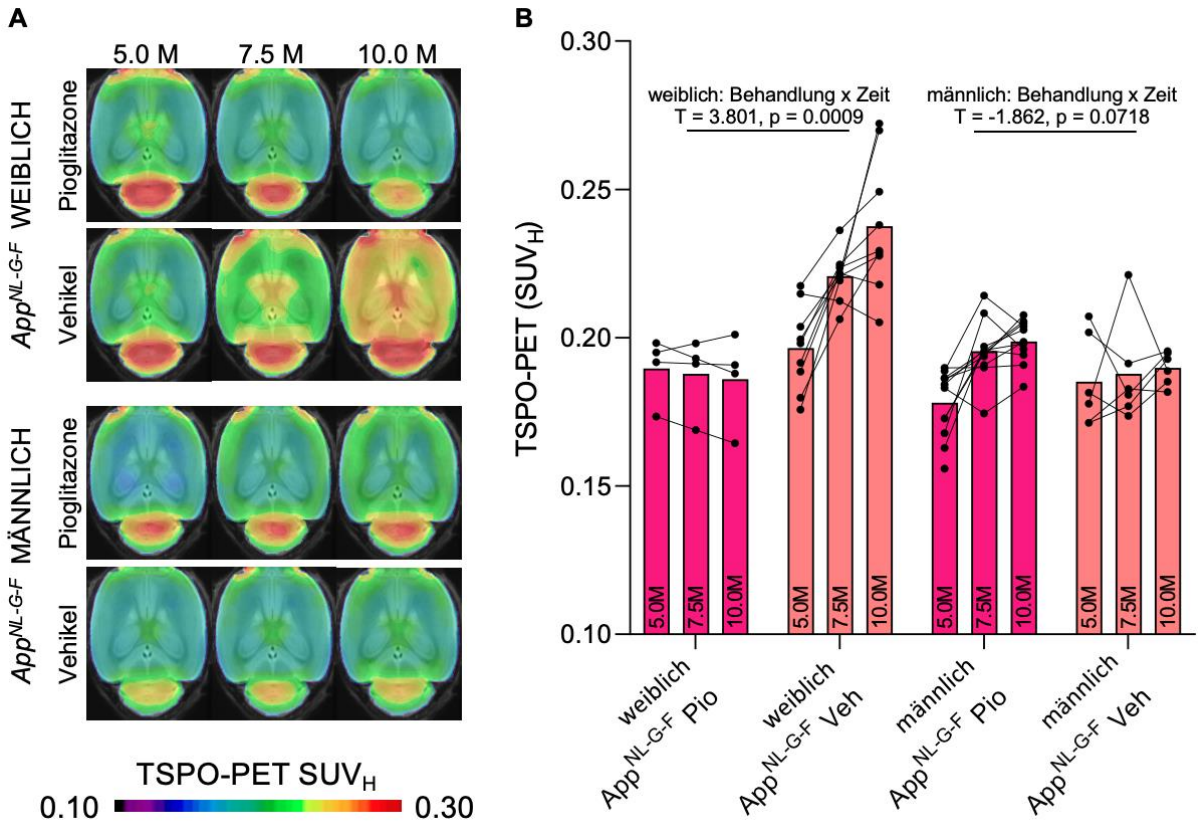

Abbildung 2: Analog zu Abbildung 1 TSPO-PET Monitoring weiblicher und männlicher *App*$^{NL\text{-}G\text{-}F}$-Mäusen mit und ohne chronische Pioglitazone-Behandlung. **A** Projiziert auf eine Standard-MRT-Vorlage zeigen axiale Bilder Gruppenmittelwerte des [^{18}F]GE-180 TSPO-PET-Signals (myocardium scaled standardized uptake value, SUV_H) zu verschiedenen Zeitpunkten mit (Pio) und ohne (Veh) immunmodulatorische Behandlung. Die Baseline-Scans fanden vor Therapieinitiation statt. **B** Individuelle Verläufe des kortikalen TSPO-PET-Signals während der pharmakologischen Behandlungsperiode. Die Statistik basiert auf einem linear mixed model. Pio = Pioglitazone Behandlung, Veh = Vehikel Behandlung. Weibliche *App*$^{NL\text{-}G\text{-}F}$ Pioglitazone n = 4, weibliche *App*$^{NL\text{-}G\text{-}F}$ Vehikel n = 9, männliche *App*$^{NL\text{-}G\text{-}F}$ Pioglitazone n = 11, männliche *App*$^{NL\text{-}G\text{-}F}$ Vehikel n = 6.

Die Gruppe der Wildtyp-Tiere ergab keinen Unterschied zwischen Behandlung und Vehikel. Außerdem bestanden keine Unterschiede zwischen den Ausgangswerten des Aβ-PET-Signals (**Abb. 3 A**) und den Aβ-PET-Veränderungsraten über die Zeit (**Abb. 3 B**) zwischen den Geschlechtern der therapienaiven *App*$^{NL\text{-}G\text{-}F}$-Mäuse.

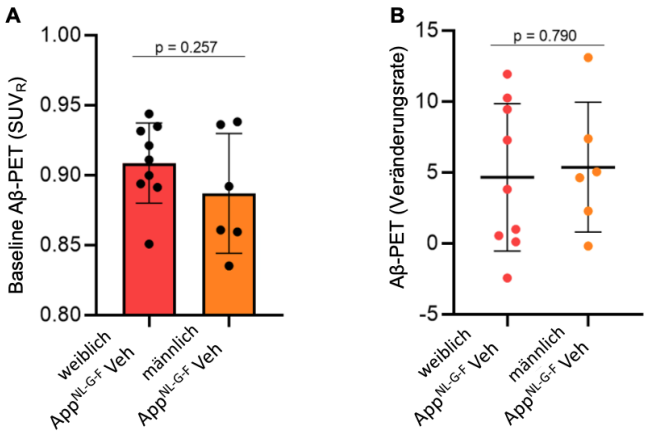

Abbildung 3: **A** Quantifizierung der Baseline SUV_R (standardized uptake value ratio) der [^{18}F]florbetaben Aβ-PET therapienaiver *App*$^{NL-G-F}$-Mäuse beider Geschlechter. **B** Vergleiche der Veränderungsrate des [^{18}F]florbetaben Aβ-PET zwischen Beginn und Ende der Beobachtungsperiode bei therapienaiven *App*$^{NL-G-F}$-Mäusen beider Geschlechter. Die p-Werte basieren auf einem ungepaarten t-Test. Veh = Vehikel Behandlung. Weibliche *App*$^{NL-G-F}$ n = 9, männliche *App*$^{NL-G-F}$ n = 6.

Darüber hinaus fiel ein starker indirekter Zusammenhang zwischen der TSPO-PET Quantifizierung zur Baseline und den darauffolgenden Veränderungen des TSPO-PET-Signals bei Pioglitazone-behandelten Tieren auf (R = -0,874; p < 0,001, **Abb. 4 A – B**). Dies spricht dafür, dass Mäuse mit hoher Mikrogliaaktivierung vor Therapiebeginn stärker auf die PPARγ-Stimulation ansprechen. Dieser nennenswerte Zusammenhang war auch bei separater Betrachtung der Kohorten von PS2APP- (R = -0,964; p < 0,0001) und *App*$^{NL-G-F}$-Mäusen (R = -0,68; p = 0,0053) mit chronischer Pioglitazone-Behandlung nachweisbar. Der oben genannte Effekt konnte in allen Hirnregionen beobachtet werden, wobei die Unterschiede zwischen Pioglitazone- und Vehikel-behandelten Mäusen in neokortikalen Arealen, Hippocampus, Striatum und Thalamus am stärksten ausgeprägt waren (**Abb. 4 C – D, Tabelle 1**). Auch in der Vehikel-Kohorte war das TSPO-PET-Signal zur Baseline in mehreren subkortikalen Regionen signifikant negativ mit Veränderungen der Mikrogliaaktivierung assoziiert (**Tabelle 1**). Diese Beobachtung stützt die Annahme,

dass Mikrogliaaktivierung zu frühen Zeitpunkten per se eine Vorhersage für den longitudinalen Verlauf und die räumliche Lernleistung treffen kann (Blume, Focke et al. 2018, Focke, Blume et al. 2019).

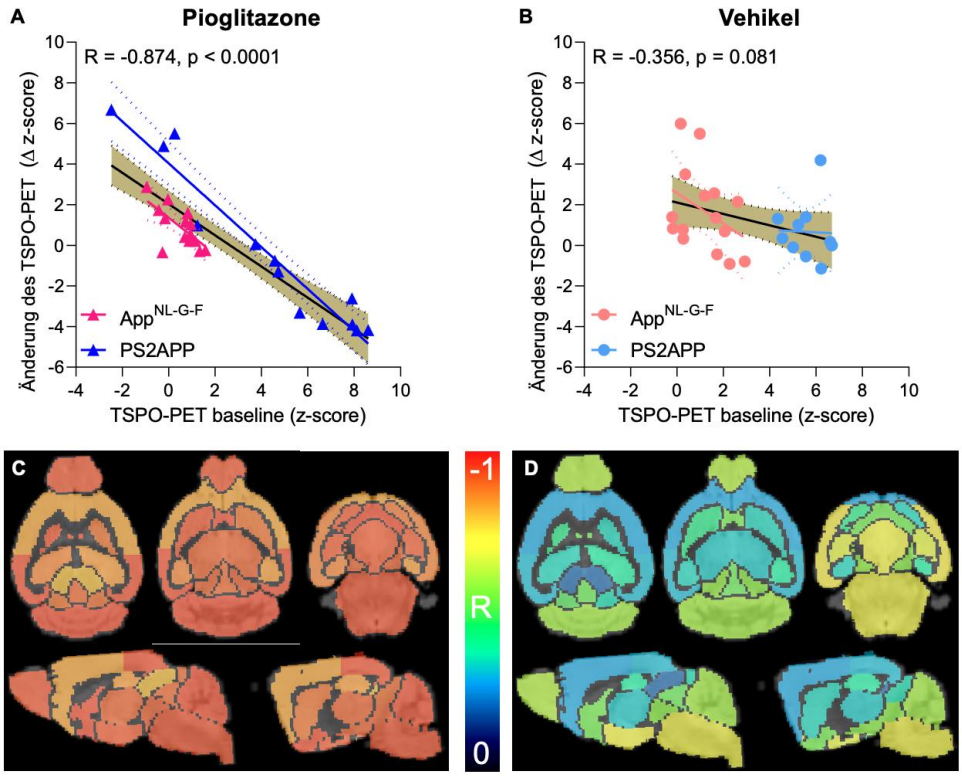

Abbildung 4: Veränderungsvorhersage der Mikrogliaaktivität anhand der initialen [^{18}F]GE-180 TSPO-PET Untersuchung. **A – B** Korrelationsanalyse zwischen den Baseline TSPO-PET Z-Scores und den Differenzen der TSPO-PET Z-Scores zwischen Studienbeginn und Studienende bei *App*$^{NL-G-F}$- und PS2APP-Mäusen mit **(A)** und ohne **(B)** Pioglitazone-Behandlung. Gold: Kombination beider Mausmodelle, Rot: *App*$^{NL-G-F}$, Blau: PS2APP

(**C – D**) Multiregionale Korrelationsanalyse zwischen dem TSPO-PET Z-Score zu Studienbeginn und der Differenz der Z-Scores zwischen Baseline- und Abschlussuntersuchung. Die Korrelationskoeffizienten projizieren sich farblich graduiert auf axiale und sagittale Schichten einer Standard-MRT-Aufnahme. Für die Pioglitazone- **(C)** und Vehikel-Behandlungsgruppe (**D**) wurden *App*$^{NL-G-F}$- und PS2APP-Mäuse gemeinsam analysiert.

Tabelle 1: Multiregionale Analyse der Veränderungsvorhersage der Mikrogliaaktivierung anhand des initialen, therapienaiven [^{18}F]GE-180 TSPO-PET.

Berechnung der Pearson Korrelationskoeffizienten (R) zwischen anfänglichen TSPO-PET Z-Scores und der Entwicklung des TSPO-PET (Δ Z-Score) während des fünfmonatigen Behandlungszeitraums beider Mauslinien. *p < 0,05; **p < 0,01; ***p < 0,001.

Region	Pioglitazone		Vehikel		Differenz
	R	p-Wert (FDR-korrigiert)	R	p-Wert (FDR-korrigiert)	ΔR
Striatum R	-0,941	4,9E-13***	-0,427	0,12	0,514
Striatum L	-0,899	1,0E-10***	-0,342	0,12	0,557
Hippocampus R	-0,879	8,6E-10***	-0,344	0,12	0,535
Hippocampus L	-0,854	8,6E-09***	-0,388	0,083	0,466
Thalamus	-0,920	7,8E-12***	-0,326	0,13	0,594
Zerebellum	-0,952	1,4E-13***	-0,584	0,0066**	0,368
Basales Vorderhirn & Septum	-0,949	1,4E-13***	-0,516	0,017*	0,433
Hypothalamus	-0,936	8,6E-13***	-0,705	0,0009***	0,231
Amygdala R	-0,935	8,6E-13***	-0,665	0,0012**	0,270
Amygdala L	-0,935	9,0E-13***	-0,666	0,0015**	0,269
Hirnstamm	-0,943	1,4E-12***	-0,691	0,0009***	0,252
Zentrales Grau	-0,914	1,8E-11***	-0,505	0,019*	0,409
Colliculus superior	-0,804	2,6E-07***	-0,199	0,34	0,605
Bulbus olfactorius	-0,938	7,5E-13***	-0,603	0,0050**	0,335
Mittelhirn R	-0,919	9,5E-12***	-0,558	0,0099**	0,361
Mittelhirn L	-0,922	6,4E-12***	-0,541	0,012*	0,381
Colliculus inferior R	-0,900	3,0E-11***	-0,486	0,11	0,414
Colliculus inferior L	-0,910	9,7E-11***	-0,357	0,024*	0,553
Piriformer/entorhinaler Kortex	-0,883	6,2E-10***	-0,742	0,0005***	0,141
Auditorischer/visueller Kortex	-0,947	1,8E-13***	-0,306	0,15	0,641
Motorischer/sensorischer Kortex	-0,836	3,2E-08***	-0,283	0,18	0,553

Diese Erkenntnisse warfen die Frage auf, ob die chronische Pioglitazone-Behandlung auch Auswirkungen auf andere Determinanten der Alzheimer Krankheit hat. In einer Korrelationsanalyse der Änderungsrate des TSPO-PET-Signals mit individuellen Defiziten räumlichen Lernens zeigte sich in der PS2APP-Kohorte ein Zusammenhang zwischen besserer Lernperformance und vermindertem Anstieg des TSPO-PET Signals (R = -0,733; p = 0,0043, **Abb. 5 A – B**). Da in der Vehikel-

Kohorte der PS2APP-Mäuse keine Auswirkungen nachgewiesen werden konnten (R = -0,032; p = 0,991), erschien dieser Effekt behandlungsspezifisch (**Abb. 5 B**). In der *App*$^{NL\text{-}G\text{-}F}$-Kohorte konnte keine statistische Signifikanz erreicht werden (R = -0,349; p = 0,221, **Abb. 5 C – D**). Darüber hinaus konnte in beiden therapierten Mausmodellen eine stärkere Zunahme fibrillären Aβs, der Hauptquelle des Aβ-PET-Signals (Biechele, Monasor et al. 2022), nachgewiesen werden, was einem Shift hin zu zunehmend fibrillärer Beschaffenheit entspricht (**Abb. 5 E und G**). In den Pioglitazone-behandelten Kohorten bestand eine Assoziation zwischen niedriger Fläche unter der Kurve (AUC) des TSPO-PET-Signals und höherer Aβ-Veränderungsrate in PS2APP- (R = -0,600; p = 0,030, **Abb. 5 E – F**) und *App*$^{NL\text{-}G\text{-}F}$-Mäusen (R = -0,553; p = 0,040, **Abb. 5 G – H**). In den Vehikel-Kontrollen konnten keinerlei solcher Assoziationen beobachtet werden.

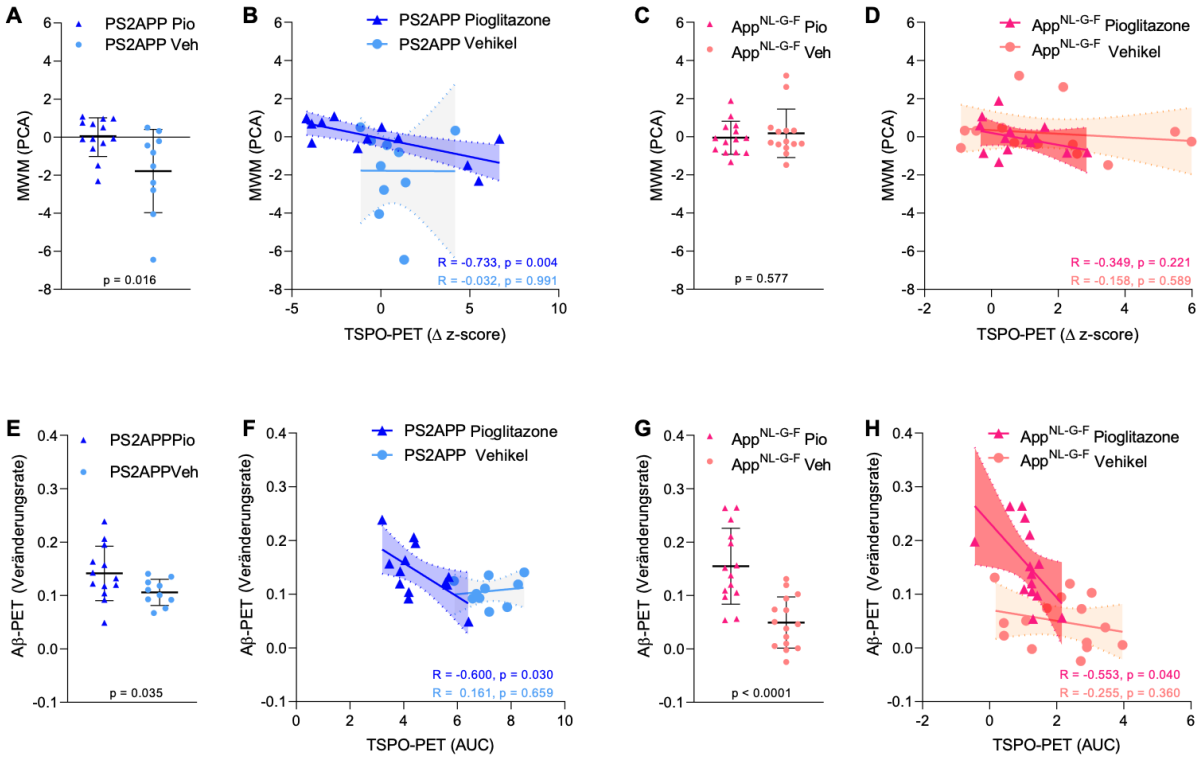

Abbildung 5: Korrelationen des [^{18}F]GE-180 TSPO-PET-Signals mit dem Leistungsindex im Wasserlabyrinth (je höher desto besser) und der Dynamik der Aβ-Akkumulation nach 5-monatiger

Pioglitazone- oder Vehikel-Behandlung. **A** Vergleich des Leistungsindex (PCA) (je höher desto besser) im Wasserlabyrinth (MWM) von Pioglitazone-behandelten PS2APP-Mäusen und ihren Vehikelkontrollen nach 5 Monaten. **B** Korrelation longitudinaler Veränderungen des TSPO-PET mit der räumlichen Lernleistung derselben Tiere. **C** Vergleich des Wasserlabyrinth-Leistungsindex von Pioglitazone behandelten *App*$^{NL\text{-}G\text{-}F}$-Mäusen und ihren Vehikelkontrollen nach 5 Monaten. **D** Korrelation longitudinaler Veränderungen des TSPO-PET mit der räumlichen Lernleistung derselben Tiere. **E** Vergleich der [^{18}F]florbetaben Aβ-PET-Veränderungsrate (Δ SUV_R) Pioglitazone-behandelter PS2APP-Mäuse und deren Vehikelkontrollen. **F** Korrelation der TSPO-PET- und Aβ-PET-Veränderungsrate behandelter (Pio) und unbehandelter (Veh) PS2APP-Tiere.
G Vergleich der [^{18}F]florbetaben Aβ-PET-Veränderungsrate (Δ SUV_R) Pioglitazone-behandelter *App*$^{NL\text{-}G\text{-}F}$-Mäuse und deren Vehikelkontrollen. **H** Korrelation der TSPO-PET- und Aβ-PET-Veränderungsrate behandelter (Pio) und unbehandelter (Veh) *App*$^{NL\text{-}G\text{-}F}$-Tiere. AUC = Fläche unter der Kurve.

Dennoch bleiben die molekularen und zellulären Korrelate während der pharmakologischen Immunmodulation mit PPARγ-Agonisten in den bis hier beschriebenen Experimenten und Vorarbeiten ungeklärt (Brendel, Probst et al. 2016, Parhizkar, Arzberger et al. 2019). Unter Verwendung eines Antikörpers gegen einen allgemeinen Marker für Mikroglia (Iba-1) und einen spezifischen Marker für mikrogliale Aktivierung (CD68) validierten wir das [^{18}F]GE-180 TSPO-PET-Signal in Subpopulationen aller Studiengruppen via (Immun-)Histochemie. Die Ergebnisse der Iba-1 Färbung ($R = 0{,}790$; $p < 0{,}0001$, **Abb. 6 A**) und der CD68 Färbung ($R = 0{,}952$; $p < 0{,}0001$, **Abb. 6 B**) korrelierten auf hohem Niveau mit der TSPO-Bindung in der PET. Dabei war ein stärkerer Zusammenhang zwischen der [^{18}F]GE-180 TSPO-PET und der CD68 Färbung festzustellen, als zwischen der [^{18}F]GE-180 TSPO-PET und der Iba-1 Färbung. Eine eingeschränkte Differenzierbarkeit der Iba-1-Immunhistochemie bei behandelten Tieren ist als Ursache denkbar, da diese nicht in der Lage war, zwischen behandelten und unbehandelten Mäusen beider Kohorten zu unterscheiden, was auch auf Einzeltierebene zu erkennen war (**Abb. 6 C**).

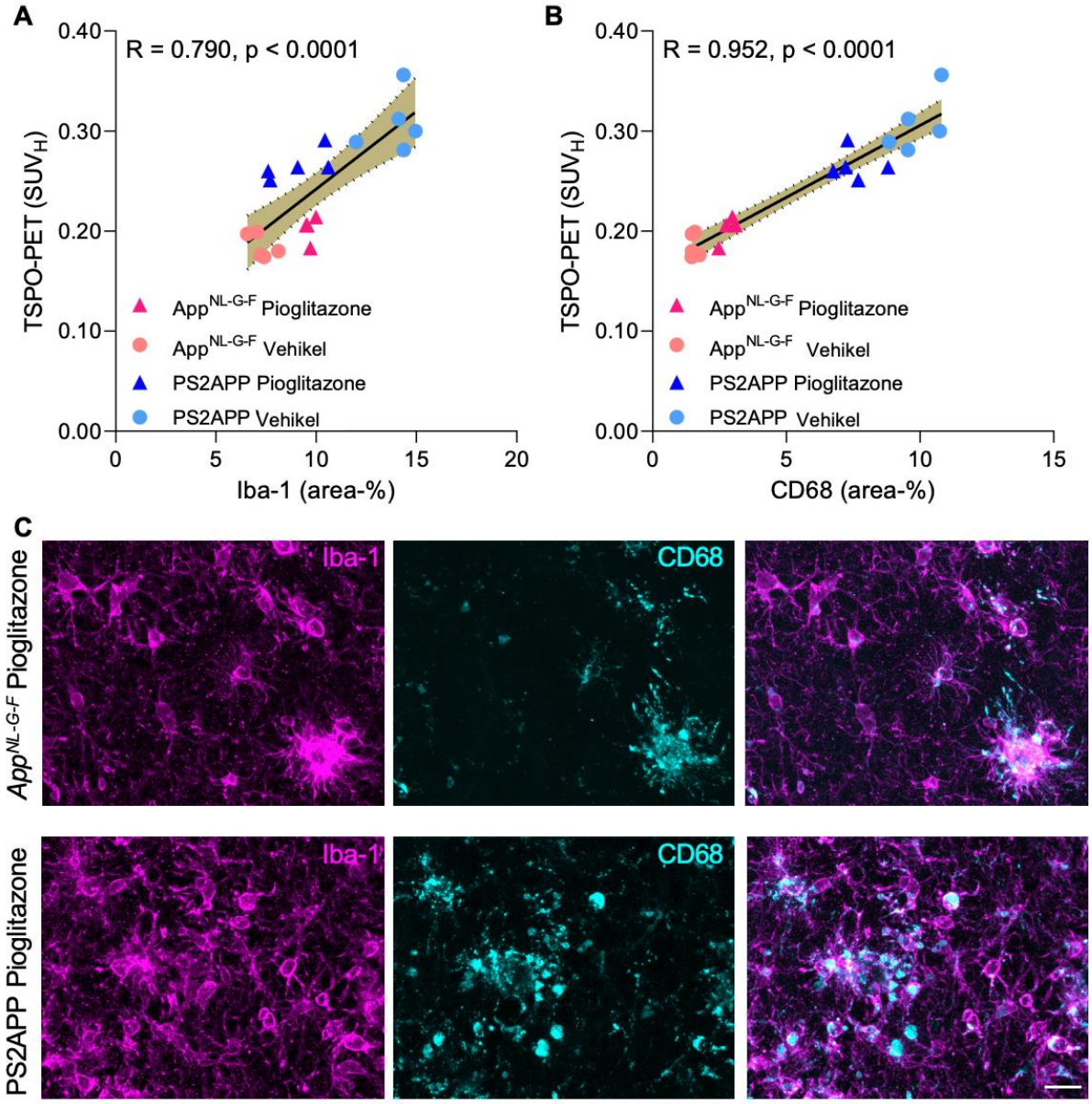

Abbildung 6: **A – B** Korrelationsanalyse der Immunhistochemie mit der finalen [^{18}F]GE-180 TSPO-PET nach Myokardkorrektur (SUV_H). *App*$^{NL-G-F}$ Pioglitazone n = 4, *App*$^{NL-G-F}$ Vehikel n = 5, PS2APP Pioglitazone n = 5, PS2APP Vehikel n = 5. Die goldenen Bänder repräsentieren die 95%-Konfidenzintervalle. **C** Individuelle Aufnahmen der immunhistochemischen Färbung von behandelten *App*$^{NL-G-F}$- und PS2APP-Mäusen. Ersichtlich wird eine ähnliche Iba-1 Flächenfärbung zwischen beiden behandelten Mausmodellen bei höherer CD68 Flächenfärbung der PS2APP-Mäuse, passend zum erhöhten TSPO-PET-Signal (siehe **A – B**). Gefärbte Mikroglia mit Iba-1 (violett), gefärbte mikrogliale Aktivierung mit CD68 (blau), Überlagerung von Iba-1 und CD68 (rechts). Maßstabsbalken = 20 µm.

Im Zuge meiner Erstautorschaft „*Pre-therapeutic microglia activation and sex determine therapy effects of chronic immunomodulation*“ konnten die genannten Erkenntnisse im August 2021 in „*Theranostics*“ publiziert werden.

2.2. Chronische PPARγ-Stimulation führt zu kompakteren Amyloid Plaques und verbessertem räumlichen Lernen

Der oben genannte experimenteller Aufbau inkludierte auch die Messung der fibrillären zerebralen Amyloidose durch [^{18}F]florbetaben Aβ-PET-Aufnahmen. Diese wurden in den gleichen Individuen der PS2APP- und *App*$^{NL\text{-}G\text{-}F}$-Kohorten mit und ohne Pioglitazone-Behandlung, sowie altersgleichen Wildtypen durchgeführt (s.o.). Da die Dynamik der Mikrogliaaktivität unter der verabreichten, chronisch immunmodulatorischen Therapie mit Veränderungen der Aβ-Last und -Zusammensetzung und veränderter kognitiver Performance einherging, wurde dieser Sachverhalt genauer evaluiert. Dazu erfolgte eine erweiterte Immunfluoreszenz- und histologische Untersuchung der konservierten Hemisphären, wie bereits beschrieben (Dorostkar, Dreosti et al. 2010, Brendel, Focke et al. 2017, Brendel, Kleinberger et al. 2017). Nach der Vorbereitung der Schnitte erfolgte die Immunfluoreszenzmarkierung von prä-fibrillärem Aβ mittels NAB228 (Thermo Fisher Scientific, USA). Fibrilläres Aβ wurde mit Methoxy-X04 (TOCRIS, Bristol, Vereinigtes Königreich) histologisch gefärbt. Zudem konnte die synaptische Dichte durch Färbung des vesikulären Glutamattransporter 1 (VGLUT1) im Hippocampus visualisiert werden.

Bei Vehikel-behandelten PS2APP-Mäusen konnte im Beobachtungszeitraum ein Anstieg der fibrillären Amyloidose durch das Aβ-PET beobachtet werden. Bei Pioglitazone-behandelten PS2APP-Mäusen fiel dieser Aβ-PET-Anstieg erstaunlicherweise signifikant stärker aus (+21.4%), als in der Vehikel-Gruppe (+14,1%, p = 0,002), was auf eine Steigerung der fibrillären Aβ-Levels unter PPARγ-Stimulation hindeutete (**Abb. 7**). Das Aβ-PET Signal der Wildtyp-Tiere hingegen blieb sowohl mit der Zeit, als auch als Reaktion auf die Behandlung wie erwartet unverändert (**Abb. 7 B**).

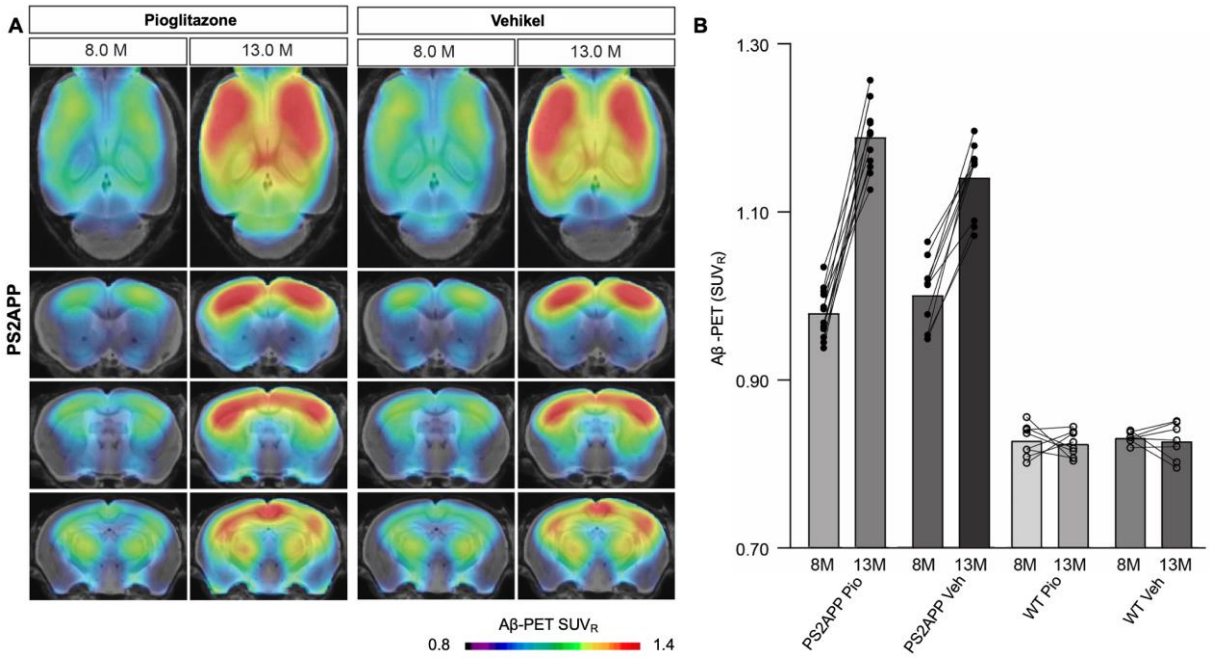

Abbildung 7: **A** Koronare und axiale Bilder gruppengemittelter SUV_R der [^{18}F]florbetaben Aβ-PET-Aufnahmen zum Beginn- und Endzeitpunkt der Beobachtungsperiode, projiziert auf eine Standard-MRT-Aufnahme. Dargestellt ist die PS2APP-Mauslinie mit und ohne Pioglitazone-Behandlung. **B** Individuelle Verläufe des standardisierten kortikalen [^{18}F]florbetaben Aβ-PET-Signals (SUV_R) von PS2APP- und Wildtyp-Tieren mit und ohne Pioglitazone-Behandlung im fünfmonatigen Intervall. PS2APP Pioglitazone n = 13, PS2APP Vehikel n = 10, WT Pioglitazone n = 8, WT Vehikel n = 7.

Analog konnte diese Beobachtung im *App*$^{NL-G-F}$-Mausmodell mit endogener APP-Expression und mehr „baumwollartiger“, weniger fibrillärer Plaque-Zusammensetzung (Sebastian Monasor, Muller et al. 2020) bestätigt werden. Bei gleichen Ausgangswerten zeigten die *App*$^{NL-G-F}$-Mäuse im Vergleich zum Vehikel (+5,3%) einen noch steileren Anstieg des Aβ-PET-Signals (+17,2%, $p < 0{,}0001$) nach fünfmonatiger Pioglitazone-Behandlungsperiode, als die PS2APP-Tiere (**Abb. 8 A**).

In beiden Mausmodellen wiesen der fronto-temporale Kortex und der Hippocampus die ausgeprägteste Dynamik auf (**Abb. 7A und 8A**).

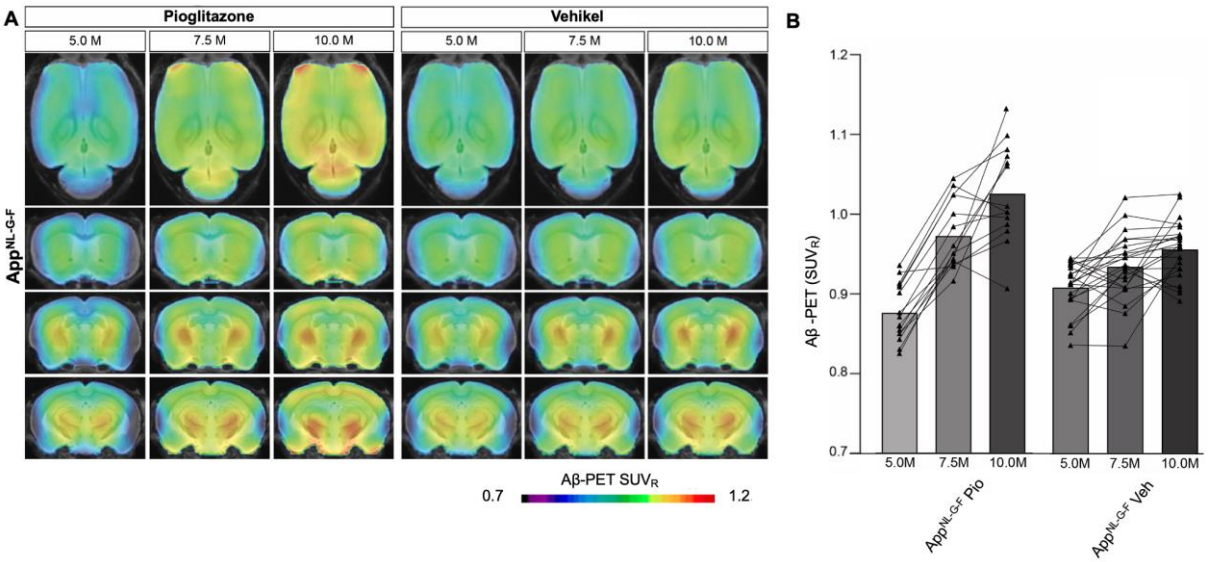

Abbildung 8: **A** Koronare und axiale Bilder gruppengemittelter SUV_R der [^{18}F]florbetaben Aβ-PET-Aufnahmen zum Beginn-, Mittel- und Endzeitpunkt der Beobachtungsperiode, projiziert auf eine Standard-MRT-Aufnahme. Dargestellt ist die *App*$^{NL-G-F}$-Mauslinie mit und ohne Pioglitazone-Behandlung. **B** Individuelle Verläufe des standardisierten kortikalen [^{18}F]florbetaben Aβ-PET-Signals von *App*$^{NL-G-F}$-Tieren mit und ohne Pioglitazone-Behandlung im fünfmonatigen Intervall. *App*$^{NL-G-F}$ Pioglitazone n = 15, *App*$^{NL-G-F}$ Vehikel n = 15.

Als Ursache konnten Veränderung der Plaque-Zusammensetzung und nicht eine Veränderung der Plaque-Dichte identifiziert werden. Beide Mauslinien verzeichneten einen signifikanten Anstieg des mit Methoxy-X04 gefärbten, fibrillären Aβs unter Pioglitazone-Behandlung im Vergleich zu den mit Vehikel behandelten Tieren (PS2APP: 29,6 ± 3,5% vs. 15,2 ± 0,7%, p = 0,0056; *App*$^{NL-G-F}$: 9,1 ± 1,6% vs. 4,4 ± 0,4%, p = 0,0001). Während aber bei PS2APP-Mäusen kein therapeutischer Effekt in der NAB2228-Färbung des prä-fibrillären Aβ-Anteils ersichtlich war, verzeichneten *App*$^{NL-G-F}$-Mäuse einen signifikanten Abfall bei behandelten Tieren (26.7 ± 1.7% vs. 34.5 ± 1.7%, p = 0.0138; **Abb. 9 A – B**). Bei natürlicherweise diffusem Plaquecharakter mit hoher prä-fibrillärer und niedriger fibrillärer Aβ-Fraktion der *App*$^{NL-G-F}$-Mäuse (Sebastian Monasor, Muller et al. 2020) spiegelt sich dies in mehr

Überlagerungszunahme von Methoxy-X04- und NAB228-positiven Plaques von unbehandelt zu behandelt im Vergleich zu PS2APP-Mäusen wider (PS2APP: 25.1 ± 2.1% vs. 40.4 ± 3.6%, p = 0.0075, **Abb. 9A**; *App*$^{NL-G-F}$: 12.9 ± 1.3% vs. 35.0 ± 3.4%, p = 0.0005; **Abb. 9B**).

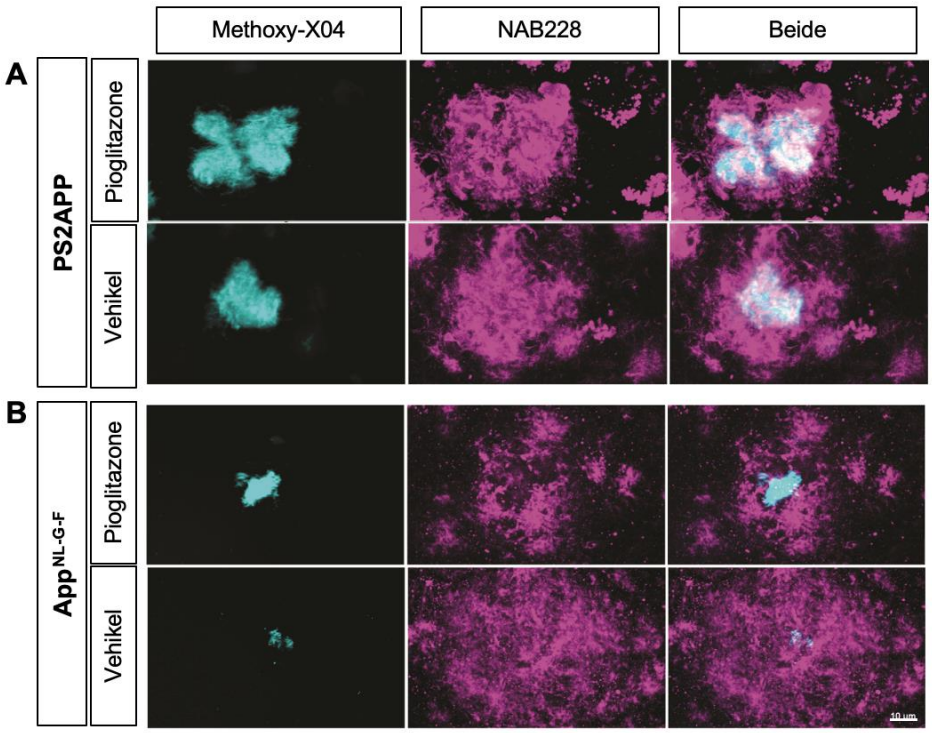

Abbildung 9: Veränderung der Plaque-Zusammensetzung bei chronischer Immunmodulation: Methoxy-X04 (blau) gefärbtes, fibrilläres Aβ und NAB228 (violett) gefärbtes, prä-fibrilläres Aβ in Pioglitazone- und Vehikel-behandelten PS2APP-Mäusen (**A**) und *App*$^{NL-G-F}$-Mäusen (**B**). Überlagerung der Methoxy-X04- und NAB228-Färbung (rechts). Maßstabsbalken = 10 µm.

Die kognitive Lernleistung im Wasserlabyrinth korrelierte bei Pioglitazone-behandelten PS2APP-Mäusen mit der Zunahme des Aβ-PET-Signals (R = 0,686; p = 0,0097) (**Abb. 10 A**). Pioglitazone behandelte PS2APP-Tiere zeigten einen signifikant verbesserten Leistungsindex im Wasserlabyrinth. Im Vergleich zur Vehikel-Gruppe mussten behandelte Tiere weniger Strecke zurücklegen, um ihr Ziel zu finden. Die räumliche Lernleistung von *App*$^{NL-G-F}$-Mäusen wurde therapeutisch

nicht beeinflusst (**Abb. 10 B**). Die Wildtypen unterschieden sich hinsichtlich ihrer Therapiegruppe nicht.

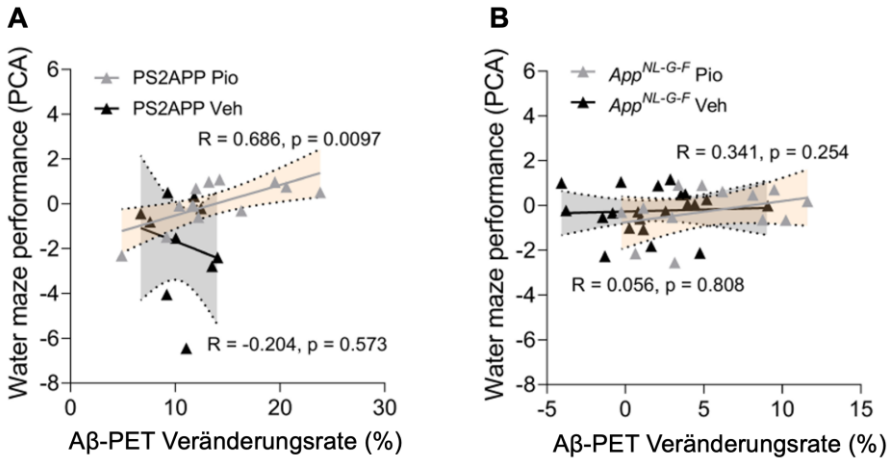

Abbildung 10: Korrelation zwischen der Aβ-PET-Veränderungsrate des [^{18}F]florbetaben Aβ-PET-Signals zwischen Beginn und Ende der 5-monatigen Beobachtungsperiode und der räumlichen Lernperformance im Wasserlabyrinth (**A**) behandelter und unbehandelter individueller PS2APP-Tiere bzw. (**B**) behandelter und unbehandelter individueller *App*$^{NL-G-F}$-Tiere. Je höher der PCA, desto besser die Leistung im Wasserlabyrinth.

Die molekulare Korrelation dieses Effektes entsprach wiederhergestellter synaptischer Plastizität im präsynaptischen Cornu ammonis 1 (CA1) Bereich des Hippocampus bei Pioglitazone-behandelten PS2APP-Mäusen. Gemessen wurde die synaptische Dichte mittels VGLUT1-Färbung. Bei Wildtypen konnte keine therapiebezogene Änderung der Synapsendichte festgestellt werden (**Abb. 11**). Diese Beobachtungen bestätigen die Hippocampus-abhängigen verbesserten Leistungen der immunmodulierten PS2APP-Mäuse im Wasserlabyrinth.

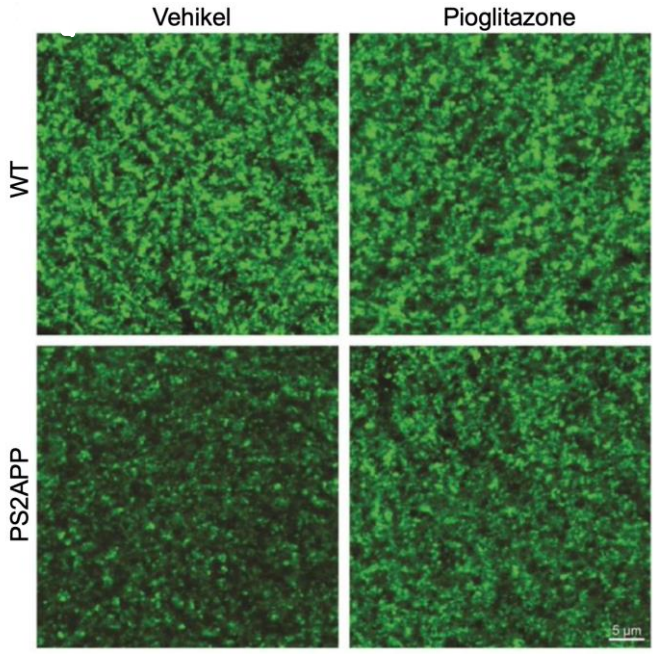

Abbildung 11: Färbung der synaptischen Dichte mittels VGLUT1 im hippocampalen CA1-Bereich. Abgebildet sind repräsentative unbehandelte und behandelte Wildtyp- (oben) sowie PS2APP-Individuen (unten). Maßstabsbalken = 5 µm

Im Rahmen meiner Koautorschaft „*Chronic PPARγ stimulation shifts amyloidosis to higher fibrillarity but improves cognition*" wurden diese Ergebnisse im März 2022 in „*Frontiers of Aging Neuroscience"* publiziert.

3. Zusammenfassung

Vielversprechende präklinische Studien konnten eine Verbesserung von Synapsendichte und kognitiven Leistungen nach immunmodulatorischen Therapien gegen die Alzheimer Krankheit zeigen. Im Rahmen dieser Arbeit sollten Therapieeffekte und Therapiemonitoring zweier Mausmodelle mit unterschiedlicher Plaque-Beschaffenheit überprüft werden. Das Ziel war die optimale Therapiezuordnung sowie die Bewertung des Ansprechens auf eine chronische PPARγ-Behandlung mittels [^{18}F]GE-180 18-kDa Translokatorprotein (TSPO)-PET.

23 PS2APP- und 15 Wildtyp-Mäuse durchliefen im Alter von 8,0, 9,5, 11,5 und 13 Monaten ein longitudinales Studiendesign mit [^{18}F]GE-180 TSPO-PET und [^{18}F]florbetaben Amyloid-PET. 33 *App*$^{NL-G-F}$-Mäuse durchliefen im Alter von 5,0, 7,5 und 10 Monaten dieselben Untersuchungen. Nach absolvierter Erstuntersuchung erhielten alle Tiere zufällig entweder das immunmodulatorische Therapiefutter Pioglitazone oder ein Vehikel-Kontrollfutter für die gesamte Studiendauer. Es wurden relative Standardaufnahmewerte (engl.: Standardized-Uptake-Value-Ratio, SUV_R) für die Aβ-PET mittels Pseudoreferenzregion und für die TSPO-PET mittels Myokardkorrektur (SUV_H) berechnet. Zuletzt fand eine kognitive Verhaltenstestung mittels Morris-Wasserlabyrinth und eine (immun)histochemische Validierung der in-vivo PET-Ergebnisse statt.

Die erste Arbeit konnte die Eignung der TSPO-PET zum Nachweis modifizierter Mikrogliaaktivierung bei chronischer PPARγ-Stimulation bestätigen. Behandelte PS2APP-Mäuse wiesen ein abgeschwächtes TSPO-PET-Signal auf (17 % Verringerung, $p = 0{,}0046$), während das TSPO-PET Signal der Vehikel-Gruppe kontinuierlich anstieg. Analog zu vorherigen Beobachtungen erwies sich das Geschlecht der Mäuse als starker Mediator der zerebralen TSPO-Expression. Pioglitazone-behandelte, weibliche *App*$^{NL-G-F}$-Tiere zeigten longitudinal eine

geringere Zunahme der mikroglialen Aktivierung in der TSPO-PET, als weibliche Vehikel-Kontrollen (21 % Verringerung, p = 0,0053), während behandelte männliche *App*$^{NL-G-F}$ -Tiere den gegenteiligen Effekt zeigten. Dabei wirkte sich neben dem Geschlecht auch das anfängliche TSPO-PET auf das Therapie-Ansprechen aus. In beiden Mausmodellen bestand ein stark negativer Zusammenhang zwischen der Baseline TSPO-PET und dessen darauffolgender Dynamik unter Pioglitazone-Behandlung (R = -0,874, p < 0,001), welcher in neokortikalen Arealen, Hippocampus, Striatum und Thalamus am stärksten ausgeprägt war. Immunmodulierte PS2APP-Tiere mit schwachem Anstieg des TSPO-PET-Signals zeigten zudem eine bessere räumliche Lernleistung (R = -0,733, p = 0,0043), als nicht-therapierte PS2APP-Tiere. Unsere Daten zeigen klar, dass weibliche Mäuse mit hoher Inflammation vor Therapiebeginn am meisten von der immunmodulatorischen Therapie profitieren. Das Geschlecht könnte gemeinsam mit der quantitativen molekularen TSPO-PET Bildgebung zur Responder Stratifizierung dienen und so einen Schritt hin zu personalisierter Medizin auf dem individuellen Patientenlevel ermöglichen. In der immunhistochemischen post-mortem Validierung der in vivo PET-Ergebnisse korrelierte die Färbung mittels mikroglialer Antikörper stark mit den TSPO-PET Ergebnissen und bestätigte somit die Affinität zu den gleichen molekularen Quellen.

Die zweite Arbeit legte ihr Augenmerk auf die Quantifizierung der fibrillären zerebralen Amyloidose unter chronischer Immunmodulation mittels [^{18}F]florbetaben Aβ-PET-Aufnahmen und (immun)histochemischen Analysen. In beiden Mausmodellen war therapieunabhängig ein Anstieg der fibrillären Amyloidose durch das Aβ-PET-Signal zu verzeichnen. In Pioglitazone-behandelten PS2APP-Mäusen (+21.4%) sowie *App*$^{NL-G-F}$-Mäusen (+17.2%) fiel diese Zunahme signifikant stärker aus, als in den Vehikel-Behandlungsgruppen (+14.1%, p=0.002 vs. +5.3%, p<0.0001). Ursächlich für die Unterschiede in der PET Bildgebung waren

Veränderungen der Plaque-Zusammensetzung hin zu höherer Fibrillarität, deren Nachweis mit Färbungen von präfibrillärem Aβ mittels NAB228 und von fibrillärem Aβ mittels Methoxy-X04 gelang. Überraschenderweise konnte ein Zusammenhang zwischen verbesserter räumlicher Lernleistung und Zunahme des Aβ-PET-Signals bei immunmodulierten PS2APP-Mäusen hergestellt werden ($R = 0,686$; $p = 0,0097$). Durch Färbung des vesikulären Glutamattransporters 1 wurde als molekulares Korrelat eine Wiederherstellung der dendritischen Synapsendichte im hippocampalen Cornu ammonis 1 unter Pioglitazone-Behandlung in PS2APP-Mäusen festgestellt. Diese translationalen Daten legen nahe, dass eine Verschiebung hin zu höherer Plaque-Fibrillarität die kognitive Funktion und die Integrität des Gehirns schützt. Entgegen der Erwartungen kann eine Zunahme des Aβ-PET-Signals bei immunmodulatorischen Behandlungen daher protektiv wirken.

4. Summary

Promising preclinical studies showed a rescue of spine density and cognitive performance after immunomodulatory therapies in Alzheimer's disease. Subject of this thesis was testing PET monitoring of an immunomodulatory therapy on two mouse models with different plaque characteristics. The general aim was to determine the optimal therapy allocation as well as the evaluation of response to a chronic PPARγ treatment using [^{18}F]GE-180 18-kDa translocator protein (TSPO)-PET.

23 PS2APP and 15 wild-type mice underwent a longitudinal study design with [^{18}F]-GE-180 TSPO-PET and [^{18}F]florbetaben amyloid PET at 8.0, 9.5, 11.5, and 13 months of age. 33 *App*$^{NL-G-F}$ mice underwent the same examinations at 5.0, 7.5, and 10 months of age. After the initial examination, all animals were randomized to either chronic immunomodulatory treatment with Pioglitazone (via chow) or to vehicle group until final examination. Relative standardized uptake value ratios (SUV_R) were calculated for Aβ-PET using pseudoreference regions and for TSPO-PET, a myocardial correction method was applied for quantification (SUV_H). Cognitive behavioral testing using Morris Water Maze and immunohistochemical validation of in vivo PET results pursued the final PET session.

The first paper confirmed suitability of TSPO-PET for detecting modified microglial activation during chronic PPARγ-stimulation. Treated PS2APP mice exhibited a decreased TSPO-PET signal (17% attenuation, $p = 0.0046$), while that of the vehicle group increased continuously. Analogous to previous observations, the sex of mice proved to be a strong mediator of cerebral TSPO expression. Via Pioglitazone immunomodulated female *App*$^{NL-G-F}$ animals recorded less increase of microglial activation measured by TSPO-PET, than vehicle controls did (21% attenuation, $p = 0.0053$), whereas treated male *App*$^{NL-G-F}$ animals showed an increase compared to

their vehicle littermates. In addition, therapy naive TSPO-PET anticipated treatment response. In both mouse models, the correlation between initial TSPO-PET and its dynamics during treatment period with pioglitazone was distinctly negative ($R = -0.874$, $p < 0.001$). Immunomodulated PS2APP animals with attenuated increase of TSPO-PET levels also showed better spatial learning performance ($R = -0.733$, $p = 0.0043$), than vehicle controls. Our data clearly showed, that female mice with high inflammation prior to therapy initiation benefit most from an immunomodulatory PPARγ targeting therapy. Sex, together with molecular imaging measures in the context of TSPO-PET quantification, can be used for responder stratification, providing a step towards personalized medicine at the individual patient level. In post-mortem (immuno)histochemical validation of in vivo PET results, microglial antibody binding strongly correlated with TSPO binding, confirming affinity to identical molecular sources.

The second work focused on quantification of cerebral fibrillar amyloidosis by [^{18}F]florbetaben Aβ-PET imaging and (immuno)histochemical analyses under chronic immunomodulatory therapy in PS2APP- and *App*$^{NL\text{-}G\text{-}F}$ mice.

In both mouse models, there was a therapy-independent increase in fibrillar amyloidosis measured by Aβ-PET. The observed increase was stronger in PS2APP (+21.4%) as well as *App*$^{NL\text{-}G\text{-}F}$ animals (+17.2%) after immunomodulatory pioglitazone treatment, compared to vehicle treatment groups (+14.1%, $p=0.002$ vs. +5.3%, $p<0.0001$). This effect was pinpointed to changes in plaque composition towards higher fibrillarity, detected by prefibrillary Aβ stain with NAB228 and fibrillar Aβ stain with Methoxy-X04. Surprisingly, a correlation between improved spatial learning performance and the Aβ-PET signal increase in immunomodulated PS2APP mice ($R = 0.686$; $p = 0.0097$) was observed. By staining the vesicular glutamate transporter 1,

the molecular origin was found to be a rescue of dendritic spine density in the hippocampal cornu ammonis 1.

Taken together, our translational data propose that hypercondensed composition of Aβ-plaques is able to ameliorate cognitive performance by reducing neurotoxicity and and hence protects brain integrity. Thus, increasing Aβ-PET signaling during an immunomodulatory therapy period can be neurologically protective.

5. Literaturverzeichnis

Ahmad, M. H., M. Fatima and A. C. Mondal (2019). "Influence of microglia and astrocyte activation in the neuroinflammatory pathogenesis of Alzheimer's disease: Rational insights for the therapeutic approaches." J Clin Neurosci **59**: 6-11.

Alzheimer´s Association. (2022). "What is Alzheimer´s Disease?", from https://www.alz.org/alzheimers-dementia/what-is-alzheimers.

Bamberger, M. E., M. E. Harris, D. R. McDonald, J. Husemann and G. E. Landreth (2003). "A cell surface receptor complex for fibrillar beta-amyloid mediates microglial activation." J Neurosci **23**(7): 2665-2674.

Biechele, G., N. Franzmeier, T. Blume, M. Ewers, J. M. Luque, F. Eckenweber, C. Sacher, L. Beyer, F. Ruch-Rubinstein, S. Lindner, F. J. Gildehaus, B. von Ungern-Sternberg, P. Cumming, P. Bartenstein, A. Rominger, G. U. Hoglinger, J. Herms and M. Brendel (2020). "Glial activation is moderated by sex in response to amyloidosis but not to tau pathology in mouse models of neurodegenerative diseases." J Neuroinflammation **17**(1): 374.

Biechele, G., L. S. Monasor, K. Wind, T. Blume, S. Parhizkar, T. Arzberger, C. Sacher, L. Beyer, F. Eckenweber, F. J. Gildehaus, B. von Ungern-Sternberg, M. Willem, P. Bartenstein, P. Cumming, A. Rominger, J. Herms, S. F. Lichtenthaler, C. Haass, S. Tahirovic and M. Brendel (2022). "Glitter in the Darkness? Nonfibrillar beta-Amyloid Plaque Components Significantly Impact the beta-Amyloid PET Signal in Mouse Models of Alzheimer Disease." J Nucl Med **63**(1): 117-124.

Birks, J. (2006). "Cholinesterase inhibitors for Alzheimer's disease." Cochrane Database Syst Rev(1): CD005593.

Blume, T., C. Focke, F. Peters, M. Deussing, N. L. Albert, S. Lindner, F. J. Gildehaus, B. von Ungern-Sternberg, L. Ozmen, K. Baumann, P. Bartenstein, A. Rominger, J. Herms and M. Brendel (2018). "Microglial response to increasing amyloid load saturates with aging: a longitudinal dual tracer in vivo muPET-study." J Neuroinflammation **15**(1): 307.

Bonsack, F. and S. Sukumari-Ramesh (2018). "TSPO: An Evolutionarily Conserved Protein with Elusive Functions." Int J Mol Sci **19**(6).

Braak, H. and E. Braak (1991). "Demonstration of amyloid deposits and neurofibrillary changes in whole brain sections." Brain Pathol **1**(3): 213-216.

Brendel, M., C. Focke, T. Blume, F. Peters, M. Deussing, F. Probst, A. Jaworska, F. Overhoff, N. Albert, S. Lindner, B. von Ungern-Sternberg, P. Bartenstein, C. Haass, G. Kleinberger, J. Herms and A. Rominger (2017). "Time Courses of Cortical Glucose Metabolism and Microglial Activity Across the Life Span of Wild-Type Mice: A PET Study." J Nucl Med **58**(12): 1984-1990.

Brendel, M., G. Kleinberger, F. Probst, A. Jaworska, F. Overhoff, T. Blume, N. L. Albert, J. Carlsen, S. Lindner, F. J. Gildehaus, L. Ozmen, M. Suarez-Calvet, P. Bartenstein, K. Baumann, M. Ewers, J. Herms, C. Haass and A. Rominger (2017). "Increase of TREM2 during Aging of an Alzheimer's Disease Mouse Model Is Paralleled by Microglial Activation and Amyloidosis." Front Aging Neurosci **9**: 8.

Brendel, M., F. Probst, A. Jaworska, F. Overhoff, V. Korzhova, N. L. Albert, R. Beck, S. Lindner, F. J. Gildehaus, K. Baumann, P. Bartenstein, G. Kleinberger, C. Haass, J. Herms and A. Rominger (2016). "Glial Activation and Glucose Metabolism in a Transgenic Amyloid Mouse Model: A Triple-Tracer PET Study." J Nucl Med **57**(6): 954-960.

Bromley-Brits, K., Y. Deng and W. Song (2011). "Morris water maze test for learning and memory deficits in Alzheimer's disease model mice." J Vis Exp(53).

Burns, D. K., C. Chiang, K. A. Welsh-Bohmer, S. K. Brannan, M. Culp, J. O'Neil, G. Runyan, P. Harrigan, B. L. Plassman, M. Lutz, E. Lai, S. Haneline, D. Yarnall, D. Yarbrough, C. Metz, S. Ponduru, S. Sundseth and A. M. Saunders (2019). "The TOMMORROW study: Design of an Alzheimer's disease delay-of-onset clinical trial." Alzheimers Dement (N Y) **5**: 661-670.
Chandra, A., P. E. Valkimadi, G. Pagano, O. Cousins, G. Dervenoulas, M. Politis and I. Alzheimer's Disease Neuroimaging (2019). "Applications of amyloid, tau, and neuroinflammation PET imaging to Alzheimer's disease and mild cognitive impairment." Hum Brain Mapp **40**(18): 5424-5442.
Citron, M., T. Oltersdorf, C. Haass, L. McConlogue, A. Y. Hung, P. Seubert, C. Vigo-Pelfrey, I. Lieberburg and D. J. Selkoe (1992). "Mutation of the beta-amyloid precursor protein in familial Alzheimer's disease increases beta-protein production." Nature **360**(6405): 672-674.
d'Angelo, M., V. Castelli, M. Catanesi, A. Antonosante, R. Dominguez-Benot, R. Ippoliti, E. Benedetti and A. Cimini (2019). "PPARgamma and Cognitive Performance." Int J Mol Sci **20**(20).
Dani, M., M. Wood, R. Mizoguchi, Z. Fan, Z. Walker, R. Morgan, R. Hinz, M. Biju, T. Kuruvilla, D. J. Brooks and P. Edison (2018). "Microglial activation correlates in vivo with both tau and amyloid in Alzheimer's disease." Brain **141**(9): 2740-2754.
Deussing, M., T. Blume, L. Vomacka, C. Mahler, C. Focke, A. Todica, M. Unterrainer, N. L. Albert, S. Lindner, B. von Ungern-Sternberg, K. Baumann, A. Zwergal, P. Bartenstein, J. Herms, A. Rominger and M. Brendel (2018). "Coupling between physiological TSPO expression in brain and myocardium allows stabilization of late-phase cerebral [(18)F]GE180 PET quantification." Neuroimage **165**: 83-91.
Deutsche Alzheimer Gesellschaft e.V. (2020). "Die häufigkeit von demenzerkrankungen." from https://www.deutsche-alzheimer.de/fileadmin/Alz/pdf/factsheets/infoblatt1_haeufigkeit_demenzerkrankungen_dalzg.pdf.
Dorostkar, M. M., E. Dreosti, B. Odermatt and L. Lagnado (2010). "Computational processing of optical measurements of neuronal and synaptic activity in networks." J Neurosci Methods **188**(1): 141-150.
Elder, G. A., M. A. Gama Sosa and R. De Gasperi (2010). "Transgenic mouse models of Alzheimer's disease." Mt Sinai J Med **77**(1): 69-81.
Fan, Z., V. Calsolaro, R. A. Atkinson, G. D. Femminella, A. Waldman, C. Buckley, W. Trigg, D. J. Brooks, R. Hinz and P. Edison (2016). "Flutriciclamide (18F-GE180) PET: First-in-Human PET Study of Novel Third-Generation In Vivo Marker of Human Translocator Protein." J Nucl Med **57**(11): 1753-1759.
FDA, U. S. F. D. A. (2021). "Aducanumab Information." from https://www.fda.gov/drugs/postmarket-drug-safety-information-patients-and-providers/aducanumab-marketed-aduhelm-information.
Focke, C., T. Blume, B. Zott, Y. Shi, M. Deussing, F. Peters, C. Schmidt, G. Kleinberger, S. Lindner, F. J. Gildehaus, L. Beyer, B. von Ungern-Sternberg, P. Bartenstein, L. Ozmen, K. Baumann, M. M. Dorostkar, C. Haass, H. Adelsberger, J. Herms, A. Rominger and M. Brendel (2019). "Early and Longitudinal Microglial Activation but Not Amyloid Accumulation Predicts Cognitive Outcome in PS2APP Mice." J Nucl Med **60**(4): 548-554.
Frigerio, I., B. D. C. Boon, C. P. Lin, Y. Galis-de Graaf, J. Bol, P. Preziosa, J. Twisk, F. Barkhof, J. J. M. Hoozemans, F. H. Bouwman, A. J. M. Rozemuller, W. D. J. van de Berg and L. E. Jonkman (2021). "Amyloid-beta, p-tau and reactive microglia are pathological correlates of MRI cortical atrophy in Alzheimer's disease." Brain Commun **3**(4): fcab281.

Geldmacher, D. S., T. Fritsch, M. J. McClendon and G. Landreth (2011). "A randomized pilot clinical trial of the safety of pioglitazone in treatment of patients with Alzheimer disease." Arch Neurol **68**(1): 45-50.
Gotzl, J. K., M. Brendel, G. Werner, S. Parhizkar, L. Sebastian Monasor, G. Kleinberger, A. V. Colombo, M. Deussing, M. Wagner, J. Winkelmann, J. Diehl-Schmid, J. Levin, K. Fellerer, A. Reifschneider, S. Bultmann, P. Bartenstein, A. Rominger, S. Tahirovic, S. T. Smith, C. Madore, O. Butovsky, A. Capell and C. Haass (2019). "Opposite microglial activation stages upon loss of PGRN or TREM2 result in reduced cerebral glucose metabolism." EMBO Mol Med **11**(6).
Hampel, H., J. Cummings, K. Blennow, P. Gao, C. R. Jack, Jr. and A. Vergallo (2021). "Developing the ATX(N) classification for use across the Alzheimer disease continuum." Nat Rev Neurol **17**(9): 580-589.
Hanslik, K. L. and T. K. Ulland (2020). "The Role of Microglia and the Nlrp3 Inflammasome in Alzheimer's Disease." Front Neurol **11**: 570711.
Heneka, M. T., M. J. Carson, J. El Khoury, G. E. Landreth, F. Brosseron, D. L. Feinstein, A. H. Jacobs, T. Wyss-Coray, J. Vitorica, R. M. Ransohoff, K. Herrup, S. A. Frautschy, B. Finsen, G. C. Brown, A. Verkhratsky, K. Yamanaka, J. Koistinaho, E. Latz, A. Halle, G. C. Petzold, T. Town, D. Morgan, M. L. Shinohara, V. H. Perry, C. Holmes, N. G. Bazan, D. J. Brooks, S. Hunot, B. Joseph, N. Deigendesch, O. Garaschuk, E. Boddeke, C. A. Dinarello, J. C. Breitner, G. M. Cole, D. T. Golenbock and M. P. Kummer (2015). "Neuroinflammation in Alzheimer's disease." Lancet Neurol **14**(4): 388-405.
Heneka, M. T., M. P. Kummer, A. Stutz, A. Delekate, S. Schwartz, A. Vieira-Saecker, A. Griep, D. Axt, A. Remus, T. C. Tzeng, E. Gelpi, A. Halle, M. Korte, E. Latz and D. T. Golenbock (2013). "NLRP3 is activated in Alzheimer's disease and contributes to pathology in APP/PS1 mice." Nature **493**(7434): 674-678.
Ishizawa, K. and D. W. Dickson (2001). "Microglial activation parallels system degeneration in progressive supranuclear palsy and corticobasal degeneration." J Neuropathol Exp Neurol **60**(6): 647-657.
Ising, C., C. Venegas, S. Zhang, H. Scheiblich, S. V. Schmidt, A. Vieira-Saecker, S. Schwartz, S. Albasset, R. M. McManus, D. Tejera, A. Griep, F. Santarelli, F. Brosseron, S. Opitz, J. Stunden, M. Merten, R. Kayed, D. T. Golenbock, D. Blum, E. Latz, L. Buee and M. T. Heneka (2019). "NLRP3 inflammasome activation drives tau pathology." Nature **575**(7784): 669-673.
Jain, P., A. M. Chaney, M. L. Carlson, I. M. Jackson, A. Rao and M. L. James (2020). "Neuroinflammation PET Imaging: Current Opinion and Future Directions." J Nucl Med **61**(8): 1107-1112.
James, M. L., N. P. Belichenko, A. J. Shuhendler, A. Hoehne, L. E. Andrews, C. Condon, T. V. Nguyen, V. Reiser, P. Jones, W. Trigg, J. Rao, S. S. Gambhir and F. M. Longo (2017). "[(18)F]GE-180 PET Detects Reduced Microglia Activation After LM11A-31 Therapy in a Mouse Model of Alzheimer's Disease." Theranostics **7**(6): 1422-1436.
Jaul, E. and J. Barron (2017). "Age-Related Diseases and Clinical and Public Health Implications for the 85 Years Old and Over Population." Front Public Health **5**: 335.
Kullenberg, T., M. Lofqvist, M. Leinonen, R. Goldbach-Mansky and H. Olivecrona (2016). "Long-term safety profile of anakinra in patients with severe cryopyrin-associated periodic syndromes." Rheumatology (Oxford) **55**(8): 1499-1506.
Lane, C. A., J. Hardy and J. M. Schott (2018). "Alzheimer's disease." Eur J Neurol **25**(1): 59-70.
Leng, F. and P. Edison (2021). "Neuroinflammation and microglial activation in Alzheimer disease: where do we go from here?" Nat Rev Neurol **17**(3): 157-172.

Lichtenthaler, S. F., N. Ida, G. Multhaup, C. L. Masters and K. Beyreuther (1997). "Mutations in the transmembrane domain of APP altering gamma-secretase specificity." Biochemistry **36**(49): 15396-15403.
Malik, A. and T. D. Kanneganti (2017). "Inflammasome activation and assembly at a glance." J Cell Sci **130**(23): 3955-3963.
Mandrekar-Colucci, S., J. C. Karlo and G. E. Landreth (2012). "Mechanisms underlying the rapid peroxisome proliferator-activated receptor-gamma-mediated amyloid clearance and reversal of cognitive deficits in a murine model of Alzheimer's disease." J Neurosci **32**(30): 10117-10128.
Masuda, A., Y. Kobayashi, N. Kogo, T. Saito, T. C. Saido and S. Itohara (2016). "Cognitive deficits in single App knock-in mouse models." Neurobiol Learn Mem **135**: 73-82.
Michalowsky, B., A. Kaczynski and W. Hoffmann (2019). "[The economic and social burden of dementia diseases in Germany-A meta-analysis]." Bundesgesundheitsblatt Gesundheitsforschung Gesundheitsschutz **62**(8): 981-992.
Nilsberth, C., A. Westlind-Danielsson, C. B. Eckman, M. M. Condron, K. Axelman, C. Forsell, C. Stenh, J. Luthman, D. B. Teplow, S. G. Younkin, J. Naslund and L. Lannfelt (2001). "The 'Arctic' APP mutation (E693G) causes Alzheimer's disease by enhanced Abeta protofibril formation." Nat Neurosci **4**(9): 887-893.
Overhoff, F., M. Brendel, A. Jaworska, V. Korzhova, A. Delker, F. Probst, C. Focke, F. J. Gildehaus, J. Carlsen, K. Baumann, C. Haass, P. Bartenstein, J. Herms and A. Rominger (2016). "Automated Spatial Brain Normalization and Hindbrain White Matter Reference Tissue Give Improved [(18)F]-Florbetaben PET Quantitation in Alzheimer's Model Mice." Front Neurosci **10**: 45.
Ozmen, L., A. Albientz, C. Czech and H. Jacobsen (2009). "Expression of transgenic APP mRNA is the key determinant for beta-amyloid deposition in PS2APP transgenic mice." Neurodegener Dis **6**(1-2): 29-36.
Parhizkar, S., T. Arzberger, M. Brendel, G. Kleinberger, M. Deussing, C. Focke, B. Nuscher, M. Xiong, A. Ghasemigharagoz, N. Katzmarski, S. Krasemann, S. F. Lichtenthaler, S. A. Muller, A. Colombo, L. S. Monasor, S. Tahirovic, J. Herms, M. Willem, N. Pettkus, O. Butovsky, P. Bartenstein, D. Edbauer, A. Rominger, A. Erturk, S. A. Grathwohl, J. J. Neher, D. M. Holtzman, M. Meyer-Luehmann and C. Haass (2019). "Loss of TREM2 function increases amyloid seeding but reduces plaque-associated ApoE." Nat Neurosci **22**(2): 191-204.
Pascoal, T. A., A. L. Benedet, N. J. Ashton, M. S. Kang, J. Therriault, M. Chamoun, M. Savard, F. Z. Lussier, C. Tissot, T. K. Karikari, J. Ottoy, S. Mathotaarachchi, J. Stevenson, G. Massarweh, M. Scholl, M. J. de Leon, J. P. Soucy, P. Edison, K. Blennow, H. Zetterberg, S. Gauthier and P. Rosa-Neto (2021). "Microglial activation and tau propagate jointly across Braak stages." Nat Med **27**(9): 1592-1599.
Platt, T. L., V. L. Reeves and M. P. Murphy (2013). "Transgenic models of Alzheimer's disease: better utilization of existing models through viral transgenesis." Biochim Biophys Acta **1832**(9): 1437-1448.
Puzzo, D., W. Gulisano, A. Palmeri and O. Arancio (2015). "Rodent models for Alzheimer's disease drug discovery." Expert Opin Drug Discov **10**(7): 703-711.
Querfurth, H. W. and F. M. LaFerla (2010). "Alzheimer's disease." N Engl J Med **362**(4): 329-344.
Richards, J. G., G. A. Higgins, A. M. Ouagazzal, L. Ozmen, J. N. Kew, B. Bohrmann, P. Malherbe, M. Brockhaus, H. Loetscher, C. Czech, G. Huber, H. Bluethmann, H. Jacobsen and J. A. Kemp (2003). "PS2APP transgenic mice, coexpressing hPS2mut and hAPPswe, show age-related cognitive deficits associated with discrete brain amyloid deposition and inflammation." J Neurosci **23**(26): 8989-9003.

Rupprecht, R., C. H. Wetzel, M. Dorostkar, J. Herms, N. L. Albert, J. Schwarzbach, M. Schumacher and I. D. Neumann (2022). "Translocator protein (18kDa) TSPO: a new diagnostic or therapeutic target for stress-related disorders?" Mol Psychiatry.
Sacher, C., T. Blume, L. Beyer, F. Peters, F. Eckenweber, C. Sgobio, M. Deussing, N. L. Albert, M. Unterrainer, S. Lindner, F. J. Gildehaus, B. von Ungern-Sternberg, I. Brzak, U. Neumann, T. Saito, T. C. Saido, P. Bartenstein, A. Rominger, J. Herms and M. Brendel (2019). "Longitudinal PET Monitoring of Amyloidosis and Microglial Activation in a Second-Generation Amyloid-beta Mouse Model." J Nucl Med **60**(12): 1787-1793.
Saito, T., Y. Matsuba, N. Mihira, J. Takano, P. Nilsson, S. Itohara, N. Iwata and T. C. Saido (2014). "Single App knock-in mouse models of Alzheimer's disease." Nat Neurosci **17**(5): 661-663.
Salliot, C., M. Dougados and L. Gossec (2009). "Risk of serious infections during rituximab, abatacept and anakinra treatments for rheumatoid arthritis: meta-analyses of randomised placebo-controlled trials." Ann Rheum Dis **68**(1): 25-32.
Scarf, A. M. and M. Kassiou (2011). "The translocator protein." J Nucl Med **52**(5): 677-680.
Scott, G., H. Zetterberg, A. Jolly, J. H. Cole, S. De Simoni, P. O. Jenkins, C. Feeney, D. R. Owen, A. Lingford-Hughes, O. Howes, M. C. Patel, A. P. Goldstone, R. N. Gunn, K. Blennow, P. M. Matthews and D. J. Sharp (2018). "Minocycline reduces chronic microglial activation after brain trauma but increases neurodegeneration." Brain **141**(2): 459-471.
Sebastian Monasor, L., S. A. Muller, A. V. Colombo, G. Tanrioever, J. Konig, S. Roth, A. Liesz, A. Berghofer, A. Piechotta, M. Prestel, T. Saito, T. C. Saido, J. Herms, M. Willem, C. Haass, S. F. Lichtenthaler and S. Tahirovic (2020). "Fibrillar Abeta triggers microglial proteome alterations and dysfunction in Alzheimer mouse models." Elife **9**.
Serrano-Pozo, A., M. P. Frosch, E. Masliah and B. T. Hyman (2011). "Neuropathological alterations in Alzheimer disease." Cold Spring Harb Perspect Med **1**(1): a006189.
Serrano-Pozo, A., M. L. Mielke, T. Gomez-Isla, R. A. Betensky, J. H. Growdon, M. P. Frosch and B. T. Hyman (2011). "Reactive glia not only associates with plaques but also parallels tangles in Alzheimer's disease." Am J Pathol **179**(3): 1373-1384.
Shi, Y., M. Cui, K. Ochs, M. Brendel, F. L. Strubing, N. Briel, F. Eckenweber, C. Zou, R. B. Banati, G. J. Liu, R. J. Middleton, R. Rupprecht, U. Rudolph, H. U. Zeilhofer, G. Rammes, J. Herms and M. M. Dorostkar (2022). "Long-term diazepam treatment enhances microglial spine engulfment and impairs cognitive performance via the mitochondrial 18 kDa translocator protein (TSPO)." Nat Neurosci **25**(3): 317-329.
St George-Hyslop, P. H. (2000). "Molecular genetics of Alzheimer's disease." Biol Psychiatry **47**(3): 183-199.
Su, L., A. Surendranathan, Y. Huang, W. R. Bevan-Jones, L. Passamonti, Y. T. Hong, R. Arnold, P. V. Rodríguez, Y. Wang, E. Mak, T. D. Fryer, F. Aigbirhio, J. B. Rowe and J. T. O'Brien (2021). "Relationship between tau, neuroinflammation and atrophy in Alzheimer's disease: The NIMROD study." Information Fusion **67**: 116-124.
Tan, M. S., X. Ji, J. Q. Li, W. Xu, H. F. Wang, C. C. Tan, Q. Dong, C. T. Zuo, L. Tan, J. Suckling, J. T. Yu and I. Alzheimer's Disease Neuroimaging (2020). "Longitudinal trajectories of Alzheimer's ATN biomarkers in elderly persons without dementia." Alzheimers Res Ther **12**(1): 55.
Thyrian, J. R., M. Boekholt, W. Hoffmann, M. Leiz, J. Monsees, T. Schmachtenberg, F. Schumacher-Schonert and U. Stentzel (2020). "[The prevalence of people with

dementia in Germany-A nationwide analysis at the district level]." Nervenarzt **91**(11): 1058-1061.
Villemagne, V. L., S. Burnham, P. Bourgeat, B. Brown, K. A. Ellis, O. Salvado, C. Szoeke, S. L. Macaulay, R. Martins, P. Maruff, D. Ames, C. C. Rowe, C. L. Masters, B. Australian Imaging and G. Lifestyle Research (2013). "Amyloid beta deposition, neurodegeneration, and cognitive decline in sporadic Alzheimer's disease: a prospective cohort study." Lancet Neurol **12**(4): 357-367.
Vivash, L. and T. J. O'Brien (2016). "Imaging Microglial Activation with TSPO PET: Lighting Up Neurologic Diseases?" J Nucl Med **57**(2): 165-168.
Wang, W. Y., M. S. Tan, J. T. Yu and L. Tan (2015). "Role of pro-inflammatory cytokines released from microglia in Alzheimer's disease." Ann Transl Med **3**(10): 136.
Weller, J. and A. Budson (2018). "Current understanding of Alzheimer's disease diagnosis and treatment." F1000Res **7**.
WHO. (2021). "Dementia." from https://www.who.int/news-room/fact-sheets/detail/dementia.
Wolf, B. J., M. Brackhan, P. Bascunana, I. Leiter, B. L. N. Langer, T. L. Ross, J. P. Bankstahl and M. Bankstahl (2020). "TSPO PET Identifies Different Anti-inflammatory Minocycline Treatment Response in Two Rodent Models of Epileptogenesis." Neurotherapeutics **17**(3): 1228-1238.
Wright, A. L., R. Zinn, B. Hohensinn, L. M. Konen, S. B. Beynon, R. P. Tan, I. A. Clark, A. Abdipranoto and B. Vissel (2013). "Neuroinflammation and neuronal loss precede Abeta plaque deposition in the hAPP-J20 mouse model of Alzheimer's disease." PLoS One **8**(4): e59586.
Zou, C., Y. Shi, J. Ohli, U. Schuller, M. M. Dorostkar and J. Herms (2016). "Neuroinflammation impairs adaptive structural plasticity of dendritic spines in a preclinical model of Alzheimer's disease." Acta Neuropathol **131**(2): 235-246.

6. Danksagung

An vorrangiger Stelle möchte ich meinem Doktorvater Herrn Priv.-Doz. Dr. med. Matthias Brendel für die Bereitstellung dieses überaus interessanten Themas herzlich danken. Insbesondere gilt mein Dank für die immer währende Unterstützung, die wirklich herausragende Betreuung und die vielen förderlichen Ratschläge sowie für die stets geöffnete Tür. Durch seine engagierte Art konnte er mich zu vielen weiteren wissenschaftliche Projekten begeistern.

Herrn Prof. Dr. med. Peter Bartenstein möchte ich für die Ermöglichung dieses Projektes danken.

Außerdem danke ich Karin Bormann-Giglmaier für die kompetente Zusammenarbeit und die harmonische Atmosphäre bei der Durchführung der Experimente.

Ganz besonderer Dank gilt meinen Eltern Claudia und Manfred Biechele und meinem Freund Robin für ihre endlose Geduld, Motivation und emotionale Unterstützung während meiner Dissertation. Vielen herzlichen Dank dafür.

7. Publikation Nr. 1

IVYSPRING INTERNATIONAL PUBLISHER

Theranostics

2021; 11(18): 8964-8976. doi: 10.7150/thno.64022

Research Paper

Pre-therapeutic microglia activation and sex determine therapy effects of chronic immunomodulation

Gloria Biechele[1], Tanja Blume[1,2], Maximilian Deussing[1], Benedikt Zott[3,4], Yuan Shi[2], Xianyuan Xiang[5], Nicolai Franzmeier[6], Gernot Kleinberger[7], Finn Peters[2], Katharina Ochs[2], Carola Focke[1], Christian Sacher[1], Karin Wind[1], Claudio Schmidt[1], Simon Lindner[1], Franz-Josef Gildehaus[1], Florian Eckenweber[1], Leonie Beyer[1], Barbara von Ungern-Sternberg[1], Peter Bartenstein[1,8], Karlheinz Baumann[9], Mario M. Dorostkar[2,10], Axel Rominger[1,8,11], Paul Cumming[11,12], Michael Willem[5], Helmuth Adelsberger[3], Jochen Herms[2,8,10], Matthias Brendel[1,8]✉

1. Dept. of Nuclear Medicine, University Hospital of Munich, LMU Munich, Munich, Germany.
2. DZNE – German Center for Neurodegenerative Diseases, Munich, Germany.
3. Institute of Neuroscience, Technical University of Munich, Munich, Germany.
4. Department of Diagnostic and Interventional Neuroradiology, Klinikum rechts der Isar, Technical University of Munich, Munich, Germany.
5. Metabolic Biochemistry, Biomedical Center (BMC), Faculty of Medicine, Ludwig-Maximilians-Universität München, Munich, Germany.
6. Institute for Stroke and Dementia Research, University Hospital of Munich, LMU Munich, Munich, Germany.
7. ISAR Bioscience GmbH, 82152 Planegg, Germany.
8. SyNergy, University of Munich, Munich, Germany.
9. Roche Pharma Research and Early Development, Neuroscience Discovery, Roche, Innovation Center Basel, F. Hoffmann-La Roche Ltd., Basel, Switzerland.
10. Center for Neuropathology and Prion Research, Ludwig-Maximilians-University of Munich, Munich, Germany.
11. Dept. of Nuclear Medicine, Inselspital Bern, Bern, Switzerland.
12. School of Psychology and Counselling, Queensland University of Technology, Brisbane, Australia.

✉ Corresponding author: Dr. Matthias Brendel, MHBA, Department of Nuclear Medicine, University Hospital of Munich, Marchioninistr.15, 81377 Munich, Germany. Phone: +49 (0) 89 4400 74650; Fax: +49 (0) 89 4400 77646; E-mail: matthias.brendel@med.uni-muenchen.de.

Received: 2021.06.18; Accepted: 2021.08.06; Published: 2021.08.19

Abstract

Modulation of the innate immune system is emerging as a promising therapeutic strategy against Alzheimer's disease (AD). However, determinants of a beneficial therapeutic effect are ill-understood. Thus, we investigated the potential of 18 kDa translocator protein positron-emission-tomography (TSPO-PET) for assessment of microglial activation in mouse brain before and during chronic immunomodulation.

Methods: Serial TSPO-PET was performed during five months of chronic microglia modulation by stimulation of the peroxisome proliferator-activated receptor (PPAR)-γ with pioglitazone in two different mouse models of AD (PS2APP, *App*$^{NL-G-F}$). Using mixed statistical models on longitudinal TSPO-PET data, we tested for effects of therapy and sex on treatment response. We tested correlations of baseline with longitudinal measures of TSPO-PET, and correlations between PET results with spatial learning performance and β-amyloid accumulation of individual mice. Immunohistochemistry was used to determine the molecular source of the TSPO-PET signal.

Results: Pioglitazone-treated female PS2APP and *App*$^{NL-G-F}$ mice showed attenuation of the longitudinal increases in TSPO-PET signal when compared to vehicle controls, whereas treated male *App*$^{NL-G-F}$ mice showed the opposite effect. Baseline TSPO-PET strongly predicted changes in microglial activation in treated mice ($R = -0.874$, $p < 0.0001$) but not in vehicle controls ($R = -0.356$, $p = 0.081$). Reduced TSPO-PET signal upon pharmacological treatment was associated with better spatial learning despite higher fibrillar β-amyloid accumulation. Immunohistochemistry confirmed activated microglia to be the source of the TSPO-PET signal ($R = 0.952$, $p < 0.0001$).

Conclusion: TSPO-PET represents a sensitive biomarker for monitoring of immunomodulation and closely reflects activated microglia. Sex and pre-therapeutic assessment of baseline microglial activation predict individual immunomodulation effects and may serve for responder stratification.

Key words: pioglitazone, TSPO-PET, *App*$^{NL-G-F}$ mice, PS2APP mice, microglia, sex, prediction

Introduction

Neuroinflammation is now recognized as an inherent part of the Alzheimer's disease (AD) pathology [1]. The key players of neuroinflammation in AD are activated microglia and astrocytes [2].

Although it is still unclear if beneficial or detrimental effects of neuroinflammation dominate in the (patho)-physiology of AD, there is considerable interest in integrating the modulation of neuroinflammation into novel treatment strategies against AD [3]. Preclinical studies showed that immunomodulation by peroxisome proliferator-activated receptor (PPAR)-γ using the antidiabetic compound pioglitazone rescues neuronal spine density [4] and spatial learning performance [5] in mouse AD models. However, a large human trial with pioglitazone in mild cognitive impairment due to AD was terminated after an interim analysis showing lack of efficacy [6]. Hence, the discrepancies between beneficial effects in preclinical studies and lacking efficacy in humans deserve detailed inquiry, with the objective of uncovering the salient factors accounting for the failure of PPARγ stimulation in clinical translation.

TSPO-PET is increasingly used to monitor therapy-related changes of microglial activation in humans [7] and rodent models [8]. In this regard, the TSPO ligand ^{18}F-GE-180 is proven effective for robust imaging of microglial activation in a mouse model of amyloidosis, and shows the normalization of TSPO binding upon treatment with a neurotrophin receptor ligand that ameliorates hyperphosphorylation and misfolding of tau, and rescues the consequent neurite degeneration [9]. Our previous data revealed excellent agreement between ^{18}F-GE-180 PET quantitation and immunohistochemistry of microglial markers [10, 11], thus indicating its potential to access and predict PPARγ stimulation effects *in vivo*.

Therefore, we aimed in this study to test the hypothesis that TSPO-PET with ^{18}F-GE-180 is a suitable tool for monitoring anti-neuroinflammatory responses to chronic immunomodulation in AD mouse models. We furthermore tested the hypothesis that microglial activation by TSPO-PET predicts therapy-related changes and outcome parameters. Furthermore, we tested for effects of mouse sex on immunomodulation. Finally, we used immunohisto-chemistry to validate *in vivo* PET findings and to confirm the cellular source of TSPO-PET signal alterations.

Material and Methods

Study design

All experiments were performed in compliance with the National Guidelines for Animal Protection, Germany, with approval of the local animal care committee of the Government of Oberbayern (Regierung Oberbayern) and overseen by a veterinarian. The experiments also complied with the ARRIVE guidelines and were carried out in accordance with the U.K. Animals (Scientific Procedures) Act, 1986 and associated guidelines, EU Directive 2010/63/EU for animal experiments. The chronic treatment study was performed in two different Aβ mouse models and a longitudinal PET imaging design was applied in both cohorts. Female PS2APP and wild-type mice had their baseline assessment at eight months of age and had follow-up PET imaging at 9.5, 11.5 and 13 months of age. Female and male *App*$^{NL-G-F}$ mice had their baseline assessment at five months of age and received follow-up PET imaging at 7.5 and 10 months of age. Cage randomization to pioglitazone treatment or control chow (vehicle) groups was initiated after the baseline PET scans, and treatments continued until after the terminal behavioural assessments. After recovering from the final PET scan, mice were transferred to the behavioural facility and rested for one week before initiation of Morris water maze (WM) testing of spatial learning. One week after the behavioural tests, mice were deeply anaesthetized prior to transcardial perfusion and fixation with 4% paraformaldehyde. We then harvested and processed the brains for immunohistochemical and biochemical analyses (randomized hemispheres). Group comparisons of longitudinal Aβ-PET monitoring and detailed Aβ analyses by immunohistochemistry and biochemistry of the same cohort are reported in a separate manuscript [12]. Shared data points between both manuscripts are indicated and cited.

Animal Models and Statistical Power Analysis

The transgenic B6.PS2APP (line B6.152H) is homozygous for human presenilin (PS) 2, the N141I mutation, and the human amyloid precursor protein (APP) K670N/M671L mutations [13]. Homozygous B6.PS2APP mice show first appearance of plaques in the cerebral cortex and hippocampus at 5–6 months of age [14]. The knock-in mouse model *App*$^{NL-G-F}$ carries a mutant APP gene encoding the humanized Aβ sequence (G601R, F606Y, and R609H) with three pathogenic mutations, namely Swedish (KM595/596NL), Beyreuther/Iberian (I641F), and Arctic (E618G). Homozygotic *App*$^{NL-G-F}$ mice progressively exhibit widespread Aβ accumulation from two months of age [15, 16]. Both transgenic models were generated on a C57Bl/6 background, which also served for wild-type controls.

Required sample sizes were calculated by G*power (V3.1.9.2, Kiel, Germany), based on assumptions for a type I error α=0.05 and a power of 0.8 for group comparisons. A drop-out rate of 10% per time-point was assumed and a treatment effect causing 5% change in the PET signal was considered significant. Estimations were based on PET measures

in previous investigations with the same mouse models [10, 17]. Calculated sample sizes at baseline were n = 14 for PS2APP, n = 8 for wild-type, and n = 9 per sex for *App*$^{NL-G-F}$.

PET Imaging

For all PET procedures, radiochemistry, data acquisition, and image pre-processing were conducted according to an established, standardized protocol [18]. In brief, ^{18}F-GE-180 TSPO-PET recordings (average dose: 11.5 ± 2.2 MBq) with an emission window of 60–90 min after injection were performed for assessment of cerebral TSPO expression. Aβ-PET recordings (^{18}F-florbetaben average dose: 12.2 ± 2.0 MBq) with an emission window of 30-60 min after injection were obtained to measure fibrillar cerebral amyloidosis, as reported elsewhere [12]. Isoflurane anesthesia was induced before tracer injection and maintained to the end of the imaging time window. Mice with different genotype and treatment arm were examined simultaneously, with random placement in a four-mouse imaging chamber, thus with exposure to an equal level of isoflurane during the PET recording. All image analyses were performed using PMOD (version 3.5; PMOD technologies, Basel, Switzerland). Static 30-60 min (Aβ-PET) and 60-90 min (TSPO-PET) datasets were co-registered to tracer specific templates (genotype specific) by a manual rigid-body transformation (TX_{rigid}) [18]. In the second step, a reader-independent affine co-registration to the tracer-specific template was performed [18]. Here, the initial manually fused images were further normalized by non-linear brain normalization (TX_{BN}) via the PMOD brain normalization tool (equal modality; smoothing by 0.6 mm; nonlinear warping; 16 iterations; frequency cutoff 3; regularization 1.0; no thresholding). The concatenation of TX_{rigid} and TX_{BN} was then used to obtain optimal resampling with a minimum of interpolation. Normalization of injected radioactivity was performed by the previously validated myocardium correction method [19] for TSPO-PET and by previously established white matter [18] (PS2APP) and periaqueductal grey [17] (*App*$^{NL-G-F}$) reference regions for Aβ-PET. Thus, the primary endpoints of PET consisted of myocardium-adjusted standardized uptake values (SUV_H) for TSPO-PET and intracerebral reference-based standardized uptake value ratios (SUVr) for Aβ-PET. TSPO- and Aβ-PET estimates (per time-point and rate of change) deriving from the same neocortical target VOI (15 mm^3) were extracted and compared between treatment and vehicle groups as well as between transgenic mice and wild-type controls by mixed linear models. The TSPO-PET z-score of each individual transgenic mouse at each time-point was calculated by subtraction of the mean TSPO-PET value of vehicle treated, age-matched wild-type mice and division by the standard deviation of wild-type mice (z-score = [$mean_{TG}$ – $mean_{WT-Veh}$]/SD_{WT-Veh}). The z-score deviation per time was defined as a TSPO-PET AUC [20] and served as an index for microglial activation during the observation time period. For the association analysis between baseline TSPO-PET and changes of TSPO-PET over time (Δ z-score = rate of change), we additionally extracted VOIs from the Mirrione atlas [21] to allow evaluation of multiple brain regions. The large cortex VOI of the atlas was divided into motor/sensory, auditory/visual and entorhinal/piriform cortices to allow evaluation within functionally similar compartments. We applied a false discovery rate correction for multiple comparisons.

Water maze

Two slightly different Morris water maze tasks were applied due to facility changes between the investigation of PS2APP and *App*$^{NL-G-F}$ cohorts. We used a principal component analysis of the standard read-outs of each water maze task to generate a robust read-out for correlation analyses [22]. Thus, one quantitative index of water maze performance per mouse was calculated via dimension reduction and correlated with PET imaging. The experimenter was blind according to the phenotype of the animals. Water maze results were also used as an endpoint in the dedicated manuscript on Aβ-PET in both mouse models [12].

PS2APP and age-matched wild-type mice were subjected to a modified water maze task as described previously [20, 23-25] yielding escape latency, distance to the correct platform, and correct choice of the platform as read outs. Mice had to distinguish between two visible platforms, one of which was weighted in such a manner that it would float when the mouse climbed on (correct choice), while the other would sink (wrong choice). The correct platform was always located at the same spot in the maze, while the wrong platform as well as the site from which the mice were released into the maze were varied in a pseudorandom fashion. Visual cues on the walls of the laboratory provided orientation. Trials were terminated if the mouse had failed to reach one of the platforms within 30 sec (error of omission). In this case, or in case of a wrong choice, the experimenter placed the mouse on the correct platform. After a three-day handling period, water maze training was performed on five consecutive days, with five trials per day, which were conducted 2-4 minutes apart. Memory performance was assessed by measuring the

escape latency at each day of training and by the travelled distance at the last training day. For measuring escape latency, we calculated the summed average time of all trials from the start point to attaining one of the platforms. On the sixth day, the correct platform was placed in the opposite quadrant of the maze to confirm that the mice indeed used spatial cues rather than rule-based learning to find it. Trials were filmed with a video camera and the swimming trace was extracted using custom written LabView software (National Instruments).

App^{NL-G-F} mice and 14 age- and sex-matched wild-type mice underwent a common Morris water maze test, which was performed according to a standard protocol with small adjustments [26] as previously described [17]. In brief, the first day was used for acclimatization with a visible platform (five minutes per mouse). The mice then underwent five training days where each mouse had to perform four trials per day with the platform visible at the first training day and the platform hidden under water for all other training days. The test day was set by only one trial with complete removal of the platform. The maximum trial length on all training and test days was set to a maximum of 70 seconds. The video tracking software EthoVision® XT (Noldus) was used for analyses of escape latency, the platform frequency and attendance in the platform quadrant at the probe trial.

The principal component of the water maze test scores was extracted from three spatial learning readouts (PS2APP: escape latency, distance, platform choice; *App*$^{NL-G-F}$: escape latency, frequency to platform, time spent in platform quadrant) using SPSS 26 statistics (IBM Deutschland GmbH, Ehningen, Germany). Prior to the PCA, the linearity of the relationship of the data was tested by a correlation matrix, and items with a correlation coefficient < 0.3 were discarded. The Kaiser-Meyer-Olkin (KMO) measure and Bartlett's test of sphericity were used to test for sampling adequacy and suitability for data reduction. Components with an Eigenvalue > 1.0 were extracted and a varimax rotation was selected.

Immunohistochemistry

Iba-1 and CD68 immunohistochemistry was performed as described previously [17, 27] and the group comparisons between treatment and vehicle groups are reported in the accompanying manuscript [12]. Correlation analyses were performed between TSPO-PET and Iba-1/CD68 quantitation. Groups of n = 4-5 PS2APP and *App*$^{NL-G-F}$ mice per treatment and vehicle groups with a successful TSPO-PET scan prior to immunohistochemistry were subjected to this analysis. In brief, we performed a standard free-floating immunofluorescence protocol with cortex areas matching the PET brain regions of interest. As previously described, perfusion-fixed 50-µm thick brain sections were rinsed either overnight or for 48 h in PBS with 0.2% Triton X-100 containing one of the following primary antibodies: rabbit monoclonal Iba-1 (1:500. Wako: 19-19741), or rat monoclonal CD68 (1:500. Bio-rad: MCA1857). After washing in PBS, sections were then incubated in a combination of three secondary antibodies (Alexa 488 goat anti-rabbit, Alexa 594 goat anti-mouse). A detailed analysis of Aβ-plaques (methoxy-X04 and NAB223) of this cohort is reported in the accompanying manuscript [12].

Statistics

Group differences (i.e. between treatment groups or sexes) in TSPO-PET trajectories over time were determined using linear mixed models using the lmer package in the R statistical software, including a random intercept. Note that we selected models including either linear or quadratic time effects based on best model fit (i.e. lower Akaike Information Criterion for better model fit).

Association analyses were performed between PET, water maze, and immunohistochemistry scores. Pearson's coefficient of correlation (R) was calculated after confirming normal distribution by a Kolmogorov-Smirnow test. Correlation analysis was performed between TSPO-PET baseline (z-score) and the rate of change of TSPO-PET signal (Δ z-score). This analysis was performed in the cortical target region and in a separate analysis of the full Mirrione atlas set of VOIs [21]. False discovery rate correction was applied for the multi-region analysis. The rate of change of TSPO-PET (Δ z-score) was correlated with the principal component of the water maze task to investigate potential associations of the PPARγ stimulation treatment effect with spatial learning performance. The index of microglial activity during a certain time-period (AUC) was correlated with the Aβ-PET rate of change to test the hypothesis of Aβ removal by activated microglia [28]. Immunohistochemistry quantification (Iba-1 and CD68) in the cortex was correlated with the cortical TSPO-PET signal of the terminal time-point.

Results

TSPO-PET detects altered microglia activation during chronic PPARγ stimulation

First, we investigated whether effects of chronic PPARγ stimulation can be detected by TSPO PET in PS2APP mice and wild-type controls. Vehicle-treated PS2APP mice showed a strong increase over time of

the TSPO-PET signal when compared to vehicle-treated wild-type mice between eight and 13 months of age, with a peak at 11.5 months (+52-67%, all time-points: $p < 0.0001$, **Figure 1**). The pre-therapeutic baseline TSPO-PET signal did not significantly differ between PS2APP mice with and without pioglitazone treatment (SUV_H: 0.24±0.05 vs. 0.26±0.01, $p = 0.647$). However, PS2APP mice with pioglitazone treatment had an attenuated TSPO-PET signal at 9.5 (-13%, $p = 0.0027$), 11.5 (-17%, $p = 0.0046$), and 13.0 (-13%, $p = 0.0071$) months of age when compared to the increasing signal of age-matched vehicle-treated PS2APP mice (**Figure 1**). Linear mixed models revealed a main effect of treatment group on TSPO-PET across time-points (b/SE = -0.036/0.006, T = 5.405, $p < 0.0001$), controlling for age (i.e. quadratic effect) and random intercept. Individual PS2APP mice indicated a heterogeneous pharmacotherapy-related change in the TSPO-PET signal, which was already conspicuous during the first six weeks of treatment (range of change: -35 to +86%). Pioglitazone-treated wild-type mice manifested a slight decrease of the TSPO-PET signal after six weeks of treatment when compared to vehicle-treated wild-type mice (-12%, $p = 0.013$), and no such differences at the other time points.

Chronic PPARγ stimulation changes microglial activation independent of APP overexpression but dependent on sex

Next, we tested whether previously observed sex differences in TSPO expression in mouse brain [29] have an impact on the responses to PPARγ pharmacological stimulation. To this end, we used the novel APP knock-in model *App*$^{NL\text{-}G\text{-}F}$ [16] mice and performed longitudinal TSPO-PET imaging during chronic pioglitazone treatment in groups of female and male mice. Furthermore, we tested whether these mice showed effects of PPARγ stimulation on the TSPO-PET signal in the absence of APP overexpression. Baseline levels of the TSPO-PET signal in female *App*$^{NL\text{-}G\text{-}F}$ mice at 5 months of age were lower compared to baseline levels of female PS2APP mice at 8 months of age (-21%, $p < 0.0001$; Figure S1). We observed sex-specific elevation of the TSPO-PET signal in vehicle-treated female *App*$^{NL\text{-}G\text{-}F}$ mice when compared to males aged 7.5 (+18%, $p = 0.017$) and 10 months (+25%, $p = 0.0007$; sex × time interaction: b/SE = -0.100/0.030, T = -3.273, $p = 0.0003$, linear mixed model controlling for random intercept). Female *App*$^{NL\text{-}G\text{-}F}$ mice with pioglitazone treatment showed a smaller TSPO-PET signal increase compared to vehicle-treated female *App*$^{NL\text{-}G\text{-}F}$ mice aged from five to ten months (**Figure 2**). This resulted from an attenuated TSPO-PET signal increase in pioglitazone-treated female *App*$^{NL\text{-}G\text{-}F}$ mice aged 7.5 (-15%, $p = 0.030$) and 10 months (-21%, $p = 0.0053$)

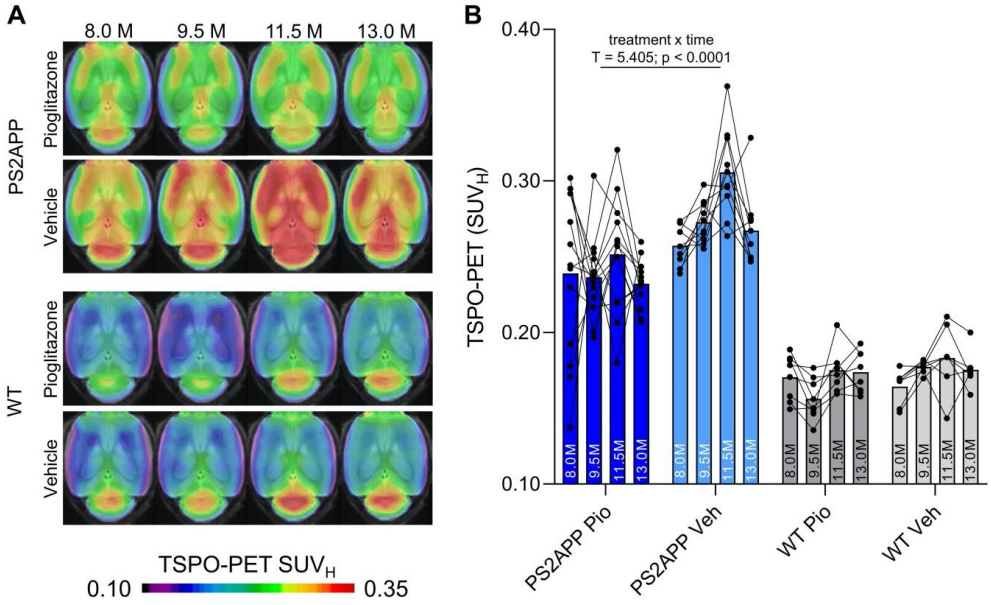

Figure 1. TSPO-PET monitoring of chronic pioglitazone treatment in PS2APP and wild-type (WT) mice. (**A**) Axial images show group levels of the ^{18}F-GE-180 TSPO-PET signal (myocardium scaled standardized uptake value, SUV_H) at different ages in treatment and vehicle groups, projected upon a standard MRI anatomic template. Baseline scans were performed prior to treatment initiation. (**B**) Individual time courses of the cortical TSPO-PET signal during the treatment period. Pio = pioglitazone treatment, Veh = vehicle treatment. Statistics derive from a linear mixed model. PS2APP pioglitazone n = 13, PS2APP vehicle n = 10, WT pioglitazone n = 8, WT vehicle n = 7.

when compared to vehicle-treated female *App*$^{NL-G-F}$ mice (treatment × time interaction: b/SE = 0.114/0.030, T = 3.801, p = 0.0009, linear mixed model controlling for random intercept, **Figure 2**). On the other hand, male *App*$^{NL-G-F}$ mice with pioglitazone treatment tended to show a slight exaggerated increase of the TSPO-PET signal from five to ten months of age when compared to vehicle treated male *App*$^{NL-G-F}$ mice (+12% vs. +2%, treatment × time interaction: b/SE = -0.041/0.022, T = -1.862, p = 0.072). Wild-type mice did not show differences in TSPO-PET signal between treated or non-treated animals for this time span. Baseline levels of Aβ-PET and the Aβ-PET rate of change did not differ between female and male *App*$^{NL-G-F}$ mice (Figure S1).

Baseline TSPO-PET predicts treatment associated changes in microglial activation during chronic PPARγ stimulation

Given the observed heterogeneity of changes in TSPO-PET after induction of PPARγ pharmacological stimulation, we asked if TSPO-PET at baseline serves to predict the individual longitudinal changes in microglial activation upon treatment. Strikingly, we observed a strong negative association between baseline TSPO-PET and subsequent changes in the TSPO-PET signal across pioglitazone treated animals (R = -0.874, p < 0.001, **Figure 3A-B**), suggesting that mice with high microglial activation at baseline respond more strongly to PPARγ stimulation. Importantly, this association was also present in independent cohorts of PS2APP mice (R = -0.964, p < 0.0001) and *App*$^{NL-G-F}$ mice (R = -0.680, p = 0.0053) mice with chronic pioglitazone treatment. On the other hand, there was only a trend towards a negative association between the baseline TSPO-PET signal and subsequent TSPO-PET changes in vehicle treated animals (R = -0.356, p = 0.081). The association between pre-therapeutic TSPO-PET results and changes in microglial activation of pioglitazone-treated mice was observed across all brain regions, with the strongest differences relative to vehicle treated mice in neocortical areas, hippocampus, striatum, and thalamus (**Figure 3C-D; Table 1**). Several subcortical regions also showed a significant negative association between the baseline TSPO-PET signal and changes in microglial activation in the vehicle cohort (**Table 1**), congruent with the observation that microglial activation at baseline *per se* has a predictive value for longitudinal alterations of microglial activity and spatial learning performance [20, 30].

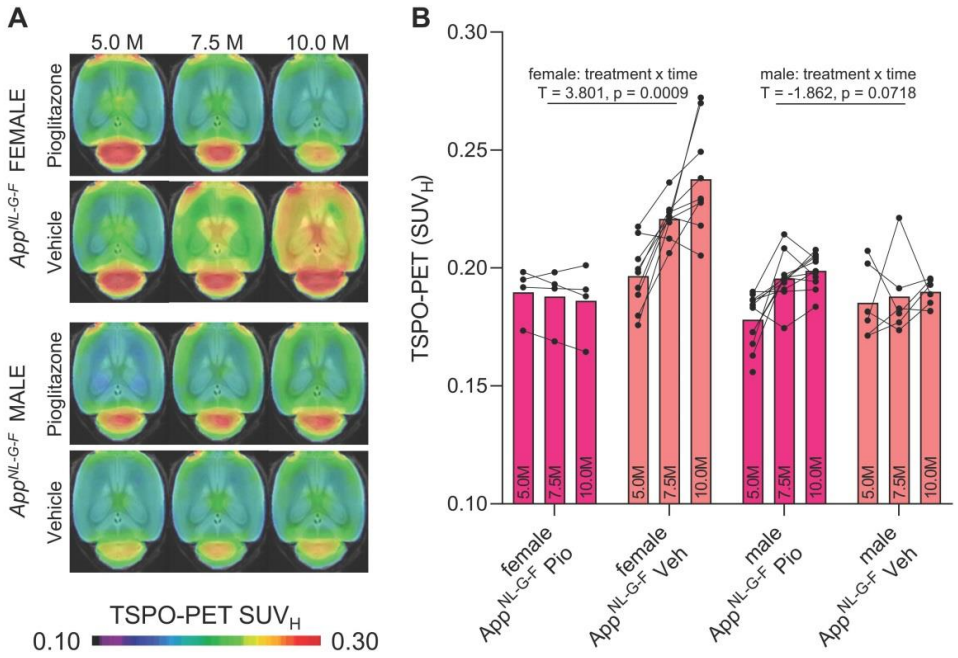

Figure 2. ^{18}F-GE-180 TSPO-PET monitoring of effects of chronic pioglitazone treatment in female and male *App*$^{NL-G-F}$ mice. (**A**) Axial images show group means of the TSPO-PET signal (myocardium scaled standardized uptake value, SUV_H) at different ages in treatment and vehicle groups, projected upon a standard MRI template. Baseline scans were performed prior to therapy initiation. (**B**) Individual time courses of the cortical TSPO-PET signal during the pharmacological treatment period. Statistics derive from a linear mixed model. Female *App*$^{NL-G-F}$ pioglitazone n = 4, female *App*$^{NL-G-F}$ vehicle n = 9, male *App*$^{NL-G-F}$ pioglitazone n = 11, male *App*$^{NL-G-F}$ vehicle n = 6. Pio = pioglitazone treatment, Veh = vehicle treatment.

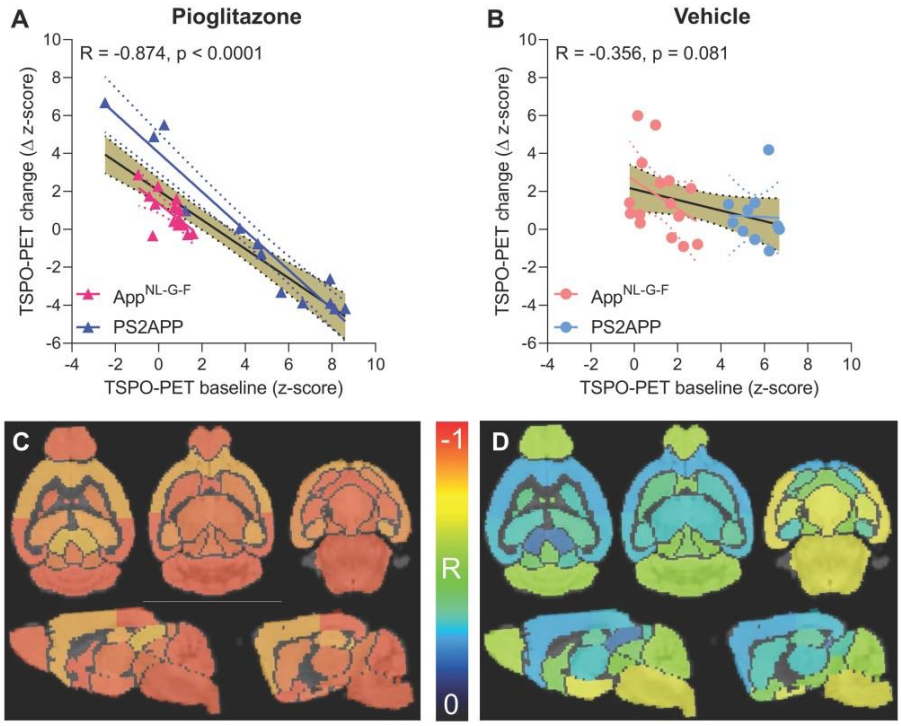

Figure 3. Prediction of changes in microglial activity by the ^{18}F-GE-180 TSPO-PET baseline examination. (**A, B**) Correlation analysis between the TSPO-PET z-score at baseline and the change of the TSPO-PET z-score (baseline to last follow-up) in *App*$^{NL-G-F}$ and PS2APP mice with pioglitazone treatment (**A**) and vehicle controls (**B**). Correlations are illustrated for the combination of both mouse models (gold) and in separate analyses of *App*$^{NL-G-F}$ (red) and PS2APP (blue) mice. (**C, D**) Multiregional analysis of the correlation between the TSPO-PET z-score at baseline and the change of the TSPO-PET z-score (baseline to last follow-up). Re-projected coefficients of correlation (R) are illustrated in axial and sagittal slices projected upon a standard MRI template. *App*$^{NL-G-F}$ and PS2APP mice were analyzed together for the pioglitazone treatment group (**C**) and vehicle controls (**D**). Levels of significance per region after false discovery rate correction for multiple comparisons are provided in **Table 1**.

Table 1. Multi-region analysis of baseline prediction of longitudinal microglial activation by baseline TSPO-PET

Region	Pioglitazone		Vehicle		Contrast
	R	p-value (FDR-corrected)	R	p-value (FDR-corrected)	ΔR
Striatum R	-0.941	4.9E-13***	-0.427	0.12	0.514
Striatum L	-0.899	1.0E-10***	-0.342	0.12	0.557
Hippocampus R	-0.879	8.6E-10***	-0.344	0.12	0.535
Hippocampus L	-0.854	8.6E-09***	-0.388	0.083	0.466
Thalamus	-0.920	7.8E-12***	-0.326	0.13	0.594
Cerebellum	-0.952	1.4E-13***	-0.584	0.0066**	0.368
Basal forebrain & septum	-0.949	1.4E-13***	-0.516	0.017*	0.433
Hypothalamus	-0.936	8.6E-13***	-0.705	0.0009***	0.231
Amygdala R	-0.935	8.6E-13***	-0.665	0.0012**	0.270
Amygdala L	-0.935	9.0E-13***	-0.666	0.0015**	0.269
Brainstem	-0.943	1.4E-12***	-0.691	0.0009***	0.252
Central grey	-0.914	1.8E-11***	-0.505	0.019*	0.409
Superior colliculi	-0.804	2.6E-07***	-0.199	0.34	0.605
Olfactory bulb	-0.938	7.5E-13***	-0.603	0.0050**	0.335
Midbrain R	-0.919	9.5E-12***	-0.558	0.0099**	0.361
Midbrain L	-0.922	6.4E-12***	-0.541	0.012*	0.381
Inferior colliculus R	-0.900	3.0E-11***	-0.486	0.11	0.414
Inferior colliculus L	-0.910	9.7E-11***	-0.357	0.024*	0.553
Piriform/entorhinal cortex	-0.883	6.2E-10***	-0.742	0.0005***	0.141
Auditory/visual cortex	-0.947	1.8E-13***	-0.306	0.15	0.641
Motor/sensory cortex	-0.836	3.2E-08***	-0.283	0.18	0.553

Person's correlation coefficients (R) were calculated between baseline TSPO-PET (z-score) and the change in TSPO-PET (Δ z-score) during the five months treatment period in pioglitazone and vehicle treated *App*$^{NL-G-F}$ and PS2APP mice. P-values were adjusted for multiple comparisons by false discovery rate correction. *p < 0.05; **p < 0.01; ***p < 0.001.

PPARγ stimulation induced changes of microglial activation predict spatial learning performance and aggregation of fibrillar Aβ

Next, we asked if altered TSPO expression during chronic pioglitazone treatment has associations with known determinants of therapeutic effects in the AD models. To this end, we correlated the rate of change in the TSPO-PET signal during the treatment period with the individual spatial learning impairment and changes in fibrillary Aβ pathology measured post mortem. Better spatial learning was associated with an attenuated increase of the TSPO-PET signal during five months of PPARγ stimulation in PS2APP mice (R = -0.733, p = 0.0043, **Figure 4A-B**), but the association did not reach statistical significance in *App*$^{NL-G-F}$ mice (R = -0.349, p = 0.221, **Figure 4C-D**). The observed effect in PS2APP mice was treatment-specific, since there was no association between altered TSPO expression and spatial learning in vehicle treated mice (R = -0.032, p = 0.991, **Figure 4B**). Our dedicated analysis of Aβ

species during chronic PPARγ stimulation in this same cohort [12] revealed a greater increase in fibrillar Aβ, which is the major source of the Aβ-PET signal [31], in both treated mouse models compared to their vehicle controls, which reflected a shift of Aβ plaques towards a more fibrillary composition. Meanwhile, the non-fibrillar proportion of plaques decreased upon the treatment, as is reported elsewhere [12]. A low area under the curve (AUC) of TSPO-PET signal during the recording period was associated with a higher rate of change of fibrillar Aβ in pioglitazone-treated PS2APP ($R = -0.600$, $p = 0.030$, **Figure 4E-F**) and *App*$^{NL\text{-}G\text{-}F}$ mice ($R = -0.553$, $p = 0.040$, **Figure 4G-H**). Vehicle controls of both models did not show significant associations between the TSPO-PET AUC and changes in fibrillary Aβ pathology.

^{18}F-GE-180 TSPO-PET signal reflects activated microglia

Finally, we set about to elucidate the molecular source of the TSPO-PET signal. Earlier studies have already validated *in vivo* TSPO-PET as a microglial marker relative to immunohistochemistry *ex vivo* [10, 11] and we have elsewhere demonstrated that PPARγ-related modulation of microglia can be detected by terminal immunohistochemistry in these mouse models [12]. However, the molecular and cellular correlates of altered TSPO expression during pharmacological PPARγ stimulation remained unclear. To establish this relationship, we performed an immunohistochemical validation of TSPO-PET in subpopulations of all study groups using antibodies against a general marker of microglia (Iba-1) and a specific marker of microglial activation (CD68).

Iba-1 ($R = 0.790$, $p < 0.0001$, **Figure 5A**) and CD68 ($R = 0.952$, $p < 0.0001$, **Figure 5B**) immunohistochemistry results correlated highly with TSPO-PET binding *in vivo*. Importantly, we saw a stronger association between TSPO-PET with CD68 labelling, which we attribute to the lesser differentiation of Iba-1 immunohistochemistry for treated *App*$^{NL\text{-}G\text{-}F}$ and PS2APP. Indeed, Iba-1 immunohistochemistry did not differentiate between treated *App*$^{NL\text{-}G\text{-}F}$ and treated PS2APP mice. The lacking differentiation of pioglitazone-treated PS2APP and *App*$^{NL\text{-}G\text{-}F}$ mice by Iba-1 immunohistochemistry was also discernible at the individual mouse level (**Figure 5C**).

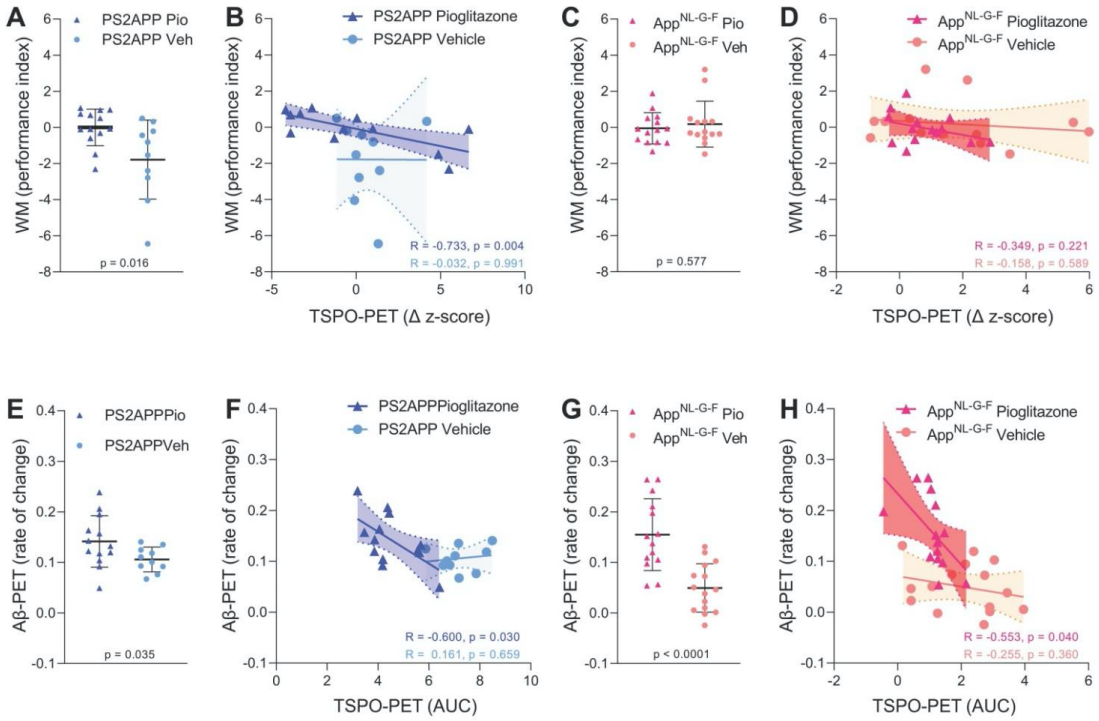

Figure 4. Associations of ^{18}F-GE-180 TSPO-PET findings with spatial learning performance and Aβ accumulation. (**A**) Water maze (WM) performance index (principal component analysis, PCA, higher score means better performance) in the comparison of PS2APP mice after five months pioglitazone treatment and their vehicle controls. (**B**) Correlation between the longitudinal change of TSPO-PET in PS2APP mice and the water maze performance index. (**C**) Water maze performance index in the comparison of *App*$^{NL\text{-}G\text{-}F}$ mice after five months pioglitazone treatment and their vehicle controls. (**D**) Correlation between the longitudinal change of TSPO-PET in *App*$^{NL\text{-}G\text{-}F}$ mice and the water maze performance index. (**E**) Aβ-PET rate of change (Δ SUVR) in the comparison of PS2APP mice after five months pioglitazone treatment and their vehicle controls [12]. (**F**) Correlation between the TSPO-PET rate of change in PS2APP mice and the Aβ-PET rate of change. (**G**) Aβ-PET rate of change (Δ SUVR) in the comparison of *App*$^{NL\text{-}G\text{-}F}$ mice after five months pioglitazone treatment and their vehicle controls [12]. (**H**) Correlation between the TSPO-PET rate of change in *App*$^{NL\text{-}G\text{-}F}$ mice and the Aβ-PET rate of change. P-values of the group comparisons derive from an unpaired two-tailed t-test. R- and P-values of the correlation analyses derive from a Pearson correlation. PS2APP pioglitazone n = 13, PS2APP vehicle n = 10, *App*$^{NL\text{-}G\text{-}F}$ pioglitazone n = 15, *App*$^{NL\text{-}G\text{-}F}$ vehicle n = 15. AUC = area under the curve.

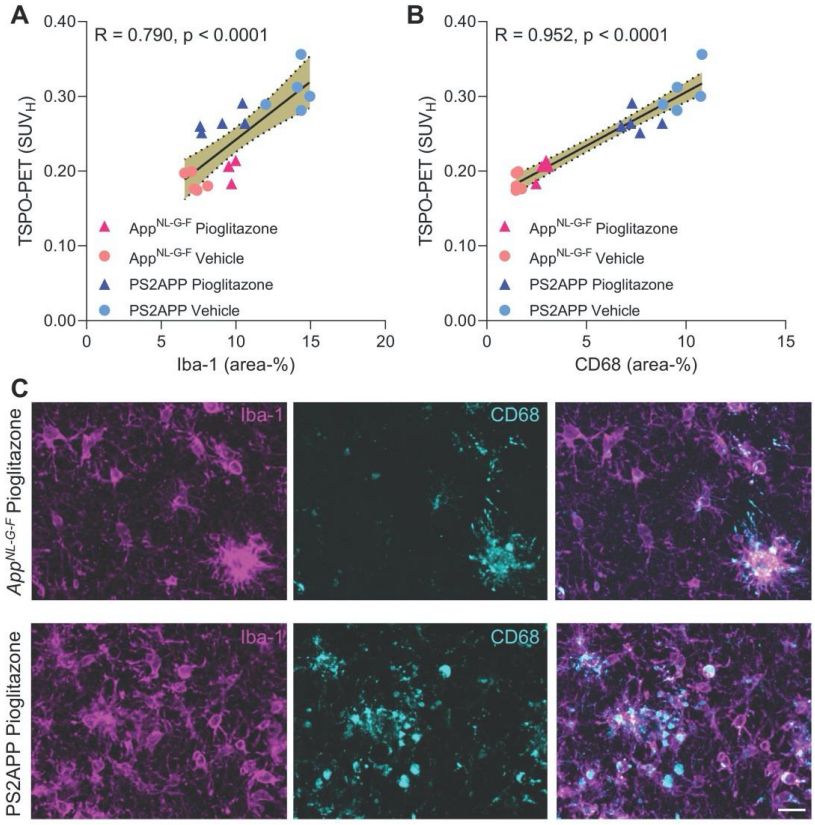

Figure 5. A, B: Correlation analysis between immunohistochemistry markers of microglial activation and ^{18}F-GE-180 TSPO-PET at the terminal time-point. *App*$^{NL-G-F}$ pioglitazone n = 4, *App*$^{NL-G-F}$ n = 5, PS2APP pioglitazone n = 5, PS2APP vehicle n = 5. Error bands represent the 95% confidence intervals. SUV$_H$ = standardized uptake value including myocardium correction. R = Pearson's coefficient of correlation. **C:** Representative immunohistochemistry images of treated *App*$^{NL-G-F}$ and PS2APP mice, indicating a similar Iba-1 area coverage but a higher CD68 area coverage of PS2APP mice compared to *App*$^{NL-G-F}$. The differentiation by CD68 fitted to corresponding TSPO-PET images, clearly showing an elevated TSPO-PET signal in PS2APP mice compared to *App*$^{NL-G-F}$. Scale bar = 20 µm.

Discussion

In this longitudinal study, we investigated serial TSPO-PET imaging as a tool for monitoring of chronic immunomodulation in two distinct mouse models of amyloidosis. Here, PET with the TSPO ligand ^{18}F-GE-180 sensitively detected changes of microglial activity upon pharmacological PPARγ stimulation. Furthermore, we discovered an important sex difference in this treatment response. Pre-therapeutic TSPO-PET measures supported the prediction of individual treatment responses across mouse models and sexes, thus indicating that baseline TSPO expression has an association with the effect of immunomodulation. Immunohistochemistry results confirmed that TSPO-PET is sensitive to activated microglia in the present models.

Our results prove that PET with the TSPO ligand ^{18}F-GE-180 can sensitively monitor pioglitazone-induced changes of microglial activity during chronic treatment of AD-model mice. This finding is important given that an earlier PET study using the less avid TSPO ligand ^{11}C-(*R*)-PK11195 failed to detect treatment-induced changes in the TSPO-PET signal during chronic pioglitazone administration in APPPS1 mice [32]. Nonetheless, the ^{11}C-(*R*)-PK11195 methodology was sufficiently sensitive to detect microglial activation in transgenic versus wild-type mice. We note that a head-to-head comparison with an equal treatment setting would be required to draw robust conclusions on the superiority of one tracer over the other. However, earlier studies support our present findings of excellent sensitivity for ^{18}F-GE-180 TSPO-PET, since the tracer outperformed ^{11}C-(R)-PK11195 in a preclinical head-to-head comparison after lipopolysaccharide challenge [33] and revealed higher specific binding *in vivo* when compared to ^{11}C-PBR23 in a human blocking study [34, 35]. Importantly, we successfully measured treatment effects on microglial activation by TSPO-PET in two distinct Aβ mouse models. Here, our use of *App*$^{NL-G-F}$ mice [16] provided evidence that TSPO expression is

altered by pharmacological PPARγ stimulation in mice without overexpression of APP. In line with our data, ^{18}F-GE-180 PET also enabled the detection of *reduced* microglial activation during neurotrophin receptor modulation by LM11A-31 [9]. Furthermore, ^{18}F-GE-180 PET sensitively detected different temporal patterns of microglial activation upon administration of several anti-pyroglutamate-3 Aβ immunotherapy agents [36]. In summary, our PET monitoring of pharmacological PPARγ stimulation clarified that the direct modulation of microglial activity can be captured *in vivo*.

The main finding of our study is that pre-therapeutic and serial TSPO-PET recordings in our chronic pioglitazone treatment paradigm were closely associated with the treatment response. First, mice with high microglial activation at baseline showed stronger treatment effects, which was underpinned by a strong association between high baseline TSPO-PET quantitation and slower rate of increase in the TSPO-PET signal during the five months of PPARγ stimulation. Thus, TSPO-PET imaging of microglial activation may potentially serve as a translational tool [1] that could allow for predictive response stratification before or during immunomodulation in the context of precision medicine. However, we note that lacking standardization of radiotracers and their quantification are hurdles that must be overcome to enable successful translation to human studies. Second, the magnitude of microglial activation during the treatment period had close associations with changes in fibrillar Aβ pathology of both models and with spatial learning performance of PS2APP mice. The present finding of stronger increases of fibrillar Aβ in mice with low baseline microglial activity is entirely in line with our translational study in mice with amyloidosis and AD patients [28]. Thus, the present results strengthen the hypothesis that it is activated microglia that mediate the clearance of excess fibrillar Aβ. Interpretation of the observed association between low microglial activation and a behavioural source of better spatial learning performance calls for some caution. Although a sufficient microglial response seems important to maintain brain function in therapy-naive AD model mice [20], the suppression of microglial activation by PPARγ stimulation was directly correlated with better spatial learning performance in the current study. Thus, we suppose that PPARγ stimulation shifted the already activated microglia (i.e., in mice with high TSPO-PET levels at baseline) towards a more pronounced neuroprotective function. Proving this conjecture might call for a more rigorous discrimination of the M1/M2 phenotypic characteristics than is afforded by present TSPO-PET radiotracers. Nonetheless, present data definitely substantiate that microglia play a major role in the histological and behavioral consequences of cerebral amyloidosis in mice.

Interestingly, we observed a pronounced sex effect on the pioglitazone treatment response in $App^{NL\text{-}G\text{-}F}$ mice. Vehicle-treated female $App^{NL\text{-}G\text{-}F}$ mice showed the previously reported stronger increase of TSPO expression when compared to their male littermates [29], but PPARγ stimulation attenuated this increase in females while tending to exacerbate the course of neuroinflammation in males. This finding may be of remarkable significance, since some pioglitazone studies used only female mice [37] or did not declare the sex of mice [38]. Thus, potential sex effects of PPARγ stimulation might have been missed in these studies. Furthermore, this sex effect merits attention consideration in planning human studies, since levels of sex hormones can impact upon microglial modulation [39]. On the other hand, our parallel detailed analysis of amyloid aggregation during chronic PPARγ stimulation in this cohort did not show relevant sex differences in the rate of increase in Aβ PET signal [12]. Still, the present results fit with our previously reported dependency of the Aβ-PET rate of change in microglial activation in AD model mice [28], since pioglitazone treatment in male and female $App^{NL\text{-}G\text{-}F}$ mice resulted in similar microglia activation levels at the end of the study. Interestingly, a study using the same TSPO radiotracer similarly found a specific response of the PET signal in female APP/PS1dE9 mice to ^{56}Fe radiation [40]. Thus, sex differences need to be taken into consideration when planning TSPO-PET imaging studies of Aβ mouse models. The small number of female mice treated with pioglitazone and the unbalanced comparison of female and male $App^{NL\text{-}G\text{-}F}$ mice must be considered as limitations of the current study. Thus, the present results should stimulate confirmatory studies in different Aβ and tau mouse models together with studies involving manipulation of sex hormones, aiming to describe more mechanistically the observed sex differences.

We initiated PPARγ therapy at ages manifesting an early phase of limited fibrillar amyloidosis in both mouse models, thus emulating an early but detectable stage of the human AD continuum [41]. In consideration of emerging plasma biomarkers for AD pathology [42], novel treatments for AD shall likely be initiated at a comparable disease stage in future clinical studies. Thus, we focused our intervention monitoring on the phase of amyloid aggregation, which revealed the greatest therapeutic response in those AD model mice with a seemingly more aggressive microglial activation during the early

amyloid build-up phase. Thus, insofar as PET, cerebrospinal fluid, or plasma biomarkers of microglial activation could serve for treatment stratification in patients with early AD that have a positive Aβ-status, we foresee opportunities emerging for personalized precision medicine. The major drawback of current mouse AD models is the missing conversion of a sole Aβ-positive stage (A+T-) to combined Aβ/tau-positivity (A+T+). Although the recent literature describes novel combinations of Aβ/tau gene modification [43, 44], these models still do not present a breakthrough in better mimicking human AD. Conceivably, cortical tau seeding in an Aβ mouse model might yield a more AD-like model of tauopathy, but such models are not yet ready for large scaled testing of drugs [45]. Thus, we note as a limitation of the present study that we were unable to investigate effects of pioglitazone on conversion to tau-positivity or during subsequent tau spreading. As a consequence, we cannot predict the efficacy of chronic PPARγ stimulation on the tauopathy encountered at late stages of AD.

The molecular sources of the TSPO-PET signal in neurodegenerative diseases remained to be fully elucidated [35]. We undertook a correlation analysis between TSPO-PET and immunohistochemistry endpoints in heterogeneous samples of two mouse models, factoring for age, sex, and presence or absence of immunomodulation. Here, we found that the activated microglial marker CD68 proved to have a much better correlation with TSPO-PET signal. In contrast, Iba-1 immunohistochemistry did not distinguish between PS2APP and *App*$^{NL\text{-}G\text{-}F}$ mice after pioglitazone treatment, although the two groups were clearly separated by TSPO-PET and CD68 immunohistochemistry. This finding is in line with the first ^{18}F-GE-180 study in rodent models of AD which showed a co-localization between TSPO and CD68 [46]. Thus, TSPO-PET is very sensitive to detect disease-associated microglial activation, which also fits to the strong correlations between CD68 and TSPO-PET reported in Trem2-deficient APPPS1 mice [11]. As a major limitation, we note that we cannot draw detailed conclusions on the specificity of the TSPO-PET signal since we did not measure associations with reactive astrocytosis to GFAP immunohistochemistry. Furthermore, although we standardized isoflurane levels across all genotype and treatment groups, we cannot exclude a general impact of isoflurane on the variance in TSPO-PET [47]. Effects of anesthesia on TSPO-PET in mice may hamper the translation to human data since patients are only very rarely imaged under general anesthesia.

PPARγ receptor agonists represent a rather unspecific drug since PPARγ is involved in various pathways in addition to peroxisome activation, notably including glucose metabolism and insulin sensitization [48]. We selected pioglitazone for immunomodulation of microglial activity in AD mouse models as the effects of this drug are well understood. Nonetheless, more specific drugs like NLRP3 regulators [49] could enable a more direct targeting of the inflammasome in neurodegenerative diseases. Optimization of immunomodulation strategies could potentially improve their effectiveness and reduce their side effects, whereupon our present TSPO-PET imaging paradigm would be readily transferable to other drugs, so long as they target activated microglia. Ultimately, specific radioligands for different microglia phenotypes [50] could enhance the monitoring of immunomodulation *in vivo*. However, it needs to be considered that the transcriptome of human microglia is more complex than that of rodent microglia [51]. This implies that development and translation of radiotracers for specific microglia phenotypes need to be conducted carefully and in close collaboration with transcriptome sequencing experts.

Conclusion

TSPO-PET serves as a sensitive biomarker for *in vivo* monitoring of immunomodulation in mouse AD models. Pre-therapeutic assessment of microglial activation in individual mice was associated with the response to immunomodulation therapy, indicating that a biomarker of microglial activation could predict treatment effects. There were pronounced sex differences in the responses to PPARγ stimulation effects *in vivo*. The observed heterogeneity of treatment responses in mice with equal genetic background calls for testing of similar concepts in the design of biomarker studies assessing effects of immunomodulation on microglial activation in translational trials in AD patients.

Supplementary Material

Supplemental Figure S1.
http://www.thno.org/v11p8964s1.pdf

Acknowledgements

The study was supported by the *FöFoLe* Program of the Faculty of Medicine of the Ludwig Maximilian University, Munich (grant to M.B.). This work was funded by the Deutsche Forschungsgemeinschaft (DFG, German Research Foundation) to A.R. and M.B. – project numbers BR4580/1-1/ RO5194/1-1. The work was supported by the Deutsche Forschungsgemeinschaft (DFG, German Research Foundation) under Germany's Excellence Strategy within the framework of the Munich Cluster for

Systems Neurology (EXC 2145 SyNergy – ID 390857198). M.B. was supported by the Alzheimer Forschung Initiative e.V (grant number 19063p). We thank Karin Bormann-Giglmaier and Rosel Oos for excellent technical assistance. We thank Christian Haass for excellent support and supervision of the project. We thank Takashi Saito and Takaomi C. Saido for providing the *App*$^{NL-G-F}$ mice. GE Healthcare made GE-180 cassettes available through an early-access model. The authors acknowledge Inglewood Biomedical Editing for professional editing of the manuscript.

Competing Interests

K.B. is an employee of Roche. M.B. received speaker honoraria from GE healthcare, Roche and LMI and is an advisor of LMI.

References

1. Heneka MT, Carson MJ, Khoury JE, Landreth GE, Brosseron F, Feinstein DL, et al. Neuroinflammation in Alzheimer's disease. Lancet Neurol. 2015; 14: 388-405.
2. Fakhoury M. Microglia and astrocytes in Alzheimer's disease: Implications for therapy. Curr Neuropharmacol. 2018; 16: 508-18.
3. Ahmad MH, Fatima M, Mondal AC. Influence of microglia and astrocyte activation in the neuroinflammatory pathogenesis of Alzheimer's disease: Rational insights for the therapeutic approaches. J Clin Neurosci. 2019; 59: 6-11.
4. Zou C, Shi Y, Ohli J, Schuller U, Dorostkar MM, Herms J. Neuroinflammation impairs adaptive structural plasticity of dendritic spines in a preclinical model of Alzheimer's disease. Acta Neuropathol. 2016; 131: 235-46.
5. Mandrekar-Colucci S, Karlo JC, Landreth GE. Mechanisms underlying the rapid peroxisome proliferator-activated receptor-gamma-mediated amyloid clearance and reversal of cognitive deficits in a murine model of Alzheimer's disease. J Neurosci. 2012; 32: 10117-28.
6. Burns DK, Chiang C, Welsh-Bohmer KA, Brannan SK, Culp M, O'Neil J, et al. The TOMMORROW study: Design of an Alzheimer's disease delay-of-onset clinical trial. Alzheimers Dement (N Y). 2019; 5: 661-70.
7. Scott G, Zetterberg H, Jolly A, Cole JH, De Simoni S, Jenkins PO, et al. Minocycline reduces chronic microglial activation after brain trauma but increases neurodegeneration. Brain. 2018; 141: 459-71.
8. Wolf BJ, Brackhan M, Bascunana P, Leiter I, Langer BLN, Ross TL, et al. TSPO PET identifies different anti-inflammatory minocycline treatment response in two rodent models of epileptogenesis. Neurotherapeutics. 2020; 17: 1228-38.
9. James ML, Belichenko NP, Shuhendler AJ, Hoehne A, Andrews LE, Condon C, et al. [(18)F]GE-180 PET detects reduced microglia activation after LM11A-31 therapy in a mouse model of Alzheimer's disease. Theranostics. 2017; 7: 1422-36.
10. Brendel M, Probst F, Jaworska A, Overhoff F, Korzhova V, Albert NL, et al. Glial activation and glucose metabolism in a transgenic amyloid mouse model: A triple-tracer PET study. J Nucl Med. 2016; 57: 954-60.
11. Parhizkar S, Arzberger T, Brendel M, Kleinberger G, Deussing M, Focke C, et al. Loss of TREM2 function increases amyloid seeding but reduces plaque-associated ApoE. Nat Neurosci. 2019; 22: 191-204.
12. Blume T, Deussing M, Biechele G, Peters F, Zott B, Schmidt C, et al. Chronic PPARγ stimulation shifts amyloidosis to higher fibrillarity but improves cognition. bioRxiv. 2021.
13. Richards JG, Higgins GA, Ouagazzal AM, Ozmen L, Kew JN, Bohrmann B, et al. PS2APP transgenic mice, coexpressing hPS2mut and hAPPswe, show age-related cognitive deficits associated with discrete brain amyloid deposition and inflammation. J Neurosci. 2003; 23: 8989-9003.
14. Ozmen L, Albientz A, Czech C, Jacobsen H. Expression of transgenic APP mRNA is the key determinant for beta-amyloid deposition in PS2APP transgenic mice. Neurodegener Dis. 2009; 6: 29-36.
15. Masuda A, Kobayashi Y, Kogo N, Saito T, Saido TC, Itohara S. Cognitive deficits in single App knock-in mouse models. Neurobiol Learn Mem. 2016; 135: 73-82.
16. Saito T, Matsuba Y, Mihira N, Takano J, Nilsson P, Itohara S, et al. Single App knock-in mouse models of Alzheimer's disease. Nat Neurosci. 2014; 17: 661-3.
17. Sacher C, Blume T, Beyer L, Peters F, Eckenweber F, Sgobio C, et al. Longitudinal PET monitoring of amyloidosis and microglial activation in a second-generation amyloid-beta mouse model. J Nucl Med. 2019; 60: 1787-93.
18. Overhoff F, Brendel M, Jaworska A, Korzhova V, Delker A, Probst F, et al. Automated spatial brain normalization and hindbrain white matter reference tissue give improved [(18)F]-florbetaben PET quantitation in Alzheimer's model mice. Front Neurosci. 2016; 10: 45.
19. Deussing M, Blume T, Vomacka L, Mahler C, Focke C, Todica A, et al. Coupling between physiological TSPO expression in brain and myocardium allows stabilization of late-phase cerebral [(18)F]GE180 PET quantification. Neuroimage. 2017; 165: 83-91.
20. Focke C, Blume T, Zott B, Shi Y, Deussing M, Peters F, et al. Early and longitudinal microglial activation but not amyloid accumulation predicts cognitive outcome in PS2APP mice. J Nucl Med. 2019; 60: 548-54.
21. Schiffer WK, Mirrione MM, Biegon A, Alexoff DL, Patel V, Dewey SL. Serial microPET measures of the metabolic reaction to a microdialysis probe implant. J Neurosci Methods. 2006; 155: 272-84.
22. Biechele G, Wind K, Blume T, Sacher C, Beyer L, Eckenweber F, et al. Microglial activation in the right amygdala-entorhinal-hippocampal complex is associated with preserved spatial learning in App(NL-G-F) mice. Neuroimage. 2020: 117707.
23. Sauvage M, Brabet P, Holsboer F, Bockaert J, Steckler T. Mild deficits in mice lacking pituitary adenylate cyclase-activating polypeptide receptor type 1 (PAC1) performing on memory tasks. Brain Res Mol Brain Res. 2000; 84: 79-89.
24. Busche MA, Kekus M, Adelsberger H, Noda T, Forstl H, Nelken I, et al. Rescue of long-range circuit dysfunction in Alzheimer's disease models. Nat Neurosci. 2015; 18: 1623-30.
25. Keskin AD, Kekus M, Adelsberger H, Neumann U, Shimshek DR, Song B, et al. BACE inhibition-dependent repair of Alzheimer's pathophysiology. Proc Natl Acad Sci U S A. 2017; 114: 8631-6.
26. Bromley-Brits K, Deng Y, Song W. Morris water maze test for learning and memory deficits in Alzheimer's disease model mice. J Vis Exp. 2011; 53: 2920.
27. Eckenweber F, Medina-Luque J, Blume T, Sacher C, Biechele G, Wind K, et al. Longitudinal TSPO expression in tau transgenic P301S mice predicts increased tau accumulation and deteriorated spatial learning. J Neuroinflammation. 2020; 17: 208.
28. Ewers M, Biechele G, Suarez-Calvet M, Sacher C, Blume T, Morenas-Rodriguez E, et al. Higher CSF sTREM2 and microglia activation are associated with slower rates of beta-amyloid accumulation. EMBO Mol Med. 2020; 12: e12308.
29. Biechele G, Franzmeier N, Blume T, Ewers M, Luque JM, Eckenweber F, et al. Glial activation is moderated by sex in response to amyloidosis but not to tau pathology in mouse models of neurodegenerative diseases. J Neuroinflammation. 2020; 17: 374.
30. Blume T, Focke C, Peters F, Deussing M, Albert NL, Lindner S, et al. Microglial response to increasing amyloid load saturates with aging: a longitudinal dual tracer *in vivo* muPET-study. J Neuroinflammation. 2018; 15: 307.
31. Biechele G, Sebastian Monasor L, Wind K, Blume T, Parhizkar S, Arzberger T, et al. Glitter in the darkness? Non-fibrillar beta-amyloid plaque components significantly impact the beta-amyloid PET signal in mouse models of Alzheimer's disease. J Nucl Med. 2021; in press.
32. Rapic S, Backes H, Viel T, Kummer MP, Monfared P, Neumaier B, et al. Imaging microglial activation and glucose consumption in a mouse model of Alzheimer's disease. Neurobiol Aging. 2013; 34: 351-4.
33. Dickens AM, Vainio S, Marjamaki P, Johansson J, Lehtiniemi P, Rokka J, et al. Detection of microglial activation in an acute model of neuroinflammation using PET and radiotracers 11C-(R)-PK11195 and 18F-GE-180. J Nucl Med. 2014; 55: 466-72.
34. Sridharan S, Raffel J, Nandoskar A, Record C, Brooks DJ, Owen D, et al. Confirmation of specific binding of the 18-kDa translocator protein (TSPO) radioligand [(18)F]GE-180: a blocking study using XBD173 in multiple sclerosis normal appearing white and grey matter. Mol Imaging Biol. 2019; 21: 935-44.
35. Cumming P, Burgher B, Patkar O, Breakspear M, Vasdev N, Thomas P, et al. Sifting through the surfeit of neuroinflammation tracers. J Cereb Blood Flow Metab. 2018; 38: 204-24.
36. Crehan H, Liu B, Kleinschmidt M, Rahfeld JU, Le KX, Caldarone BJ, et al. Effector function of anti-pyroglutamate-3 Abeta antibodies affects cognitive benefit, glial activation and amyloid clearance in Alzheimer's-like mice. Alzheimers Res Ther. 2020; 12: 12.
37. Dorostkar MM, Burgold S, Filser S, Barghorn S, Schmidt B, Anumala UR, et al. Immunotherapy alleviates amyloid-associated synaptic pathology in an Alzheimer's disease mouse model. Brain. 2014; 137: 3319-26.
38. Seok H, Lee M, Shin E, Yun MR, Lee YH, Moon JH, et al. Low-dose pioglitazone can ameliorate learning and memory impairment in a mouse model of dementia by increasing LRP1 expression in the hippocampus. Sci Rep. 2019; 9: 4414.
39. Pike CJ. Sex and the development of Alzheimer's disease. J Neurosci Res. 2017; 95: 671-80.
40. Liu B, Hinshaw RG, Le KX, Park MA, Wang S, Belanger AP, et al. Space-like (56)Fe irradiation manifests mild, early sex-specific behavioral and neuropathological changes in wildtype and Alzheimer's-like transgenic mice. Sci Rep. 2019; 9: 12118.
41. Jack CR, Jr., Bennett DA, Blennow K, Carrillo MC, Dunn B, Haeberlein SB, et al. NIA-AA Research Framework: Toward a biological definition of Alzheimer's disease. Alzheimers Dement. 2018; 14: 535-62.
42. Bateman RJ, Blennow K, Doody R, Hendrix S, Lovestone S, Salloway S, et al. Plasma biomarkers of AD emerging as essential tools for drug development: An EU/US CTAD task force report. J Prev Alzheimers Dis. 2019; 6: 169-73.

43. Saito T, Mihira N, Matsuba Y, Sasaguri H, Hashimoto S, Narasimhan S, et al. Humanization of the entire murine Mapt gene provides a murine model of pathological human tau propagation. J Biol Chem. 2019; 294: 12754-65.
44. Cohen RM, Rezai-Zadeh K, Weitz TM, Rentsendorj A, Gate D, Spivak I, et al. A transgenic Alzheimer rat with plaques, tau pathology, behavioral impairment, oligomeric abeta, and frank neuronal loss. J Neurosci. 2013; 33: 6245-56.
45. He Z, Guo JL, McBride JD, Narasimhan S, Kim H, Changolkar L, et al. Amyloid-beta plaques enhance Alzheimer's brain tau-seeded pathologies by facilitating neuritic plaque tau aggregation. Nat Med. 2018; 24: 29-38.
46. Liu B, Le KX, Park MA, Wang S, Belanger AP, Dubey S, et al. *In vivo* detection of age- and disease-related increases in neuroinflammation by 18F-GE180 TSPO microPET imaging in wild-type and Alzheimer's transgenic mice. J Neurosci. 2015; 35: 15716-30.
47. Saba W, Goutal S, Kuhnast B, Dolle F, Auvity S, Fontyn Y, et al. Differential influence of propofol and isoflurane anesthesia in a non-human primate on the brain kinetics and binding of [(18)F]DPA-714, a positron emission tomography imaging marker of glial activation. Eur J Neurosci. 2015; 42: 1738-45.
48. Tyagi S, Gupta P, Saini AS, Kaushal C, Sharma S. The peroxisome proliferator-activated receptor: A family of nuclear receptors role in various diseases. J Adv Pharm Technol Res. 2011; 2: 236-40.
49. Swanson KV, Deng M, Ting JP. The NLRP3 inflammasome: molecular activation and regulation to therapeutics. Nat Rev Immunol. 2019; 19: 477-89.
50. Götzl JK, Brendel M, Werner G, Parhizkar S, Sebastian Monasor L, Kleinberger G, et al. Opposite microglial activation stages upon loss of PGRN or TREM2 result in reduced cerebral glucose metabolism. EMBO Molecular Medicine. 2019: e9711.
51. Gerrits E, Heng Y, Boddeke E, Eggen BJL. Transcriptional profiling of microglia; current state of the art and future perspectives. Glia. 2020; 68: 740-55.

8. Publikation Nr. 2

frontiers in Aging Neuroscience

ORIGINAL RESEARCH
published: 30 March 2022
doi: 10.3389/fnagi.2022.854031

Chronic PPARγ Stimulation Shifts Amyloidosis to Higher Fibrillarity but Improves Cognition

Tanja Blume[1†], Maximilian Deussing[2†], Gloria Biechele[3], Finn Peters[1], Benedikt Zott[4,5], Claudio Schmidt[2], Nicolai Franzmeier[6], Karin Wind[1,2], Florian Eckenweber[2], Christian Sacher[2], Yuan Shi[1], Katharina Ochs[1], Gernot Kleinberger[7,8], Xianyuan Xiang[7], Carola Focke[2], Simon Lindner[2], Franz-Josef Gildehaus[2], Leonie Beyer[2], Barbara von Ungern-Sternberg[2], Peter Bartenstein[2], Karlheinz Baumann[9], Helmuth Adelsberger[3], Axel Rominger[10,11], Paul Cumming[2,12], Michael Willem[7], Mario M. Dorostkar[1,13], Jochen Herms[1,10,13†] and Matthias Brendel[1,2,10†]*

[1] DZNE – German Center for Neurodegenerative Diseases, Munich, Germany, [2] Department of Nuclear Medicine, University Hospital of Munich, Ludwig Maximilian University of Munich, Munich, Germany, [3] Department of Radiology, University Hospital of Munich, Ludwig Maximilian University of Munich, Munich, Germany, [4] Institute of Neuroscience, Technical University of Munich, Munich, Germany, [5] Department of Diagnostic and Interventional Neuroradiology, Klinikum Rechts der Isar, Technical University of Munich, Munich, Germany, [6] Institute for Stroke and Dementia Research, University Hospital of Munich, Ludwig Maximilian University of Munich, Munich, Germany, [7] Metabolic Biochemistry, Faculty of Medicine, Biomedical Center (BMC), Ludwig Maximilian University of Munich, Munich, Germany, [8] ISAR Bioscience GmbH, Planegg, Germany, [9] Roche Pharma Research and Early Development, Neuroscience Discovery, Roche Innovation Center Basel, F. Hoffmann-La Roche Ltd., Basel, Switzerland, [10] SyNergy, Ludwig Maximilian University of Munich, Munich, Germany, [11] Department of Nuclear Medicine, Inselspital Bern, Bern, Switzerland, [12] School of Psychology and Counselling, Queensland University of Technology, Brisbane, QLD, Australia, [13] Center for Neuropathology and Prion Research, Ludwig Maximilian University of Munich, Munich, Germany

We undertook longitudinal β-amyloid positron emission tomography (Aβ-PET) imaging as a translational tool for monitoring of chronic treatment with the peroxisome proliferator-activated receptor gamma (PPARγ) agonist pioglitazone in Aβ model mice. We thus tested the hypothesis this treatment would rescue from increases of the Aβ-PET signal while promoting spatial learning and preservation of synaptic density. Here, we investigated longitudinally for 5 months PS2APP mice (N = 23; baseline age: 8 months) and App^{NL-G-F} mice (N = 37; baseline age: 5 months) using Aβ-PET. Groups of mice were treated with pioglitazone or vehicle during the follow-up interval. We tested spatial memory performance and confirmed terminal PET findings by immunohistochemical and biochemistry analyses. Surprisingly, Aβ-PET and immunohistochemistry revealed a shift toward higher fibrillary composition of Aβ-plaques during upon chronic pioglitazone treatment. Nonetheless, synaptic density and spatial learning were improved in transgenic mice with pioglitazone treatment, in association with the increased plaque fibrillarity. These translational data suggest that a shift toward higher plaque fibrillarity protects cognitive function and brain integrity. Increases in the Aβ-PET signal upon immunomodulatory treatments targeting Aβ aggregation can thus be protective.

Keywords: pioglitazone, Aβ-PET, App^{NL-G-F} mice, PS2APP mice, microglia, Aβ-plaque composition

OPEN ACCESS

Edited by:
Rodrigo Morales, University of Texas Health Science Center at Houston, United States

Reviewed by:
Jaqueline Generoso, Universidade do Extremo Sul Catarinense, Brazil
Raquel Sanchez-Varo, Universidad de Málaga, Spain

***Correspondence:**
Matthias Brendel
matthias.brendel@med.uni-muenchen.de

† These authors have contributed equally to this work

Specialty section:
This article was submitted to Alzheimer's Disease and Related Dementias, a section of the journal Frontiers in Aging Neuroscience

Received: *13 January 2022*
Accepted: *25 February 2022*
Published: *30 March 2022*

Citation:
Blume T, Deussing M, Biechele G, Peters F, Zott B, Schmidt C, Franzmeier N, Wind K, Eckenweber F, Sacher C, Shi Y, Ochs K, Kleinberger G, Xiang X, Focke C, Lindner S, Gildehaus F-J, Beyer L, von Ungern-Sternberg B, Bartenstein P, Baumann K, Adelsberger H, Rominger A, Cumming P, Willem M, Dorostkar MM, Herms J and Brendel M (2022) Chronic PPARγ Stimulation Shifts Amyloidosis to Higher Fibrillarity but Improves Cognition. Front. Aging Neurosci. 14:854031. doi: 10.3389/fnagi.2022.854031

INTRODUCTION

Alzheimer's disease (AD) has become the most common cause of dementia, and is imposing a significant burden on health care systems of societies with aging populations (Ziegler-Graham et al., 2008). During the past few decades, research on AD pathogenesis led to the formulation of a model that accumulation of amyloid beta (Aβ)-plaques and neurofibrillary tangles, the histologically characterizing hallmarks of AD (Braak and Braak, 1991), triggers a cascade of neurodegenerative events, leading to disease progression (Sasaguri et al., 2017). Additionally, novel emerging evidence indicates that neuroinflammation plays an important role in pathogenesis and progression of AD and many other neurodegenerative diseases (Zimmer et al., 2014; Heneka et al., 2015). In AD, activated microglial cells are able to bind and phagocytize soluble Aβ, and to some degree also the fibrillary Aβ aggregates, as part of the increased inflammatory response (Heneka et al., 2015). However, others report that Aβ-recognition receptors on microglia downregulate during the progression of AD, such that microglial cells eventually undergo senescence, characterized by reduced phagocytosis of Aβ-aggregates (Hickman et al., 2008). With time, the decreased microglial activity is permissive to expansion of fibrillar amyloidosis (Heppner et al., 2015; Blume et al., 2018) and a high proportion of dystrophic microglia were observed in human AD brain *post mortem* (Streit et al., 2014). These observations have led some to speculate that the microglial response is overwhelmed by the massive Aβ-deposition occurring in advanced AD, such that their chronic activation has a detrimental impact on disease progression (Hickman et al., 2008; Lee and Landreth, 2010).

It might follow that treatment with anti-inflammatory drugs should alleviate AD progression. Pioglitazone is an anti-inflammatory insulin sensitizer widely used to treat hyperglycemia in type 2 diabetes *via* activation of peroxisome proliferator-activated receptor gamma (PPAR-γ). Treatment with pioglitazone enables microglial cells to undergo a phenotypic conversion from a pro-inflammatory toward an anti-inflammatory and neuroprotective phenotype (Mandrekar-Colucci et al., 2012; Yamanaka et al., 2012). Furthermore, activation of PPAR-γ in the brains of AD mice initiate a coupled metabolic cycle with the Liver X Receptor to increase brain apolipoprotein E levels, which promotes the ability of microglial cells to phagocyte and degrade both soluble and fibrillary Aβ (Mandrekar-Colucci et al., 2012; Yamanaka et al., 2012). However, another study showed that only low-dose PPAR-γ agonist treatment, but not the conventional doses, promotes an Aβ-clearing effect by increasing (LDL Receptor Related Protein 1 (LRP1) in human brain microvascular endothelial cells (HBMECs) (Moon et al., 2012). Despite this compelling preclinical evidence, a meta-analysis encompassing nine clinical studies did not compelling support a beneficial effect of PPAR-γ agonist treatment on cognition and memory in in patients with mild-to-moderate AD (Cheng et al., 2016). Furthermore, a phase III trial of pioglitazone in patients with mild AD was discontinued due to lacking efficacy (Geldmacher et al., 2011). It remains a conundrum why the translation of PPARγ stimulation into human AD failed, which calls for further investigation to uncover the basis of the seemingly false lead. Conceivably, the efficacy of pioglitazone may be confined to a specific stage of AD, or in cases distinguished by a particular biomarker.

Given this background, we hypothesized that Aβ-load and composition would determine the individual efficacy of PPARγ stimulation effect in the progression of AD mouse models. Therefore, we undertook serial small animal positron emission tomography (μPET) with the Aβ-tracer [^{18}F]florbetaben (Manook et al., 2012; Rominger et al., 2013; Brendel et al., 2015a,b) in two AD mouse models with distinct Aβ-plaque composition. The transgenic PS2APP-line develops dense fibrillary Aβ-plaques with late debit whereas the knock-In mouse model App^{NL-G-F} develops more diffuse oligomeric Aβ-plaques with early debut. Both strains of mice were treated with pioglitazone or vehicle for 5 months during the phase of main Aβ accumulation. We conducted behavioral assessments of spatial learning and confirmed longitudinal PET findings by immunohistochemical analysis and biochemical analysis, thus aiming to test the hypothesis that response to pioglitazone would depend on the type of Aβ-plaques formed in transgenic mice.

MATERIALS AND METHODS

Study Design

Groups of PS2APP and App^{NL-G-F} mice were randomized to either treatment (PS2APP-PIO $N = 13$, all female; App^{NL-G-F}-PIO $N = 14$, $N = 10$ male, $N = 4$ female) or vehicle (PS2APP-VEH $N = 10$, all female; App^{NL-G-F}-VEH $N = 23$ $N = 9$ male, $N = 14$ female) groups at the age of 8 (PS2APP) and 5 (App^{NL-G-F}) months. In PS2APP mice, the baseline [^{18}F]florbetaben-PET scan (Aβ-PET) was performed at the age of 8 months, followed by initiation of pioglitazone treatment or vehicle for a period of 5 months and a follow-up Aβ-PET scan at 13 months. In App^{NL-G-F} mice, the baseline Aβ-PET scan was performed at the age of 5 month, followed by initiation of pioglitazone treatment or vehicle, for a period of 5 months. Follow-up Aβ-PET scans were acquired at 7.5 and 10 months of age, which was the study termination in App^{NL-G-F} mice. Mice were fed *ad libitum* with food pellets formulated with pioglitazone at a dose of 350 mg/kg or unaltered control pellets. The food was available to the mice without restriction.

For all mice, behavioral testing after the terminal PET scan was followed by immunohistochemical and biochemical analyses of randomized hemispheres. The TSPO-PET arm of the study and detailed analyses of neuroinflammation imaging are reported in a separate manuscript focusing on the predictive value of TSPO-PET for outcome of PPARγ-related immunomodulation (Biechele et al., 2022). The sample size estimation of the *in vivo* PET study was based on previous experience and calculated by G*power (V3.1.9.2, Kiel, Germany), assuming a type I error $\alpha = 0.05$ and a power of 0.8 for group comparisons, a 10% drop-out rate per time-point (including TSPO-PET), and a treatment effect of 5% change in the PET signal. Shared datapoints between the study arms are indicated.

Animals

PS2APP transgenic (Ozmen et al., 2008), App^{NL-G-F} APP knock-in (Saito et al., 2014) and wild-type C57Bl/6 mice were used in this investigation (for details see **Supplementary Material**). All experiments were performed in compliance with the National Guidelines for Animal Protection, Germany, with approval of the local animal care committee of the Government of Oberbayern (Regierung Oberbayern) and overseen by a veterinarian. The experiments complied with the ARRIVE guidelines and were carried out in accordance with the U.K. Animals (Scientific Procedures) Act, 1986 and associated guidelines, EU Directive 2010/63/EU for animal experiments. Animals were housed in a temperature and humidity-controlled environment with a 12-h light–dark cycle, with free access to food (Ssniff) and water.

Aβ-PET Acquisition and Reconstruction

[^{18}F]florbetaben radiosynthesis was performed as previously described (Rominger et al., 2013). This procedure yielded a radiochemical purity exceeding 98% and a specific activity of 80 ± 20 GBq/μmol at the end of synthesis. Mice were anesthetized with isoflurane (1.5%, delivered *via* a mask at 3.5 L/min in oxygen) and received a bolus injection [^{18}F]florbetaben 12 ± 2 MBq in 150 μL of saline to a tail vein. Following placement in the tomograph (Siemens Inveon DPET), a single frame emission recording for the interval 30–60 min p.i., which was preceded by a 15-min transmission scan obtained using a rotating [^{57}Co] point source. The image reconstruction procedure consisted of three-dimensional ordered subset expectation maximization (OSEM) with four iterations and twelve subsets followed by a maximum *a posteriori* (MAP) algorithm with 32 iterations. Scatter and attenuation correction were performed and a decay correction for [^{18}F] was applied. With a zoom factor of 1.0 and a 128 × 128 × 159 matrix, a final voxel dimension of 0.78 × 0.78 × 0.80 mm was obtained.

Small-Animal PET Data Analyses

Volumes of interest (VOIs) were defined on the MRI mouse atlas (Dorr et al., 2007). A forebrain target VOI (15 mm^3) was used for group comparisons and an additional hippocampal target VOI (8 mm^3) served for correlation analysis with spatial learning. We calculated [^{18}F]florbetaben standard-uptake-value ratios (SUVRs) using the established white matter (PS2APP; 67 mm^3; pons, midbrain, hindbrain and parts of the subcortical white matter) and periaqueductal gray (App^{NL-G-F}; 20 mm^3) reference regions (Brendel et al., 2016; Overhoff et al., 2016; Sacher et al., 2019).

Water Maze

Two different water maze tasks were applied due to changing facilities between the investigations of PS2APP and App^{NL-G-F} cohorts. We used a principal component analysis of the common read outs of each water maze task to generate a robust index for correlation analyses in individual mice (Biechele et al., 2020). The principal component of the water maze test was extracted from three spatial learning read-outs (PS2APP: escape latency, distance, platform choice; App^{NL-G-F}: escape latency, frequency to platform, time spent in platform quadrant). Thus, one quantitative index of water maze performance per mouse was generated for correlation with PET imaging readouts. The experimenter was blind to the phenotype of the animals.

Water Maze in PS2APP Mice

PS2APP and age-matched wild-type mice were subjected to a modified Morris water maze task as described previously (Sauvage et al., 2000; Busche et al., 2015; Keskin et al., 2017; Focke et al., 2019) yielding escape latency, distance to the correct platform and correct choice of the platform as read-outs.

Water Maze in App^{NL-G-F} Mice

App^{NL-G-F} mice (treated and vehicle) and 14 age- and sex-matched wild-type mice (vehicle) underwent a classical Morris water maze test, which was performed according to a standard protocol with small adjustments (Bromley-Brits et al., 2011) as previously described (Sacher et al., 2019). Details are provided in the **Supplementary Material**.

Immunohistochemistry

Immunohistochemistry in brain regions corresponding to PET analyses was performed for fibrillary as well as pre-fibrillary Aβ, microglia and synaptic density as previously published (Dorostkar et al., 2010; Brendel et al., 2017a,b). We obtained immunofluorescence labeling of pre-fibrillary Aβ using NAB228 (Thermo Fisher Scientific, Waltham, Massachusetts, United States) with a dilution of 1:500 (Monasor et al., 2020). For histological staining against fibrillar Aβ, we used methoxy-X04 (TOCRIS, Bristol, United Kingdom) at a dilution of 0.01 mg/ml in the same slice as for NAB228 staining. We obtained immunofluorescence labeling of microglia using an Iba-1 antibody (Wako, Richmond, United States) with a dilution of 1:200 co-stained with CD68 (BioRad, Hercules, CA, United States) with a dilution of 1:100. The synaptic density was measured using an anti-vesicular glutamate transporter 1 (VGLUT1) primary antibody (1:500, MerckMillipore, Billerica, Massachusetts, United States). Quantification was calculated as area-%. Details are provided in the **Supplementary Material**.

Biochemical Characterization of Brain Tissue

DEA (0.2% Diethylamine in 50 mM NaCl, pH 10) and RIPA lysates (20 mM Tris-HCl (pH 7.5), 150 mM NaCl, 1 mM Na2EDTA, 1% NP-40, 1% sodium deoxycholate, 2.5 mM sodium pyrophosphate) were prepared from brain hemispheres. The later was centrifuged at 14,000 g (60 min at 4°C) and the remaining pellet was homogenized in 70% formic acid (FA fraction). The FA fraction was neutralized with 20 × 1 M Tris-HCl buffer at pH 9.5 and used further diluted for Aβ analysis. Aβ contained in FA fractions was quantified by a sandwich immunoassay using the Meso Scale Aβ Triplex plates and Discovery SECTOR Imager 2400 as described previously (Page et al., 2008). Samples were measured in triplicates.

Statistics

The principal component of the water maze test was extracted using SPSS 26 statistics (IBM Deutschland GmbH, Ehningen,

Germany). Prior to the PCA, the linear relationship of the data was tested by a correlation matrix and items with a correlation coefficient < 0.3 were discarded. The Kaiser-Meyer-Olkin (KMO) measure and Bartlett's test of sphericity were used to test for sampling adequacy and suitability for data reduction. Components with an Eigenvalue >1.0 were extracted and a varimax rotation was selected. Water maze results were also used as an endpoint in the dedicated manuscript on serial TSPO-PET in both cohorts (Biechele et al., 2022). For immunohistochemistry quantifications GraphPad Prism (GraphPad Software, San Diego, California, United States) was used. All analyses were performed by an operator blinded to the experimental conditions. Data were normally distributed according to Shapiro—Wilk or D'Agostino-Pearson test. One-way analysis of variance (ANOVA) including Bonferroni *post-hoc* correction was used for group comparisons >2 subgroups. For assessment of inter-group differences at single time points, Student's *t*-test (unpaired, two-sided) was applied. All results are presented as mean ± SEM. *P*-values <0.05 are defined as statistically significant.

RESULTS

Long-Term Pioglitazone Treatment Provokes a Significant Increase of the Aβ-PET Signal in PS2APP Mice

First, we analyzed serial changes of fibrillar amyloidosis under chronic pioglitazone treatment by [^{18}F]florbetaben Aβ-PET in PS2APP mice and wild-type controls. Vehicle treated PS2APP mice showed an elevated Aβ-PET SUVR when compared to vehicle treated wild-type at 8 (+20.4%, $p < 0.0001$) and 13 months of age (+37.9%, $p < 0.0001$). As expected, the Aβ-PET SUVR of wild-type mice did not change between 8 and 13 months of age (0.831 ± 0.003 vs. 0.827 ± 0.008: $p = 0.645$). Surprisingly, pioglitazone treatment provoked a stronger longitudinal increase in the Aβ-PET signal of PS2APP mice (+21.4%) when compared to vehicle treated PS2APP mice (+14.1%, $p = 0.002$). At the follow-up time point, the Aβ-PET SUVR was significantly elevated when compared to untreated PS2APP mice (**Figure 1**; 1.140 ± 0.014 vs. 1.187 ± 0.011; $p = 0.0017$). Pioglitazone treatment in wild-type mice provoked no changes of Aβ-PET SUVR compared to vehicle-treated wild-type mice at the follow-up time-point (0.827 ± 0.008 vs. 0.823 ± 0.005: $p = 0.496$; for images of wild-type mice see **Supplementary Figure 1**). Taken together, we found a significant increase in the Aβ-PET signal, which implied an increase in fibrillary Aβ-levels under pioglitazone treatment in PS2APP mice.

Aβ-PET Detects a Strong Increase of the Fibrillar Aβ-Load in App^{NL-G-F} Mice During Chronic PPARγ Stimulation

Next, we sought to validate our unexpected findings in PS2APP mice a mouse model with differing Aβ plaque composition, namely the App^{NL-G-F} mouse, which has limited fibrillarity due to endogenous expression of APP with three FAD mutations (Saito et al., 2014). Strikingly, the effect of pioglitazone treatment on the Aβ-PET signal was even stronger in App^{NL-G-F} mice than in PS2APP mice. There was a pronounced increase of the Aβ-PET signal during chronic pioglitazone treatment (+17.2%) compared to vehicle (+5.3%, $p < 0.0001$). App^{NL-G-F} mice with pioglitazone treatment had a higher Aβ-PET SUVR at 7.5 (+4.6%, $p = 0.0071$) and 10 (+7.7%, $p < 0.0001$) months of age when compared to vehicle-treated App^{NL-G-F} mice (**Figure 2**). The baseline level of Aβ-PET SUVR was non-significantly lower in treated compared to untreated App^{NL-G-F} mice (0.878 ± 0.010 vs. 0.906 ± 0.006, $p = 0.1350$). In both mouse models, the Aβ-signal increase after pioglitazone-treatment compared to baseline scans was pronounced in the frontotemporal cortex and hippocampal area (**Figures 1A, 2A**). In summary, the pioglitazone treatment augmented the Aβ-PET signal increase in both mouse models; this unexpected result was more pronounced in the App^{NL-G-F} model, which expresses less fibrillary Aβ plaques.

Pioglitazone Triggers A Shift Toward Increased Aβ-Plaque Fibrillarity in Two Distinct Mouse Models of Amyloidosis

Given the unexpected *in vivo* findings, we set about to evaluate the molecular correlates of the potentiation of Aβ-PET signal during pioglitazone treatment in AD model mice. The (immuno)histochemical analysis showed that the observed increase of the Aβ-PET signal was predominantly explicable by a change in plaque composition rather than by a change in plaque density (**Figure 3**). In both mouse models, the proportion of fibrillary Aβ stained with methoxy-X04 increased significantly under pioglitazone treatment compared to vehicle treated animals (PS2APP: 29.6 ± 3.5% vs. 15.2 ± 0.7%, $p = 0.0056$, **Figure 3C**; App^{NL-G-F}: 9.1 ± 1.6% vs. 4.4 ± 0.4%, $p = 0.0001$, **Figure 3D**). Pioglitazone treatment had no significant effect on the proportion of pre-fibrillary Aβ stained with NAB228 in PS2APP mice (PS2APP: 65.4 ± 6.1% vs. 67.0 ± 6.9%, $p = 0.865$, **Figure 3C**). In App^{NL-G-F} mice, however, the proportion of pre-fibrillary Aβ decreased significantly in treated animals (App^{NL-G-F}: 26.7 ± 1.7% vs. 34.5 ± 1.7%, $p = 0.0138$, **Figure 3E**). The effect size of pioglitazone treatment on plaque morphology was larger in App^{NL-G-F} mice than in PS2APP mice, which was reflected by a significantly increased overlay of methoxy-X04 and NAB228 positive plaques proportions in relation to untreated mice (PS2APP: 40.4 ± 3.6% vs. 25.1 ± 2.1%, $p = 0.0075$, **Figure 3C**; App^{NL-G-F}: 35.0 ± 3.4% vs. 12.9 ± 1.3%, $p = 0.0005$, **Figure 3E**). We attribute this effect to the generally diffuse nature of the plaque composition of App^{NL-G-F} mice, which predominantly contain high oligomeric and low fibrillary fractions of Aβ (Monasor et al., 2020) (compare **Figures 3A,B**).

The number of methoxy positive Aβ-plaques were similar between vehicle and pioglitazone treated groups for PS2APP (1,016 ± 107 vs. 1,118 ± 121, $p = 0.547$, **Figure 3D**) and App^{NL-G-F} mice (242 ± 56 vs. 266 ± 33, $p = 0.722$, **Figure 3F**). Notably there was no significant effect of chronic pioglitazone treatment on the different insoluble Aβ species (Aβ40, Aβ42) as well as on the level of the soluble Aβ42-isoform observed in

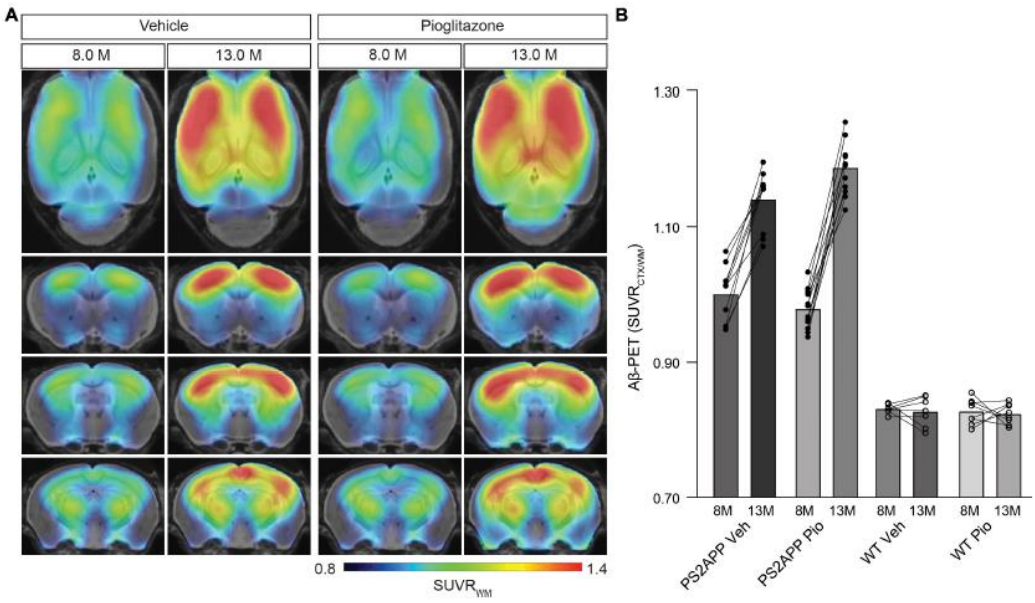

FIGURE 1 | PPARγ stimulation in PS2APP mice provokes an increase in the Aβ-PET signal. **(A)** Regional analysis of group-averaged standardized uptake value ratio (SUVR) images of the Aβ-PET radiotracer [^{18}F]florbetaben in untreated and in pioglitazone-treated PS2APP mice aged 8 and 13 months. Coronal and axial slices are projected upon a standard MRI template. **(B)** Plots show cortical SUVR values of [^{18}F]florbetaben in PS2APP and wild-type (WT) mice between 8 and 13 months of age under vehicle (Veh) or pioglitazone (Pio) treatment. The Aβ-PET signal increased in PS2APP mice during aging, but the increase was more pronounced in pioglitazone treated mice [$F_{(1,\ 12)} = 12.9$; $p = 0.0017$]. In wild-type animals, no difference was observed between untreated and treated animals during aging [$F_{(1,\ 13)} = 0.490$; $p = 0.496$]. Data are presented as mean ± SEM. P values of Bonferroni *post-hoc* test result from two-way ANOVA. $N = 10$–13 PS2APP; $N = 7$–8 WT. PET images of wild-type mice are provided in **Supplementary Figure 1**.

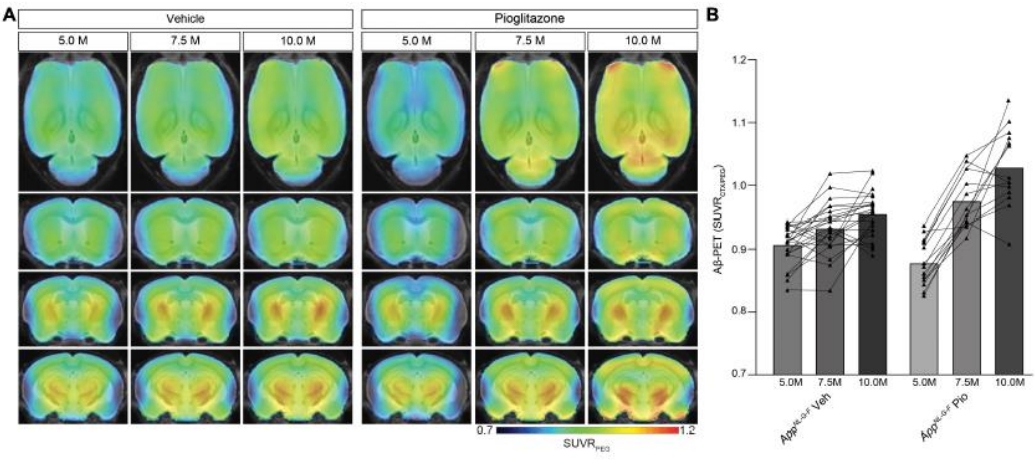

FIGURE 2 | Distinct Aβ-PET signal increase upon PPARγ stimulation in $App^{NL\text{-}G\text{-}F}$ mice with limited plaque fibrillarity and without overexpression of APP. **(A)** Regional analysis of group-averaged standardized uptake value ratios (SUVR) of the Aβ-PET radiotracer [^{18}F]florbetaben in untreated and in pioglitazone treated $App^{NL\text{-}G\text{-}F}$ animals at the age of 5, 7.5, and 10 months. Coronal and axial slices are projected upon a standard MRI template. **(B)** Plots show cortical SUVR of [^{18}F]florbetaben in $App^{NL\text{-}G\text{-}F}$ mice between the age of 5 and 10 months under vehicle or pioglitazone treatment. Aβ-PET signal increased in untreated mice during age but the increase was more pronounced in pioglitazone treated $App^{NL\text{-}G\text{-}F}$ mice [$F_{(2,\ 70)} = 20.12$; $p < 0.0001$]. Data are presented as mean ± SEM. *P*-values of Bonferroni *post-hoc* test result from two-way ANOVA. $N = 14$–23.

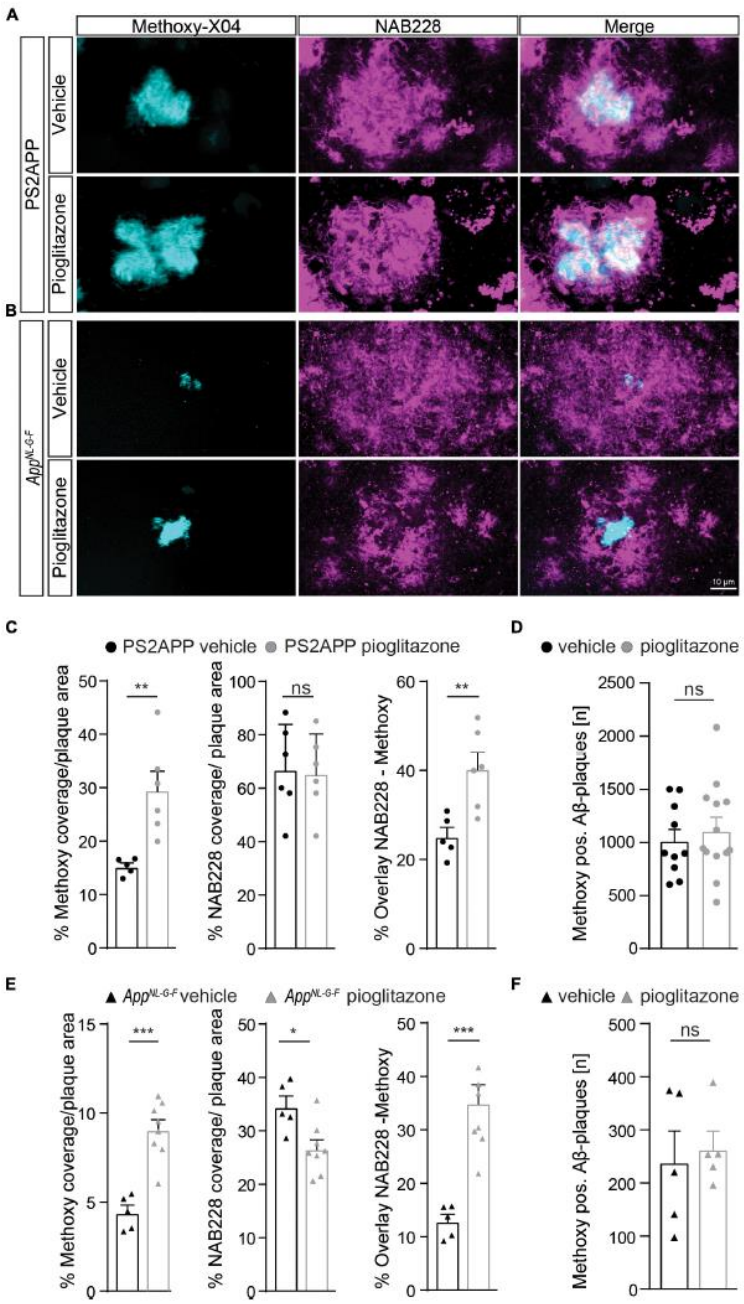

FIGURE 3 | Pioglitazone treatment triggers a change in plaque composition in two different mouse models of amyloidosis. Staining of fibrillary Aβ (methoxy-X04, cyan) and pre-fibrillary Aβ (NAB228, magenta) in vehicle and pioglitazone treated PS2APP mice **(A)** and App^{NL-G-F} mice **(B)**. **(C)** The plaque area covered by methoxy-X04 staining was significantly higher [$t_{(9)} = 3.612$; $p = 0.0056$], whereas the plaque area covered by NAB228 staining remained equal [$t_{(10)} = 0.175$; $p = 0.865$] in pioglitazone treated PS2APP mice. The overlay of NAB228 and methoxy staining increased under pioglitazone treatment [$t_{(9)} = 3.432$; $p = 0.0075$]. **(D)** The number of methoxy positive Aβ-plaques did not change under pioglitazone treatment in PS2APP-mice. **(E)** In App^{NL-G-F} mice, methoxy coverage [$t_{(11)} = 5.802$; $p = 0.0001$], NAB228 coverage [$t_{(11)} = 5.80$; $p = 0.0001$], as well as the overlay of both staining [$t_{(11)} = 2.93$; $p = 0.0138$], increased under pioglitazone treatment. **(F)** In App^{NL-G-F} mice, the number of methoxy positive Aβ-plaques did not change under pioglitazone. Data are presented as mean ± SEM; $n = 5$–13 mice. Two-sample student's *t*-test results: $^*p < 0.05$; $^{**}p < 0.01$; $^{***}p < 0.001$.

either mouse model (**Supplementary Figure 2**). Taken together, our results indicate that the potentiated increase of the Aβ-PET signal upon pioglitazone treatment reflected a change in plaque composition from less dense pre-fibrillar amyloid aggregates to fibrillary Aβ-fractions.

Microglial Activation Is Reduced Upon PPARγ Stimulation in Both Alzheimer's Disease Mouse Models

To confirm changes in the activation state of microglial cells, we performed Iba1 as well as CD68 immunohistochemical staining of activated microglia in both mouse models. We observed that pioglitazone treatment significantly decreased microglial activation in both mouse models (**Figure 4**). In PS2APP mice, PPARγ stimulation provoked a one-third reduction of area coverage of Iba1-positive microglial cells (area: 9.1 ± 0.6%) compared to untreated mice (14.0 ± 0.5%, $p = 0.0003$), and also a significant reduction of CD68-positive microglial cells area (7.6 ± 0.4% vs. 9.9 ± 0.3%, $p = 0.0018$). In pioglitazone treated App^{NL-G-F} mice, the area reduction was less pronounced, but still significant for Iba1-positive microglial cells (9.4 ± 0.2% vs. 10.6 ± 0.2%, $p = 0.0015$) and CD68-positive microglial cells (2.7 ± 0.1% vs. 3.0 ± 0.1%, $p = 0.0141$) compared to untreated mice. Thus, we observed a consistent net reduction of activated microglial coverage in both models; the lesser effect in App^{NL-G-F} mice might indicate partial compensation by triggering of microglial activation due to increased fibrillary Aβ levels (Sebastian et al., 2020).

Cognitive Function Is Improved by Chronic Pioglitazone Treatment in Association With an Increasing Aβ-PET Rate of Change

Finally, we aimed to elucidate whether the observed longitudinal changes in the composition of Aβ-plaques affected synaptic density and hippocampus related cognitive performance.

In PS2APP mice, treatment with pioglitazone resulted in a significant reduction of the water maze performance index compared to untreated mice during the probe trial (**Figure 5A**; $p = 0.0155$), whereas in wild-type animals there was no difference between treated and untreated animals ($p > 0.999$). The water maze performance index of pioglitazone treated PS2APP mice correlated strongly with the rate of increase in Aβ-PET signal (**Figure 5C**; $R = 0.686$; $p = 0.0097$). In App^{NL-G-F} mice, pioglitazone treatment did not result in a significant change of spatial learning performance (**Figure 5B**; $p > 0.999$). Accordingly, the water maze performance index and the rate of change in the Aβ-PET signal of pioglitazone treated App^{NL-G-F} mice did not correlate significantly (**Figure 5D**; $R = 0.341$; $p = 0.254$). There was no significant association between the water maze performance index and the Aβ-PET rate of change in vehicle treated PS2APP or App^{NL-G-F} mice.

To explore the basis of water maze results in PS2APP mice at the molecular level, we performed staining of synaptic density in the hippocampus. Aβ-oligomers are the primary neurotoxic forms of Aβ, while Aβ-fibrils have less neurotoxicity (Hardy and Selkoe, 2002; Haass and Selkoe, 2007; Zott et al., 2019). Thus, we hypothesized that pre-synaptic density in the hippocampal CA1-Area would be rescued upon pioglitazone-treatment. In wild-type mice we did not observe altered changed VGLUT1 density under pioglitazone treatment (**Figure 5E, F**; 0.519 ± 0.007 1/µm vs. 0.502 ± 0.008 1/µm, $p = 0.810$). In PS2APP mice, however, we found that pioglitazone treatment significantly rescued spine density in the CA1-region of the hippocampus compared to untreated animals (**Figures 5E,F**; 0.497 ± 0.006 1/µm vs. 0.459 ± 0.007 1/µm, $p = 0.0012$), supporting the hippocampal-dependent water maze results.

DISCUSSION

To our knowledge, this is the first large-scale longitudinal PET study of cerebral Aβ-deposition in two distinct AD mouse models treated with the PPARγ agonist pioglitazone. We combined *in vivo* PET monitoring with behavioral testing and detailed immunohistochemical analysis. Our main finding was an unexpected potentiation in both mouse models of the increasing Aβ-PET signal during 5 months of pioglitazone treatment. This increase occurred despite an improvement of spatial learning and prevention of synaptic loss in the PS2APP mice. Immunohistochemistry revealed a shift toward plaque composition of higher fibrillarity as the molecular correlate of the Aβ-PET signal in both mouse models. In PS2APP mice this increase was directly associated with improved cognitive performance, whereas in App^{NL-G-F} mice such an effect was not observed.

Aβ-PET enables longitudinal *in vivo* detection of Aβ-plaques, which plays an important role in AD diagnosis, monitoring disease progression, and as an endpoint for therapeutic treatment effects (Valotassiou et al., 2018). In our preceding observational and interventional studies, we validated in AD model mice the clinically established Aβ-PET tracer [^{18}F]florbetaben relative to histologically defined indices Aβ deposition (Brendel et al., 2015a,b). So far, an enhanced or increasing [^{18}F]florbetaben-PET signal has been interpreted as an indicator of disease progression or treatment failure (Laforce et al., 2018). Unexpectedly, we found that pioglitazone potentiated the increasing Aβ-PET signal in two mouse models compared to vehicle controls; in both cases, this increase was due to a shift of the plaque composition toward higher fibrillarity, and away from the more neurotoxic oligomeric form. However, ELISA measurements of plaque associated fibrillary Aβ extracted with formic acid did not indicate a change in the Aβ species composition in brain. This suggests that Aβ-PET imaging and immunohistochemical analysis detect treatment effects on Aβ-plaque composition that do not arise from a shift in the levels of Aβ species, and which may thus evade detection in studies of CSF or plasma content (Hansson et al., 2018).

Furthermore, our study provides evidence that rescued spatial learning deficits and prevented hippocampal synaptic loss can occur despite an increasing Aβ-PET signal upon immunomodulation. The combined results might sound contradictory, but according to the amyloid cascade hypothesis,

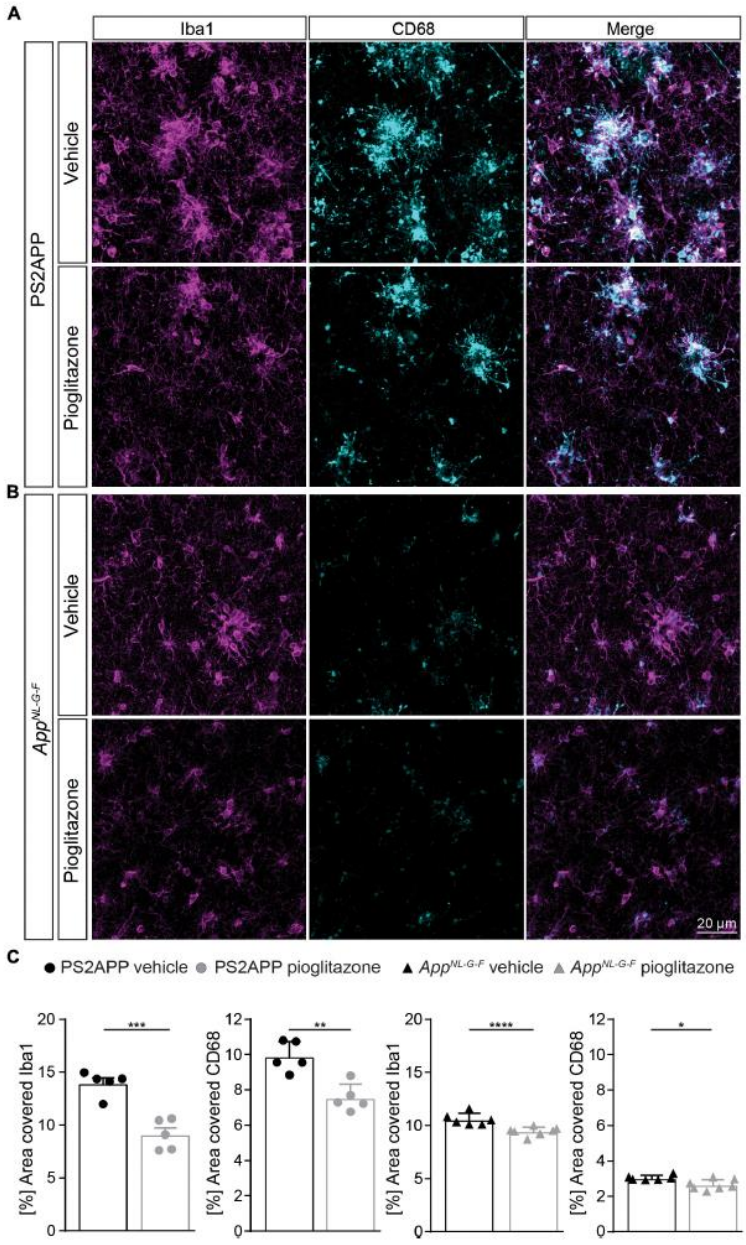

FIGURE 4 | Pioglitazone treatment reduces microglial activation in both AD mouse models. Iba1- (magenta) as well as CD68-(cyan) positive microglial cells in PS2APP **(A)** and App^{NL-G-F} mice **(B)**. **(C)** The area of Iba1 positive microglial cells [$t_{(8)} = 5.95$; $p = 0.0003$] as well as CD68 positive microglial cells [$t_{(8)} = 4.58$; $p = 0.0018$] decreased in treated PS2APP mice. The same effect was observed in App^{NL-G-F} mice were the area covered by Iba1 positive [$t_{(11)} = 4.21$; $p = 0.0015$] as well as CD68 positive microglial cells [$t_{(11)} = 2.91$; $p = 0.014$] were significantly reduced in treated compared to untreated mice. Data are presented as mean ± SEM; $n = 5$–7 mice. Two-sample student's *t*-test results: $^{*}p < 0.05$; $^{**}p < 0.01$; $^{****}p < 0.0001$.

Aβ-oligomers rather than Aβ-fibrils are the neurotoxic Aβ-forms (Haass and Selkoe, 2007; Selkoe and Hardy, 2016). Indeed, high concentrations of Aβ-oligomers isolated from brain of AD patients correlated significantly with the degree of cognitive impairment prior to death (Lue et al., 1999; McLean et al., 1999; Wang et al., 1999). Furthermore, Aβ-oligomers have been shown

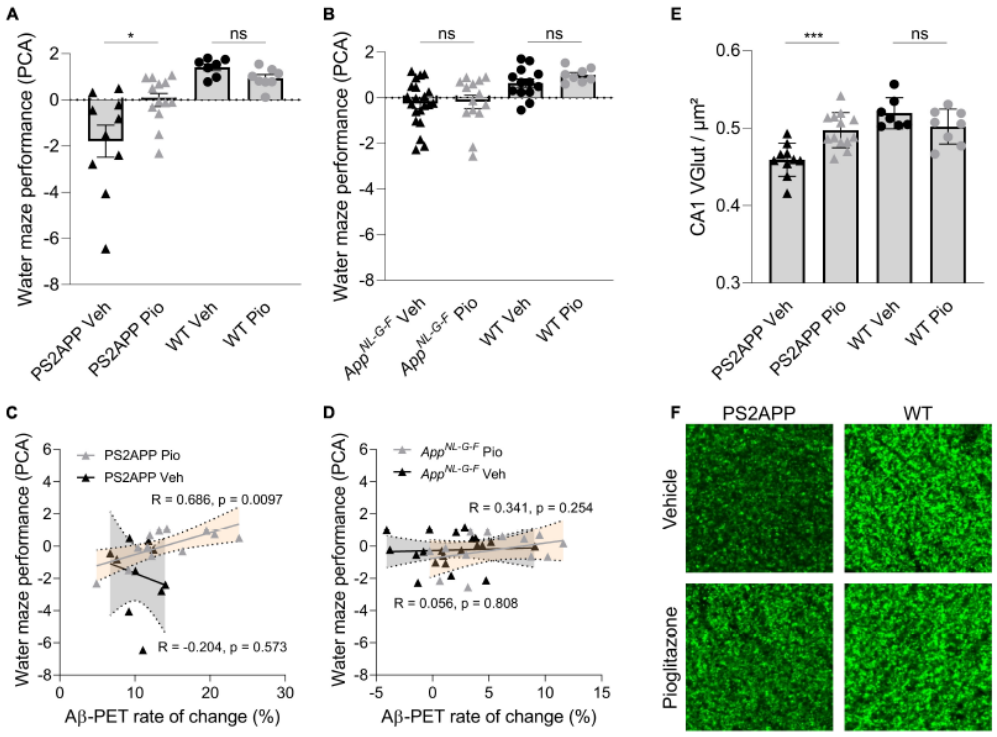

FIGURE 5 | Improved spatial learning correlates with an increased Aβ-PET rate of change in PS2APP mice. **(A)** One-way ANOVA revealed a significant difference of the water maze performance index between pioglitazone treated and untreated PS2APP and wild-type groups [$F_{(3,\ 34)} = 10.37$; $p < 0.0001$; $N = 7–13$]. Group-wise comparisons revealed that pioglitazone treated PS2APP mice achieved a higher performance index in the water maze test compared to untreated PS2APP mice ($p = 0.016$), whereas wild-type animals showed no significant difference between treatment groups ($p > 0.999$). **(B)** One-way ANOVA revealed a significant difference of the water maze performance index between pioglitazone treated and untreated App^{NL-G-F} and WT groups [$F_{(3,\ 34)} = 5.825$; $p = 0.0016$]. However, pioglitazone treated App^{NL-G-F} mice showed no difference in the water maze performance index when compared to untreated App^{NL-G-F} mice ($p > 0.999$) and wild-type animals again showed no significant difference between treatment groups ($p > 0.999$). Scatter plots show correlations between the Aβ-PET rate of change ([^{18}F]florbetaben; ΔSUVR) during the treatment period and individual cognitive testing scores in **(C)** PS2APP mice and in **(D)** App^{NL-G-F} mice (R indicates Pearson's coefficient of correlation) **(E)** The decrease in synaptic density in the hippocampal CA1-region as assessed by VGLUT1 staining was ameliorated in treated PS2APP mice when compared to untreated mice ($p = 0.0012$), whereas no such treatment effect was seen in wild-type animals [$p = 0.810$; group effect: $F_{(3,\ 34)} = 12.03$; $p < 0.0001$; $N = 7–13$]. **(F)** VGLUT1 staining in the hippocampal CA1-region of representative untreated and treated PS2APP mice (left column) as well as of representative untreated and treated wild-type (WT) mice (right column). Statistics of group wise comparisons derive from one-way ANOVA with Bonferroni *post-hoc* correction: $^*p < 0.05$; $^{***}p < 0.005$. Data are presented as mean ± SEM.

to disrupt long-term potentiation at synapses and provoke long-term depression (Cullen et al., 1997; Hu et al., 2008; Klyubin et al., 2014). Thus, improved spatial learning and rescued synaptic density could reflect a therapeutically induced shift of Aβ to hypercondensed plaques, in keeping with observations of greater neuritic damage in association with more diffuse plaques (Ulrich et al., 2014; Wang et al., 2016). Furthermore, strongly in line with our present data, a recent study argued that microglia promoted formation of dense-core plaques may play a protective role in AD (Huang et al., 2021).

The shift in plaque composition was more pronounced in App^{NL-G-F} mice than in the PS2APP model. Due to the expression of the Arctic mutation (Saito et al., 2014), the Aβ-deposits of the App^{NL-G-F} line consist predominantly of Aβ-oligomers (Sacher et al., 2019; Monasor et al., 2020). However, we observed no improvement in cognition in the APP knock-in mouse line after pioglitazone treatment. We attribute the lacking improvement of spatial learning to the minor deterioration of this model in water maze assessment at 10 months of age (Masuda et al., 2016; Sacher et al., 2019). Our present observation stand in contrast with previous studies showing that PPAR-γ agonists reduced Aβ-plaque formation by increasing Aβ-clearance (Camacho et al., 2004; Mandrekar-Colucci et al., 2012; Yamanaka et al., 2012). However, those studies only performed endpoint analyses, in part after short-term treatment of 9 days (Mandrekar-Colucci et al., 2012); the current work is the first to perform longitudinal *in vivo* monitoring of Aβ-deposition over a 5-month chronic PPAR-γ treatment period. We note that the divergent results could also reflect the different markers used for immunohistochemistry

compared to our present differentiated analysis of fibrillar and less dense pre-fibrillar Aβ components. As such, the decreased NAB228-positive plaque fraction in our treated App^{NL-G-F} mice fits to the earlier reported decrease of the 6E10-positive area in APPPS1 mice (Mandrekar-Colucci et al., 2012). We note that the biochemical source of the Aβ-PET signal is still a matter of controversy, since some studies found no impact of non-fibrillar plaque components (Catafau et al., 2016) whereas others postulated a significant contribution of non-fibrillar Aβ to the Aβ-PET signal (Ikonomovic et al., 2016, 2018, 2020). Recently, we were able to show that non-fibrillar components of Aβ plaques indeed contribute to the net Aβ-PET signal (Biechele et al., 2022). Therefore, increases in the [^{18}F]florbetaben-PET signal must be precisely differentiated and interpreted with caution. Development of new PET tracers that selectively target oligomeric Aβ may realize a more precise discrimination of neurotoxic Aβ plaque manifestation (Sehlin et al., 2016; Fang et al., 2019) and its impact on disease severity.

In line with previous pioglitazone studies (Mandrekar-Colucci et al., 2012; Yamanaka et al., 2012), we observed a decrease in microglial activity (Biechele et al., 2021), thus confirming the immunomodulatory effect of the drug. Since earlier studies have shown that fibrillary Aβ-deposits activate microglial cells (Sebastian et al., 2020) which then migrate toward the fibrillar deposits (Füger et al., 2017), resulting in an increased number of activated microglial cells surrounding Aβ-plaques (Blume et al., 2018), the inactivation and migration effects could cancel each other out. Based on our findings in both AD models, we conclude that, by increasing plaque fibrillarity, the immunomodulatory effect of pioglitazone overweighs the potential triggering of activated microglia. Modulating microglial phenotype to restore their salutogenic effects may prove crucial in new therapeutic trials (Lewcock et al., 2020). In several preclinical and clinical trials, pioglitazone proved to be a promising immunomodulatory approach for treatment of AD, especially in patients with comorbid diabetes (Liu et al., 2015; Cao et al., 2018). However, a large phase III trial of pioglitazone in patients with mild AD was discontinued due to lacking efficacy (Geldmacher et al., 2011). Our data calls for monitoring of the effects of PPARγ agonists by Aβ-PET, which may help to stratify treatment responders based on their individual rates of Aβ plaque accumulation. Based on our results, we submit that personalized PPARγ agonist treatment might be effective when the patient has capacity to successfully shift toxic pre-fibrillar Aβ toward fibrillar parts of the plaque.

We note as a limitation that PPARγ receptor agonists represent a rather unspecific class of drugs since PPARγ is involved in various pathways in addition to peroxisome activation, notably including glucose metabolism and insulin sensitization [48]. Future studies should address if the observed effects on Aβ plaque composition are also present for more selective immunomodulation strategies such as NLRP3 regulators [49]. Two different water maze examinations were performed in the present study due a switch of the laboratory. Hence, although we calculated a similar water maze performance index by a PCA of the main read-outs of each examination, the obtained results and the sensitivity to detect spatial learning deficits are not comparable between both Aβ mouse models.

CONCLUSION

In conclusion, chronic pioglitazone treatment provoked a longitudinal Aβ-PET signal increase in transgenic and knock-in mice due to a shift toward hypercondensed fibrillar Aβ plaques. The increasing rate of Aβ-PET signal increase with time was accompanied by ameliorated cognitive performance and attenuated synaptic loss after pioglitazone treatment. It follows that increasing Aβ-PET signal need not always indicate a treatment failure, since it is the composition of Aβ plaques that determines their neurotoxiticy. In summary, our preclinical data indicate that a shift toward increasing fibrillar amyloidosis can be beneficial for the preservation of cognitive function and synaptic integrity.

DATA AVAILABILITY STATEMENT

The raw data supporting the conclusions of this article will be made available by the authors, without undue reservation.

ETHICS STATEMENT

The animal study was reviewed and approved by the Regierung von Oberbayern. Written informed consent was obtained from the owners for the participation of their animals in this study.

AUTHOR CONTRIBUTIONS

KB, HA, AR, PC, MW, MMD, JH, and MB conceived the study and analyzed the results. TB, MD, and MB wrote the manuscript with further input from all co-authors. MD, GB, CSc, KW, FE, CSa, and CF performed the small animal, PET experiments, and small animal PET data analyses. TB, FP, YS, KO, GK, XX, MMD, and JH performed immunohistochemistry experiments, analyses, and interpretation. F-JG and SL performed PET tracer synthesis and analyses. NF analyzed and interpreted serial PET data and contributed to their analysis. GB, BZ, KW, and HA performed spatial learning tests and interpretation. BU-S, KB, and MW supplied the study with animal models and interpreted the dedicated results. All authors contributed with intellectual content.

FUNDING

This study was supported by the FöFoLe Program of the Faculty of Medicine of the Ludwig Maximilian University, Munich (grant to MB). This work was funded by the Deutsche Forschungsgemeinschaft (DFG, German Research Foundation) to AR and MB—project numbers BR4580/1-1/RO5194/1-1. The work was supported by the Deutsche Forschungsgemeinschaft (DFG, German Research Foundation)

under Germany's Excellence Strategy within the framework of the Munich Cluster for Systems Neurology (EXC 2145 SyNergy—ID 390857198). MB was supported by the Alzheimer Forschung Initiative e.V (Grant No. 19063p).

ACKNOWLEDGMENTS

We thank Karin Bormann-Giglmaier and Rosel Oos for excellent technical assistance. Florbetaben precursor was provided by Piramal Imaging. We thank Takashi Saito and Takaomi C. Saido for providing the App^{NL-G-F} mice.

SUPPLEMENTARY MATERIAL

The Supplementary Material for this article can be found online at: https://www.frontiersin.org/articles/10.3389/fnagi.2022.854031/full#supplementary-material

REFERENCES

Biechele, G., Blume, T., Deussing, M., Zott, B., Shi, Y., Xiang, X., et al. (2021). Chronic PPARγ Stimulation Shifts Amyloidosis to Higher Fibrillarity but Improves Cognition. *bioRxiv* [Preprint]. doi: 10.1101/2021.05.30.446348

Biechele, G., Monasor, L. S., Wind, K., Blume, T., Parhizkar, S., Arzberger, T., et al. (2022). Glitter in the Darkness? Non-fibrillar β-Amyloid Plaque Components Significantly Impact the β-Amyloid PET Signal in Mouse Models of Alzheimer Disease. *J. Nucl. Med.* 63, 117–124. doi: 10.2967/jnumed.120.261858

Biechele, G., Wind, K., Blume, T., Sacher, C., Beyer, L., Eckenweber, F., et al. (2020). Microglial Activation in the Right Amygdala-Entorhinal-Hippocampal Complex is Associated with Preserved Spatial Learning in AppNL-G-F mice. *NeuroImage* 230:117707. doi: 10.1016/j.neuroimage.2020.117707

Blume, T., Focke, C., Peters, F., Deussing, M., Albert, N. L., Lindner, S., et al. (2018). Microglial response to increasing amyloid load saturates with aging: a longitudinal dual tracer *in vivo* μPET-study. *J. Neuroinflammation* 15:307. doi: 10.1186/s12974-018-1347-6

Braak, H., and Braak, E. (1991). Neuropathological stageing of Alzheimer-related changes. *Acta Neuropathol.* 82, 239–259. doi: 10.1007/BF00308809

Brendel, M., Kleinberger, G., Probst, F., Jaworska, A., Overhoff, F., Blume, T., et al. (2017b). Increase of TREM2 during Aging of an Alzheimer's Disease Mouse Model Is Paralleled by Microglial Activation and Amyloidosis. *Front. Aging Neurosci.* 9:8. doi: 10.3389/fnagi.2017.00008

Brendel, M., Focke, C., Blume, T., Peters, F., Deussing, M., Probst, F., et al. (2017a). Time Courses of Cortical Glucose Metabolism and Microglial Activity Across the Life Span of Wild-Type Mice: a PET Study. *J. Nucl. Med.* 58, 1984–1990. doi: 10.2967/jnumed.117.195107

Brendel, M., Jaworska, A., Grießinger, E., Rötzer, C., Burgold, S., Gildehaus, F. J., et al. (2015a). Cross-sectional comparison of small animal [18F]-florbetaben amyloid-PET between transgenic AD mouse models. *PLoS One* 10:e0116678. doi: 10.1371/journal.pone.0116678

Brendel, M., Jaworska, A., Herms, J., Trambauer, J., Rötzer, C., Gildehaus, F.-J., et al. (2015b). Amyloid-PET predicts inhibition of de novo plaque formation upon chronic γ-secretase modulator treatment. *Mol. Psychiatry* 20, 1179–1187. doi: 10.1038/mp.2015.74

Brendel, M., Probst, F., Jaworska, A., Overhoff, F., Korzhova, V., Albert, N. L., et al. (2016). Glial Activation and Glucose Metabolism in a Transgenic Amyloid Mouse Model: a Triple-Tracer PET Study. *J. Nucl. Med.* 57, 954–960. doi: 10.2967/jnumed.115.167858

Bromley-Brits, K., Deng, Y., and Song, W. (2011). Morris water maze test for learning and memory deficits in Alzheimer's disease model mice. *J. Vis. Exp.* 53:2920. doi: 10.3791/2920

Busche, M. A., Kekuš, M., Adelsberger, H., Noda, T., Förstl, H., Nelken, I., et al. (2015). Rescue of long-range circuit dysfunction in Alzheimer's disease models. *Nat. Neurosci.* 18, 1623–1630. doi: 10.1038/nn.4137

Camacho, I. E., Serneels, L., Spittaels, K., Merchiers, P., Dominguez, D., and De, S. B. (2004). Peroxisome-proliferator-activated receptor gamma induces a clearance mechanism for the amyloid-beta peptide. *J. Neurosci.* 24, 10908–10917. doi: 10.1523/JNEUROSCI.3987-04.2004

Cao, B., Rosenblat, J. D., Brietzke, E., Park, C., Lee, Y., Musial, N., et al. (2018). Comparative efficacy and acceptability of antidiabetic agents for Alzheimer's disease and mild cognitive impairment: a systematic review and network meta-analysis. *Diabetes Obes. Metab.* 20, 2467–2471. doi: 10.1111/dom.13373

Catafau, A. M., Bullich, S., Seibyl, J. P., Barthel, H., Ghetti, B., Leverenz, J., et al. (2016). Cerebellar Amyloid-β Plaques: how Frequent Are They, and Do They Influence 18F-Florbetaben SUV Ratios? *J. Nucl. Med.* 57, 1740–1745. doi: 10.2967/jnumed.115.171652

Cheng, H., Shang, Y., Jiang, L., Shi, T., and Wang, L. (2016). The peroxisome proliferators activated receptor-gamma agonists as therapeutics for the treatment of Alzheimer's disease and mild-to-moderate Alzheimer's disease: a meta-analysis. *Int. J. Neurosci.* 126, 299–307. doi: 10.3109/00207454.2015.1015722

Cullen, W. K., Suh, Y. H., Anwyl, R., and Rowan, M. J. (1997). Block of LTP in rat hippocampus *in vivo* by beta-amyloid precursor protein fragments. *Neuroreport* 8, 3213–3217. doi: 10.1097/00001756-199710200-00006

Dorostkar, M. M., Dreosti, E., Odermatt, B., and Lagnado, L. (2010). Computational processing of optical measurements of neuronal and synaptic activity in networks. *J. Neurosci. Methods* 188, 141–150. doi: 10.1016/j.jneumeth.2010.01.033

Dorr, A., Sled, J. G., and Kabani, N. (2007). Three-dimensional cerebral vasculature of the CBA mouse brain: a magnetic resonance imaging and micro computed tomography study. *NeuroImage* 35, 1409–1423. doi: 10.1016/j.neuroimage.2006.12.040

Fang, X. T., Hultqvist, G., Meier, S. R., Antoni, G., Sehlin, D., and Syvänen, S. (2019). High detection sensitivity with antibody-based PET radioligand for amyloid beta in brain. *NeuroImage* 184, 881–888. doi: 10.1016/j.neuroimage.2018.10.011

Focke, C., Blume, T., Zott, B., Shi, Y., Deussing, M., Peters, F., et al. (2019). Early and Longitudinal Microglial Activation but Not Amyloid Accumulation Predicts Cognitive Outcome in PS2APP Mice. *J. Nucl. Med.* 60, 548–554. doi: 10.2967/jnumed.118.217703

Füger, P., Hefendehl, J. K., Veeraraghavalu, K., Wendeln, A. C., Schlosser, C., Obermüller, U., et al. (2017). Microglia turnover with aging and in an Alzheimer's model *via* long-term *in vivo* single-cell imaging. *Nat. Neurosci.* 20, 1371–1376. doi: 10.1038/nn.4631

Geldmacher, D. S., Fritsch, T., McClendon, M. J., and Landreth, G. (2011). A randomized pilot clinical trial of the safety of pioglitazone in treatment of patients with Alzheimer disease. *Arch. Neurol.* 68, 45–50. doi: 10.1001/archneurol.2010.229

Haass, C., and Selkoe, D. J. (2007). Soluble protein oligomers in neurodegeneration: lessons from the Alzheimer's amyloid β-peptide. *Nat. Rev. Mol. Cell Biol.* 8, 101–112. doi: 10.1038/nrm2101

Hansson, O., Seibyl, J., Stomrud, E., Zetterberg, H., Trojanowski, J. Q., Bittner, T., et al. (2018). CSF biomarkers of Alzheimer's disease concord with amyloid-β PET and predict clinical progression: a study of fully automated immunoassays in BioFINDER and ADNI cohorts. *Alzheimers Dement.* 14, 1470–1481. doi: 10.1016/j.jalz.2018.01.010

Hardy, J., and Selkoe, D. J. (2002). The amyloid hypothesis of Alzheimer's disease: progress and problems on the road to therapeutics. *Science* 297, 353–356. doi: 10.1126/science.1072994

Heneka, M. T., Carson, M. J., Khoury, J. E., Landreth, G. E., Brosseron, F., Feinstein, D. L., et al. (2015). Neuroinflammation in Alzheimer's disease. *Lancet Neurol.* 14, 388–405. doi: 10.1016/S1474-4422(15)70016-5

Heppner, F. L., Ransohoff, R. M., and Becher, B. (2015). Immune attack: the role of inflammation in Alzheimer disease. Nature reviews. *Neuroscience* 16, 358–372. doi: 10.1038/nrn3880

Hickman, S. E., Allison, E. K., and El Khoury, J. (2008). Microglial Dysfunction and Defective -Amyloid Clearance Pathways in Aging Alzheimer's Disease Mice. *J. Neurosci.* 28, 8354–8360. doi: 10.1523/JNEUROSCI.0616-08.2008

Hu, N. W., Smith, I. M., Walsh, D. M., and Rowan, M. J. (2008). Soluble amyloid-beta peptides potently disrupt hippocampal synaptic plasticity in the absence of cerebrovascular dysfunction *in vivo*. *Brain* 131, 2414–2424. doi: 10.1093/brain/awn174

Huang, Y., Happonen, K. E., Burrola, P. G., O'Connor, C., Hah, N., Huang, L., et al. (2021). Microglia use TAM receptors to detect and engulf amyloid β plaques. *Nat. Immunol.* 22, 586–594. doi: 10.1038/s41590-021-00913-5

Ikonomovic, M. D., Buckley, C. J., Abrahamson, E. E., Kofler, J. K., Mathis, C. A., Klunk, W. E., et al. (2020). Post-mortem analyses of PiB and flutemetamol in diffuse and cored amyloid-β plaques in Alzheimer's disease. *Acta Neuropathol.* 140, 463–476. doi: 10.1007/s00401-020-02175-1

Ikonomovic, M. D., Buckley, C. J., Heurling, K., Sherwin, P., Jones, P. A., Zanette, M., et al. (2016). Post-mortem histopathology underlying β-amyloid PET imaging following flutemetamol F 18 injection. *Acta Neuropathol. Commun.* 4:130. doi: 10.1186/s40478-016-0399-z

Ikonomovic, M. D., Fantoni, E. R., Farrar, G., and Salloway, S. (2018). Infrequent false positive [18 F]flutemetamol PET signal is resolved by combined histological assessment of neuritic and diffuse plaques. *Alzheimers Res. Ther.* 10, 1–4. doi: 10.1186/s13195-018-0387-6

Keskin, A. D., Kekuš, M., Adelsberger, H., Neumann, U., Shimshek, D. R., Song, B., et al. (2017). BACE inhibition-dependent repair of Alzheimer's pathophysiology. *Proc. Natl. Acad. Sci. U. S. A.* 114, 8631–8636. doi: 10.1073/pnas.1708106114

Klyubin, I., Ondrejcak, T., Hayes, J., Cullen, W. K., Mably, A. J., Walsh, D. M., et al. (2014). Neurotransmitter receptor and time dependence of the synaptic plasticity disrupting actions of Alzheimer's disease Aβ *in vivo*. *Philos. Trans. R. Soc. Lond. B Biol. Sci.* 369:20130147. doi: 10.1098/rstb.2013.0147

Laforce, R., Soucy, J.-P., Sellami, L., Dallaire-Théroux, C., Brunet, F., Bergeron, D., et al. (2018). Molecular imaging in dementia: past, present, and future. *Alzheimers Dement.* 14, 1522–1552. doi: 10.1016/j.jalz.2018.06.2855

Lee, C. Y., and Landreth, G. E. (2010). The role of microglia in amyloid clearance from the AD brain. *J. Neural Transm.* 117, 949–960. doi: 10.1007/s00702-010-0433-4

Lewcock, J. W., Schlepckow, K., Di Paolo, G., Tahirovic, S., Monroe, K. M., and Haass, C. (2020). Emerging Microglia Biology Defines Novel Therapeutic Approaches for Alzheimer's Disease. *Neuron* 108, 801–821. doi: 10.1016/j.neuron.2020.09.029

Liu, J., Wang, L. N., and Jia, J. P. (2015). Peroxisome proliferator-activated receptor-gamma agonists for Alzheimer's disease and amnestic mild cognitive impairment: a systematic review and meta-analysis. *Drugs Aging* 32, 57–65. doi: 10.1007/s40266-014-0228-7

Lue, L.-F., Kuo, Y.-M., Roher, A. E., Brachova, L., Shen, Y., Sue, L., et al. (1999). Soluble Amyloid β Peptide Concentration as a Predictor of Synaptic Change in Alzheimer's Disease. *Am. J. Pathol.* 155, 853–862. doi: 10.1016/s0002-9440(10)65184-x

Mandrekar-Colucci, S., Karlo, J. C., and Landreth, G. E. (2012). Mechanisms Underlying the Rapid Peroxisome Proliferator-Activated Receptor- -Mediated Amyloid Clearance and Reversal of Cognitive Deficits in a Murine Model of Alzheimer's Disease. *J. Neurosci.* 32, 10117–10128. doi: 10.1523/JNEUROSCI.5268-11.2012

Manook, A., Yousefi, B. H., Willuweit, A., Platzer, S., Reder, S., Voss, A., et al. (2012). Small-Animal PET Imaging of Amyloid-Beta Plaques with [11C]PiB and Its Multi-Modal Validation in an APP/PS1 Mouse Model of Alzheimer's Disease. *PLoS One* 7:e31310. doi: 10.1371/journal.pone.0031310

Masuda, A., Kobayashi, Y., Kogo, N., Saito, T., Saido, T. C., and Itohara, S. (2016). Cognitive deficits in single App knock-in mouse models. *Neurobiol. Learn. Mem.* 135, 73–82. doi: 10.1016/j.nlm.2016.07.001

McLean, C. A., Cherny, R. A., Fraser, F. W., Fuller, S. J., Smith, M. J., Beyreuther, K., et al. (1999). Soluble pool of Abeta amyloid as a determinant of severity of neurodegeneration in Alzheimer's disease. *Ann. Neurol.* 46, 860–866. < 860:aid-ana8 > 3.0.co;2-m doi: 10.1002/1531-8249(199912)46:6

Monasor, L. S., Müller, S. A., Colombo, A. V., Tanrioever, G., König, J., Roth, S., et al. (2020). Fibrillar Aβ triggers microglial proteome alterations and dysfunction in Alzheimer mouse models. *eLife* 9:e54083 doi: 10.7554/eLife.54083

Moon, J. H., Kim, H. J., Yang, A. H., Kim, H. M., Lee, B.-W., Kang, E. S., et al. (2012). The effect of rosiglitazone on LRP1 expression and amyloid β uptake in human brain microvascular endothelial cells: a possible role of a low-dose thiazolidinedione for dementia treatment. *Int. J. Neuropsychopharmacol.* 15, 135–142. doi: 10.1017/S1461145711001611

Overhoff, F., Brendel, M., Jaworska, A., Korzhova, V., Delker, A., Probst, F., et al. (2016). Automated Spatial Brain Normalization and Hindbrain White Matter Reference Tissue Give Improved [18F]-Florbetaben PET Quantitation in Alzheimer's Model Mice. *Front. Neurosci.* 10:45. doi: 10.3389/fnins.2016.00045

Ozmen, L., Albientz, A., Czech, C., and Jacobsen, H. (2008). Expression of Transgenic APP mRNA Is the Key Determinant for Beta-Amyloid Deposition in PS2APP Transgenic Mice. *Neurodegener. Dis.* 6, 29–36. doi: 10.1159/000170884

Page, R. M., Baumann, K., Tomioka, M., Pérez-Revuelta, B. I., Fukumori, A., Jacobsen, H., et al. (2008). Generation of Abeta38 and Abeta42 is independently and differentially affected by familial Alzheimer disease-associated presenilin mutations and gamma-secretase modulation. *J. Biol. Chem.* 283, 677–683. doi: 10.1074/jbc.M708754200

Rominger, A., Brendel, M., Burgold, S., Keppler, K., Baumann, K., Xiong, G., et al. (2013). Longitudinal Assessment of Cerebral -Amyloid Deposition in Mice Overexpressing Swedish Mutant -Amyloid Precursor Protein Using 18F-Florbetaben PET. *J. Nucl. Med.* 54, 1127–1134. doi: 10.2967/jnumed.112.114660

Sacher, C., Blume, T., Beyer, L., Peters, F., Eckenweber, F., Sgobio, C., et al. (2019). Longitudinal PET Monitoring of Amyloidosis and Microglial Activation in a Second-Generation Amyloid-β Mouse Model. *J. Nucl. Med.* 60, 1787–1793. doi: 10.2967/jnumed.119.227322

Saito, T., Matsuba, Y., Mihira, N., Takano, J., Nilsson, P., Itohara, S., et al. (2014). Single App knock-in mouse models of Alzheimer's disease. *Nat. Neurosci.* 17, 661–663. doi: 10.1038/nn.3697

Sasaguri, H., Nilsson, P., Hashimoto, S., Nagata, K., Saito, T., Strooper, B., et al. (2017). APP mouse models for Alzheimer's disease preclinical studies. *EMBO J.* 36, 2473–2487. doi: 10.15252/embj.201797397

Sauvage, M., Brabet, P., Holsboer, F., Bockaert, J., and Steckler, T. (2000). Mild deficits in mice lacking pituitary adenylate cyclase-activating polypeptide receptor type 1 (PAC1) performing on memory tasks. *Mol. Brain Res.* 84, 79–89. doi: 10.1016/S0169-328X(00)00219-9

Sebastian, M. L., Müller, S. A., Colombo, A. V., Tanrioever, G., König, J., Roth, S., et al. (2020). Fibrillar Aβ triggers microglial proteome alterations and dysfunction in Alzheimer mouse models. *eLife* 9:e54083.

Sehlin, D., Fang, X. T., Cato, L., Antoni, G., Lannfelt, L., and Syvänen, S. (2016). Antibody-based PET imaging of amyloid beta in mouse models of Alzheimer's disease. *Nat. Commun.* 7:306. doi: 10.1038/ncomms10759

Selkoe, D. J., and Hardy, J. (2016). The amyloid hypothesis of Alzheimer's disease at 25 years. *EMBO Mol. Med.* 8, 595–608. doi: 10.15252/emmm.201606210

Streit, W. J., Xue, Q. S., Tischer, J., and Bechmann, I. (2014). Microglial pathology. *Acta Neuropathol. Commun.* 2, 1–17. doi: 10.1186/s40478-014-0142-6

Ulrich, J. D., Finn, M. B., Wang, Y., Shen, A., Mahan, T. E., Jiang, H., et al. (2014). Altered microglial response to Aβ plaques in APPPS1-21 mice heterozygous for TREM2. *Mol. Neurodegener.* 9, 1–9. doi: 10.1186/1750-1326-9-20

Valotassiou, V., Malamitsi, J., Papatriantafyllou, J., Dardiotis, E., Tsougos, I., Psimadas, D., et al. (2018). SPECT and PET imaging in Alzheimer's disease. *Ann. Nucl. Med.* 32, 583–593. doi: 10.1007/s12149-018-1292-6

Wang, J., Dickson, D. W., Trojanowski, J. Q., and Lee, V. M. (1999). The levels of soluble versus insoluble brain Abeta distinguish Alzheimer's disease from normal and pathologic aging. *Exp. Neurol.* 158, 328–337. doi: 10.1006/exnr.1999.7085

Wang, Y., Ulland, T. K., Ulrich, J. D., Song, W., Tzaferis, J. A., Hole, J. T., et al. (2016). TREM2-mediated early microglial response limits diffusion and toxicity of amyloid plaques. *J. Exp. Med.* 213, 667–675. doi: 10.1084/jem.20151948

Yamanaka, M., Ishikawa, T., Griep, A., Axt, D., Kummer, M. P., and Heneka, M. T. (2012). PPAR/RXR -Induced and CD36-Mediated Microglial Amyloid-Phagocytosis Results in Cognitive Improvement in Amyloid Precursor Protein/Presenilin 1 Mice. *J. Neurosci.* 32, 17321–17331. doi: 10.1523/JNEUROSCI.1569-12.2012

Ziegler-Graham, K., Brookmeyer, R., Johnson, E., and Arrighi, H. M. (2008). Worldwide variation in the doubling time of Alzheimer's disease incidence rates. *Alzheimers Dement.* 4, 316–323. doi: 10.1016/j.jalz.2008.05.2479

Zimmer, E., Leuzy, A., Benedet, A., Breitner, J., Gauthier, S., and Rosa-Neto, P. (2014). Tracking neuroinflammation in Alzheimer's disease: the role of positron

emission tomography imaging. *J. Neuroinflammation* 11:120. doi: 10.1186/1742-2094-11-120

Zott, B., Simon, M. M., Hong, W., Unger, F., Chen-Engerer, H.-J., Frosch, M. P., et al. (2019). A vicious cycle of β amyloid-dependent neuronal hyperactivation. *Science* 365, 559–565. doi: 10.1126/science.aay0198

Conflict of Interest: GK is an employee of ISAR bioscience. KB is an employee of Roche. AR has received research support and speaker honoraria from Siemens. MB received speaker honoraria from GE healthcare, Roche, and LMI and is an advisor of LMI.

The remaining authors declare that the research was conducted in the absence of any commercial or financial relationships that could be construed as a potential conflict of interest.

Publisher's Note: All claims expressed in this article are solely those of the authors and do not necessarily represent those of their affiliated organizations, or those of the publisher, the editors and the reviewers. Any product that may be evaluated in this article, or claim that may be made by its manufacturer, is not guaranteed or endorsed by the publisher.